DEPARTMENT OF TRANSPORTATION

Investigation of Cracking Resistance of Asphalt Mixtures and Binders

Mihai Marasteanu, Principal Investigator
Civil, Environmental, and Geo- Engineering

January 2019

Research Project
Final Report 2019-03

To request this document in an alternative format, such as braille or large print, call 651-366-4718 or 1-800-657-3774 (Greater Minnesota) or email your request to ADArequest.dot@state.mn.us. Please request at least one week in advance.

Technical Report Documentation Page

1. Report No.	2.	3. Recipients Accession No.
MN/RC 2019-03		

4. Title and Subtitle	5. Report Date
Investigation of Cracking Resistance of Asphalt Mixtures and Binders	January 2019
	6.

7. Author(s)	8. Performing Organization Report No.
Mihai Marasteanu, Mugurel Turos, Debaroti Ghosh, Jhenyffer Lorrany Matias de Oliveira, Tianhao Yan	

9. Performing Organization Name and Address	10. Project/Task/Work Unit No.
Civil, Environmental, and Geo- Engineering University of Minnesota - Twin Cities 500 Pillsbury Drive, Minneapolis, MN	CTS#2017008
	11. Contract (C) or Grant (G) No. (C) 99008 (WO) 239

12. Sponsoring Organization Name and Address	13. Type of Report and Period Covered
Minnesota Department of Transportation Research Services & Library 395 John Ireland Boulevard, MS 330 St. Paul, Minnesota 55155-1899	Final Report
	14. Sponsoring Agency Code

15. Supplementary Notes
http://mndot.gov/research/reports/2019/201903.pdf

16. Abstract (Limit: 250 words)

In this study, the viability of using three test methods for asphalt mixtures and one test method for asphalt binders are investigated. These test methods are: Bending Beam Rheometer (BBR) for creep and strength of asphalt mixtures; low temperature Semi Circular Bend (SCB) test for fracture energy of asphalt mixtures; Dynamic Modulus (E*) test of asphalt mixtures using the Indirect Tensile Test (IDT) configuration; and BBR strength test of asphalt binders. The materials used in the experimental work were used in MnROAD cells constructed in the summer of 2016 as part of the MnROAD Cracking Group (CG) experiment, a 3-year pooled-fund project.

The results show that the testing methods investigated provide repeatable results that follow trends similar to the one observed using traditional methods. The results also show that the properties are highly temperature dependent and the ranking observed at one temperature can change at a different temperature. In addition, it is observed that materials with similar rheological properties, such as complex modulus absolute value |E*|, creep stiffness S, and m-value, do not necessarily have the same fracture resistance. These results confirm one more time the need for a fracture/strength test for correctly evaluating cracking resistance of asphalt materials.

17. Document Analysis/Descriptors	18. Availability Statement
Asphalt mixtures, Binders, Cracking, Fracture tests, Rheological properties	No restrictions. Document available from: National Technical Information Services, Alexandria, Virginia 22312

19. Security Class (this report)	20. Security Class (this page)	21. No. of Pages	22. Price
Unclassified	Unclassified	107	

INVESTIGATION OF CRACKING RESISTANCE OF ASPHALT MIXTURES AND BINDERS

FINAL REPORT

Prepared by:
Mihai Marasteanu
Mugurel Turos
Debaroti Ghosh
Jhenyffer Lorrany Matias de Oliveira
Tianhao Yan

Department of Civil, Environmental, and Geo- Engineering
University of Minnesota

JANUARY 2019

Published by:

Minnesota Department of Transportation
Research Services & Library
395 John Ireland Boulevard, MS 330
St. Paul, Minnesota 55155-1899

ACKNOWLEDGMENTS

The authors gratefully acknowledge the financial support provided by the Minnesota Department of Transportation.

The guidance and logistical support to obtain the testing materials provided by MnDOT Office of Materials and Road Research, and in particular by the project champion, David Van Deusen, are acknowledged.

TABLE OF CONTENTS

CHAPTER 1: INTRODUCTION 1

1.1 Background 1

1.2 Objective 1

1.3 Organization of the Report 1

CHAPTER 2: PRELIMINARY TESTING 2

2.1 Bending Beam Rheometer Test 3

2.2 Dynamic Modulus Test 8

2.3 Semi Circular Bend (SCB) Test 11

2.4 Conclusions 13

CHAPTER 3: MATERIAL SELECTION 14

CHAPTER 4: BBR TESTING OF ASPHALT BINDERS 20

CHAPTER 5: BBR TESTING OF ASPHALT MIXTURES 30

5.1 Specimen preparation 30

5.2 Testing Procedure 31

5.3 Guidelines for limiting creep and strength criteria for asphalt mixtures 38

5.3.1 Limiting criteria for BBR creep stiffness of asphalt mixtures 38

5.3.2 Limiting cracking temperature from BBR creep and strength of asphalt mixtures 40

5.3.3 Limiting criteria for BBR creep stiffness and m-value of asphalt mixtures 42

CHAPTER 6: SCB AND E* TESTING OF ASPHALT MIXTURES 45

6.1 Specimen preparation 45

6.2 Semi Circular Bending (SCB) Test 45

6.3 Diametral E* Test 46

6.4 Indirect Tensile Test (IDT) Creep Compliance and Tensile Strength 47

6.5 SCB Test Results 48

6.6 Diametral E* Results 53

6.7 IDT Creep Compliance and Tensile Strength Results 55

CHAPTER 7: DATA ANALYSIS 58

7.1 Binders ANOVA 58

7.2 Binders Tukey Analysis 64

7.3 Mixtures ANOVA 70

7.4 Mixtures Tukey Analysis 81

7.5 Correlations 86

CHAPTER 8: SUMMARY, CONCLUSIONS, AND RECOMMENDATIONS 90

REFERENCES 91

LIST OF FIGURES

Figure 2.1: BBR Mixture Creep Stiffness for Cell 20 at Different Temperatures. 4
Figure 2.2: BBR Mixture Creep Stiffness at 0ºC. 4
Figure 2.3: BBR Mixture Creep Stiffness at -12ºC. 4
Figure 2.4: BBR Mixture Creep Stiffness at -24ºC. 5
Figure 2.5: BBR Mixture S(60) at 0C, -12C and -24C. 5
Figure 2.6: Stress vs Strain for Cell 20 at Different Temperatures. 6
Figure 2.7: BBR Mixture Strength at 0C, -12C and -24C. 6
Figure 2.8: Fitted dynamic modulus master curves for all Cells of MnROAD. 9
Figure 2.9: |E*| values at 25 Hz for all Cells. 10
Figure 2.10: Fracture Energy for All Asphalt Mixtures. 12
Figure 2.11: Fracture Toughness for All Asphalt Mixtures. 13
Figure 2.12: Cell 19 loading deflection curves at -12°C. 13
Figure 3.1: Gradation curve of the eight mixtures on the 0.45 power chart. 16
Figure 3.2: Percentage of total and effective asphalt content. 16
Figure 3.3: Percentage of RAP and RAS 17
Figure 3.4: Voids in the mineral aggregate (VMA). 18
Figure 3.5: Adjusted Asphalt Film Thickness (AFT). 19
Figure 4.1: Loading rate for strength test performed at -24ºC on Cell 23 asphalt binder. 21
Figure 4.2: Predicted and experimentally determined stress-strain curves for two binders. 22
Figure 4.3: Burgers model. 23
Figure 4.4: Using Burgers model to fit creep and recovery experimental data. 24
Figure 4.5: Prediction of strength test using Burgers model. 25
Figure 4.6: Creep Stiffness at 60 sec for binders from Cell 16, 20-23. 27
Figure 4.7: m-value at 60 sec for binders from Cell 16, 20-23. 27
Figure 4.8: BBR Strength of Binders from Cell 16, 20-23. 28
Figure 4.9: Strain at Failure of Binders from Cell 16, 20-23. 28
Figure 4.10: Creep Stiffness vs Time of Binders from Cell 16-23 at PGLT+10C. 29
Figure 4.11: Stress-Strain Curve of Binders from Cell 16-23 @ PGLT+10C. 29
Figure 5.1: BBR Mixture Creep Stiffness at 60 seconds. 31
Figure 5.2: BBR m-values at 60 seconds. 32
Figure 5.3: BBR Mixture Strength. 34

Figure 5.4: BBR Mixture Strain at Failure. 34
Figure 5.5: Creep Stiffness for Cell 17 at 0°C. 36
Figure 5.6: m-value for Cell 17 at 0°C. 37
Figure 5.7: Stress Strain curve for Cell 17. 37
Figure 5.8: Stress Strain curve for Cell 20. 38
Figure 5.9: Predicting RTFOT Binder S(60s) at PAV Binder Critical Temperature, TCR. 39
Figure 5.10: Cell 18 thermal stress and strength obtained from BBR creep and strength tests. 42
Figure 5.11: Cell 17 thermal stress and strength obtained from BBR creep and strength tests. 42
Figure 5.12: Example of diagram used for a design temperature of -22ºC. 43
Figure 5.13: Hypothetical diagram for a design temperature of -22ºC. 44
Figure 5.14: Hypothetical diagram for a design temperature of -34ºC. 44
Figure 6.1: The original (left) and the the new loading fixture (right two photos). 45
Figure 6.2: Fracture energy for all mixtures. 49
Figure 6.3: Fracture toughness for all mixtures. 50
Figure 6.4: Cell 22 LLD and actuator displacement at -12°C. 51
Figure 6.5: Cell 22 LLD and actuator displacement at -24°C. 52
Figure 6.6: Fitted dynamic modulus master curves for all cells. 55
Figure 6.7: Creep stiffness curves at -12°C for all cells. 56
Figure 6.8: Creep stiffness curves at -24°C for all cells. 56
Figure 6.9: Average tensile strength at -24°C and -12°C. 57
Figure 7.1: (a) Confidence intervals (Tukey) for PAV binder BBR Creep Stiffness at PGLT+10°C. (b) Boxplot for pairwise comparison. 65
Figure 7.2: (a) Confidence intervals (Tukey) for PAV binder BBR Creep Stiffness at PGLT+4°C. (b) Boxplot for pairwise comparison. 65
Figure 7.3: (a) Confidence intervals (Tukey) for PAV binder BBR m-value at PGLT+10°C. (b) Boxplot for pairwise comparison. 66
Figure 7.4: (a) Confidence intervals (Tukey) for PAV binder BBR m-value at PGLT+4°C. (b) Boxplot for pairwise comparison. 66
Figure 7.5: (a) Confidence intervals (Tukey) for PAV binder BBR Strength at PGLT+10°C. (b) Boxplot for pairwise comparison. 67
Figure 7.6: (a) Confidence intervals (Tukey) for PAV binder BBR Strength at PGLT+4°C. (b) Boxplot for pairwise comparison. 67
Figure 7.7: (a) Confidence intervals (Tukey) for PAV binder BBR Strain at failure at PGLT+10°C. (b) Boxplot for pairwise comparison. 68

Figure 7.8: (a) Confidence intervals (Tukey) for PAV binder BBR Strain at failure at PGLT+4°C. (b) Boxplot for pairwise comparison 68
Figure 7.9: Summary of boxplots for PAV binder results. 69
Figure 7.10: (a) Confidence intervals (Tukey) for BBR Creep Stiffness at -12°C. (b) Boxplot for pairwise comparison. 82
Figure 7.11: (a) Confidence intervals (Tukey) for BBR Creep Stiffness at -24°C. (b) Boxplot for pairwise comparison. 82
Figure 7.12: (a) Confidence intervals (Tukey) for BBR m-value at -12°C. (b) Boxplot for pairwise comparison. 83
Figure 7.13: (a) Confidence intervals (Tukey) for BBR m-value at -24°C. (b) Boxplot for pairwise comparison. 83
Figure 7.14: (a) Confidence intervals (Tukey) for BBR strength at -24°C. (b) Boxplot for pairwise comparison. 84
Figure 7.15(a) Confidence intervals (Tukey) for BBR % strain at failure at -12°C. (b) Boxplot for pairwise comparison. 84
Figure 7.16: (a) Confidence intervals (Tukey) for fracture energy at -12°C. (b) Boxplot for pairwise comparison. 85
Figure 7.17: Summary of boxplots for mixture results. 86

LIST OF TABLES

Table 2.1: Testing Matrix for Preliminary Work. 3
Table 2.2: BBR Creep Stiffness and Strength of Asphalt Mixtures. 7
Table 2.3: |E*| master curve fitting parameters. 9
Table 2.4: Calculated values for |E*| [GPa]. 10
Table 2.5: Fracture Energy and Fracture Toughness at -12°C and -24°C. 12
Table 3.1: Asphalt Mixture Samples for CG Study. 14
Table 3.2: Inventory of Materials Received. 14
Table 3.3: Gradation and asphalt content of 2016 mixtures. 15
Table 3.4: Adjusted AFT for cells 16 to 23. 18
Table 4.1: Asphalt Binder Testing Matrix. 20
Table 4.2: Creep Stiffness and m-value of Asphalt Binder. 26
Table 4.3: Strength and Strain at Failure of Asphalt Binder. 26
Table 5.1: Testing Matrix for Asphalt Mixtures. 30
Table 5.2: BBR Creep Stiffness and m-value Results. 32
Table 5.3: BBR Strength Results. 35
Table 5.4: Predicted Mixture S(60) at PAV Binder Critical Temperature. 39
Table 5.5: Critical Temperature for all Cells. 42
Table 6.1: Fracture energy and apparent fracture toughness. 49
Table 6.2: Comparison of the SCB results obtained with the two fixtures. 50
Table 6.3: |E*| values for all cells, average values. 53
Table 6.4: |E*| master curve fitting parameters. 54
Table 6.5: Creep stiffness and tensile strength at -12oC. 55
Table 6.6: Creep stiffness and tensile strength at -24oC. 56
Table 7.1: Summary and ANOVA: PAV binder BBR Creep Stiffness at PGLT+10°C. 58
Table 7.2: Summary and ANOVA: PAV binder BBR Creep Stiffness at PGLT+4°C. 59
Table 7.3: Summary and ANOVA: PAV binder BBR m-value at PGLT+10°C. 60
Table 7.4: Summary and ANOVA: PAV binder BBR m-value at PGLT+4°C. 60
Table 7.5: Summary and ANOVA: PAV binder BBR Strength at PGLT+10°C. 61
Table 7.6: Summary and ANOVA: PAV binder BBR Strength at PGLT+4°C. 62
Table 7.7: Summary and ANOVA: PAV binder BBR Strain at PGLT+10°C. 63
Table 7.8: Summary and ANOVA: Single Factor for PAV binder BBR Strain at PGLT+4°C. 64

Table 7.9: Summary and ANOVA: BBR Creep Stiffness at -12°C. 70
Table 7.10: Summary and ANOVA: BBR Creep Stiffness at -24°C. 71
Table 7.11: Summary and ANOVA: BBR m-value at -12°C. 72
Table 7.12: Summary and ANOVA: BBR m-value at -24°C. 73
Table 7.13: Summary and ANOVA: BBR Strength at -12°C. 74
Table 7.14: Summary and ANOVA: BBR Strength at -24°C. 75
Table 7.15: Summary and ANOVA: BBR strain at failure at -12°C. 76
Table 7.16: Summary and ANOVA: BBR strain at failure at -24°C. 77
Table 7.17: Summary and ANOVA: SCB Fracture Energy at -12°C. 78
Table 7.18: Summary and ANOVA: SCB Fracture Energy at -24°C. 79
Table 7.19: Summary and ANOVA: IDT Creep Stiffness at -12°C. 80
Table 7.20: Summary and ANOVA: IDT Creep Stiffness at -24°C. 81
Table 7.21: Correlation matrix for properties from cells 16 to 23 at -12°C. 88
Table 7.22: Correlation matrix for properties from cells 16 to 23 at -24°C. 89

EXECUTIVE SUMMARY

In this study, the viability of using three test methods for asphalt mixtures and one test method for asphalt binders was investigated. The methods were: Bending Beam Rheometer (BBR) for creep and strength of asphalt mixtures; low temperature Semi Circular Bend (SCB) fracture testing for asphalt mixtures; Dynamic Modulus (E*) testing of asphalt mixtures using the Indirect Tensile Test (IDT) configuration; and BBR strength testing of asphalt binders. The materials investigated in the experimental work were used in MnROAD cells constructed in the summer of 2016 as part of the MnROAD Cracking Group (CG) experiment, a 3-year pooled-fund project.

In the beginning of the project, preliminary testing was performed using the proposed asphalt mixture testing methods to further improve the existing procedures. Testing was done on cores taken from the existing 2008 MnROAD sections 16 through 23 before reconstruction of these cells in 2016. The preliminary results did not reveal any problems with the proposed testing methods, as shown in Chapter 2.

In Chapter 3, the materials used in the experimental plan are described in detail. These materials represent loose asphalt mixtures collected from cells 16 through 23 at the time of construction of these cells during the summer of 2016 and the original asphalt binders used.

Chapter 4 details the BBR creep and strength testing performed on the five binders that correspond to MnROAD Cells 16-19, 20, 21, 22 and 23, constructed in 2016. The binders were short and then long-term aged using RTFO and PAV procedures, respectively. All binders passed the stiffness and m-value criteria at PGLT+10C. However, strength results showed clear differences between the binders, which indicate the need for a binder strength test, similar to the original SHRP specification.

In Chapter 5, the experimental work performed to obtain the BBR creep stiffness and strength of the asphalt mixtures is presented. In addition, three approaches are proposed to develop asphalt mixtures selection criteria based on BBR creep and strength results at low temperature. The first one proposes a limiting criterion for BBR creep stiffness of asphalt mixtures, similar to the current PG criterion for binders. The second approach is based on determining a limiting cracking temperature from BBR creep and strength of asphalt mixtures, while the third is based on a BBR creep stiffness and m-value diagram proposed by Utah DOT and University of Utah.

Chapter 6 details the experimental work performed on asphalt mixtures using SCB fracture testing, and E* complex modulus testing using diametral compression loading. Although not part of the work plan, IDT creep and tensile strength were also conducted to compare IDT and BBR test results.

The data obtained in the previous chapters is analyzed in Chapter 7. Statistical analyses including analysis of variance (ANOVA), Tukey's method, which represents a pairwise comparison technique, and correlation matrices based on Pearson's correlation were performed to identify significant factors. The results showed that correlations change with temperature and correlations that are significant at one temperature are not significant at the other temperature, which indicates the need to perform testing at multiple temperatures. No significant correlations were observed between the mechanical properties and the mix design parameters, most likely due to the different combinations of design parameters in each mix design.

Chapter 8 provides conclusions and recommendations. It was found that the testing methods investigated provide repeatable results that follow trends similar to the one observed using traditional methods. It was observed that materials with similar rheological properties do not necessarily have the same fracture resistance. These results confirm the need for a failure test to correctly evaluate cracking resistance of asphalt materials. In general, the mixtures used in this experiment have similar properties, which may indicate similar service performance, except for the mixture from cell 20 that has the highest RAP content and the mixture from cell 23 that contains a highly modified binder. To fully evaluate the value of these test methods in the selection process, it is recommended that cores are taken at periodic intervals of time and tested. Most importantly, distress surveys should be performed periodically and correlations should be developed to determine the best predictors of performance.

CHAPTER 1: INTRODUCTION

1.1 BACKGROUND

The Minnesota Road Research Project (MnROAD) and the National Center for Asphalt Technology (NCAT) have formed a partnership to execute asphalt mixture performance testing experiments with a nationwide implementation impact.

The MnROAD Cracking Group (CG) experiment is a 3-year pooled-fund project sponsored by five states including Illinois, Michigan, Minnesota, New York, and Wisconsin. The CG experiment at MnROAD focused on low-temperature cracking, although research components addressed other types of cracking, such as fatigue and top-down. The construction of the test cells at MnROAD was performed in the summer of 2016.

The Minnesota Department of Transportation (MnDOT) was interested in investigating performance tests in addition to those investigated as part of the CG experiment. These additional test methods have been used by a number of agencies and research laboratories and have shown significant potential for predicting the cracking behavior of the materials tested.

1.2 OBJECTIVE

The main objective of this research is to determine the viability of using three test methods for asphalt mixtures and one test method for asphalt binders in the material selection process, quality control, and forensic investigations of asphalt paving materials. These test methods are the Bending Beam Rheometer (BBR) for creep and strength of asphalt mixtures; low temperature SCB fracture testing for asphalt mixtures; E* testing of asphalt mixtures using the IDT configuration; and BBR strength testing of asphalt binders.

1.3 ORGANIZATION OF THE REPORT

First, preliminary testing is performed to refine the current procedures for the proposed testing methods. The preliminary testing is done on cores taken from the existing MnROAD sections 16 through 23, before reconstruction of these cells in 2016. Next, details regarding the asphalt binders and asphalt mixtures from the new cells constructed in 2016, and used in this study, are provided.

Chapter 4 details the experimental work performed to obtain flexural strength of asphalt binders and Chapter 5 details the experimental work performed on small mixture beams to obtain the creep and strength of the CG asphalt mixtures using the same BBR-Pro device. In Chapter 6, SCB and diametral E* testing is described and the results are presented.

Chapter 7 details the statistical analyses performed and the correlations identified between the different parameters. Chapter 8 consists of a summary of the work followed by conclusions and recommendations.

CHAPTER 2: PRELIMINARY TESTING

In the beginning of the project, preliminary testing was performed using the proposed asphalt mixture testing methods to further improve the existing procedures:

1. Bending Beam Rheometer (BBR) for creep and strength of asphalt mixtures
2. Low temperature Semi Circular Beam fracture testing for asphalt mixtures
3. E* testing of asphalt mixtures using the Indirect Tensile Test (IDT) configuration
4. Creep compliance and strength using the Indirect Tensile Test Device.

The preliminary testing was performed on cores that were taken from the existing MnROAD sections 16 through 23 before reconstruction of these cells in 2016. From each cell, 12 cores were extracted in summer of 2016 and were delivered to University of Minnesota. The cores were numbered during the collection, and the same number was used for samples preparation. The cores included the surface treatment applied during service life. For cell 23, the core height was 7", and for the cells 16 to 22, the core height was 5''.

The cores were cut to prepare testing specimens for the four test methods proposed. Testing was performed only on specimens obtained from the top surface layer of each core. For this reason, and given the number of cores available, two to three replicate cores were used for each test method. For some tests (BBR and SCB), the surface treatment layer was removed from the test specimen, since its presence would significantly affect the results. For the dynamic modulus and the IDT creep and strength test, the surface treatment was not removed, since its presence would not impact the results and the test specimen thickness is approximately 38mm, and allows cutting the test specimen from the top 1.5" lift only. The testing matrix used for each cell is presented in Table 2.1. Since IDT creep and strength is a mature testing method (AASHTO T322-07), no preliminary IDT testing was performed.

MnDOT will use the preliminary experimental results to supplement the existing database of material parameters previously obtained on these older cells, and develop correlations between the parameters obtained from testing original materials and cores taken at the time of reconstruction.

Table 2.1: Testing Matrix for Preliminary Work.

Test	Number of cores used	Number of samples prepared	Testing Temperatures and Number of Replicates	Surface treatment
E* in IDT	2	2 (1 per core)	(-12°C, 12°C and 36°C) x 2	Kept
SCB	3	6 (2 per core)	(-12°C) x 3 (-24°C) x 3	Removed
BBR Mixture	2	18 (9 per core)	(-24°C creep, recovery, strength) x 5 (-12°C creep, recovery, strength) x 5 (0°C creep, recovery, strength) x 5	Removed
Creep and strength in IDT	3	3 (1 per core)	(-24°C creep, -12°C creep) x 2 (-12°C strength) x 2 (will be performed as part of Task 5)	Kept

2.1 BENDING BEAM RHEOMETER TEST

Previous research performed at the University of Minnesota showed that the Bending Beam Rheometer (BBR), currently used for asphalt binder specifications, can be used to obtain creep and strength properties of asphalt mixtures. The sample preparation method includes several cutting steps, starting with a gyratory compacted (GC) cylinder or field core, and ending with the actual BBR beams. Each core receives first one horizontal cut, and each layer is then cut into ten beams with the dimensions of approximately l = 125.0 mm, b = 12.5 mm, D = 6.25 mm.

In this preliminary testing, each beam was first tested in creep, followed by a recovery period and then a strength test, without removing the beam from the supports. The creep test consisted of 1000 sec loading duration. The creep loading was chosen to be 2N, 4N and 6N for testing at 0°C, -12°C and -24°C, respectively. The creep was followed by a recovery of 500 seconds, without any applied load, after which, a constant loading rate was applied, such that a load of 44N was obtained in 60 sec. The test ended when the beam broke.

The tests were performed on 5 replicates at each temperature, for each cell. 105 beams were tested from 7 out of the 8 cells. The beams cut from cell 18 cores were very weak and could not be tested. This observation is in agreement with visual observation of the cores when extracted from the pavement structure.

Examples of test result are shown below. The results reported represent the average of 5 replicates. Figure 2.1 shows the creep stiffness results for Cell 20 at 3 different temperatures. As expected, stiffness decreases with increase in temperature. Figures 2.2 to 2.4 show the creep stiffness results for all cells at all three testing temperatures.

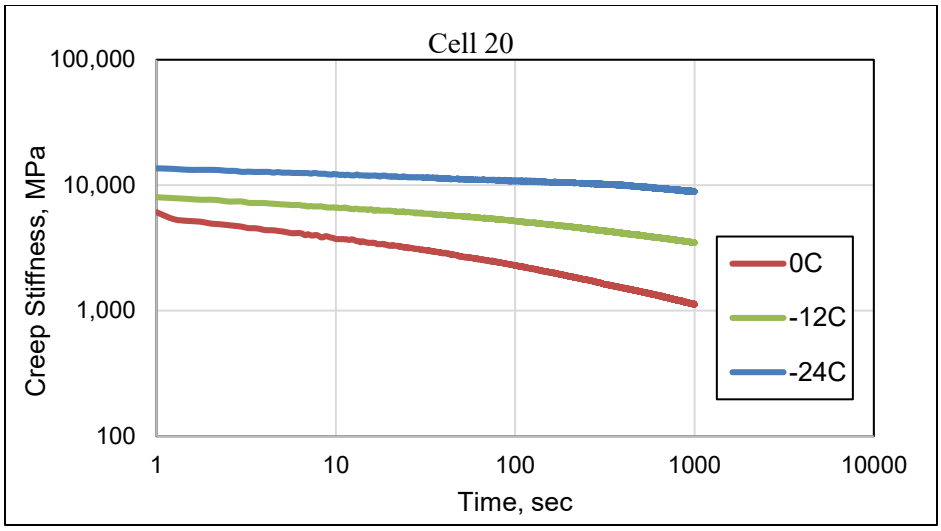

Figure 2.1: BBR Mixture Creep Stiffness for Cell 20 at Different Temperatures.

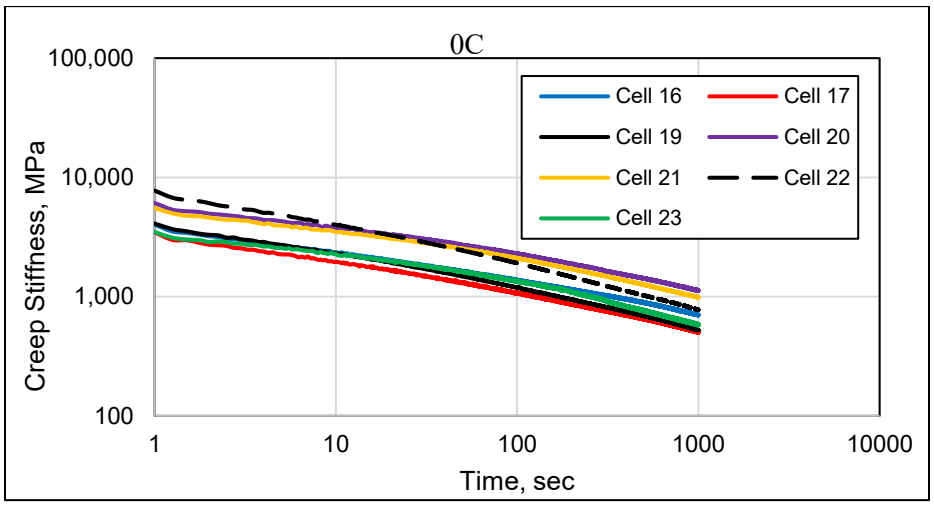

Figure 2.2: BBR Mixture Creep Stiffness at 0ºC.

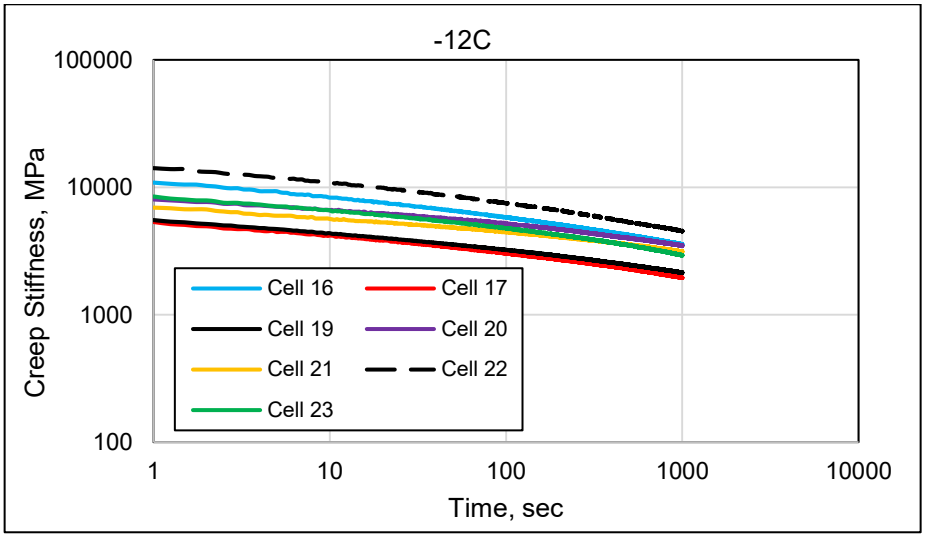

Figure 2.3: BBR Mixture Creep Stiffness at -12ºC.

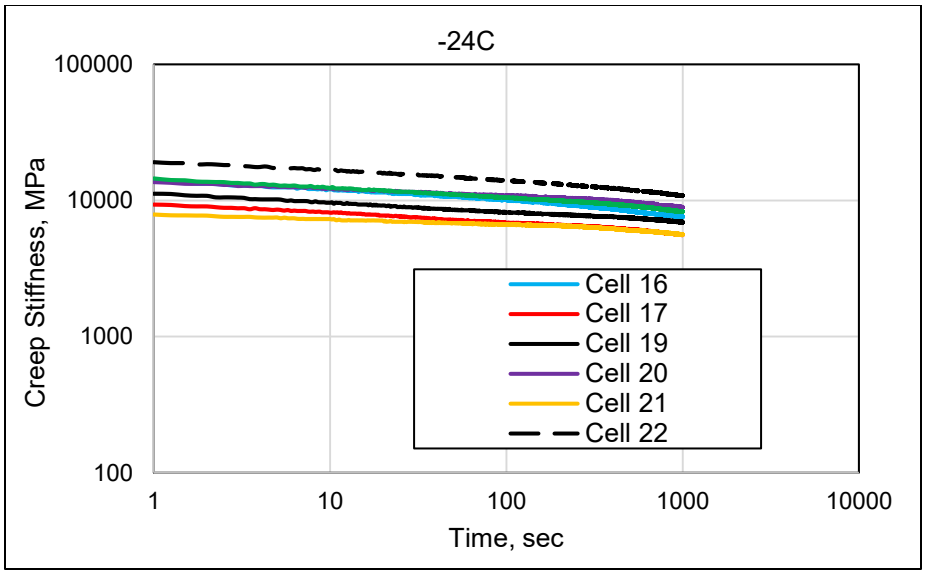

Figure 2.4: BBR Mixture Creep Stiffness at -24ºC.

The creep stiffness at 60 sec of asphalt mixture from different cells at three different temperatures are presented in Figure 2.5. Strength tests were performed on the same beams used for creep testing. An example of stress-strain curves is presented in Figure 2.6.

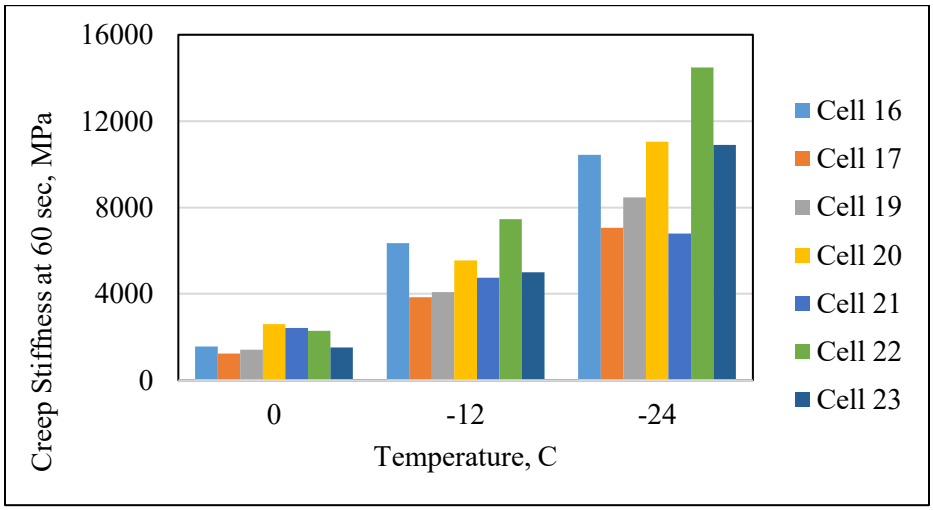

Figure 2.5: BBR Mixture S(60) at 0C, -12C and -24C.

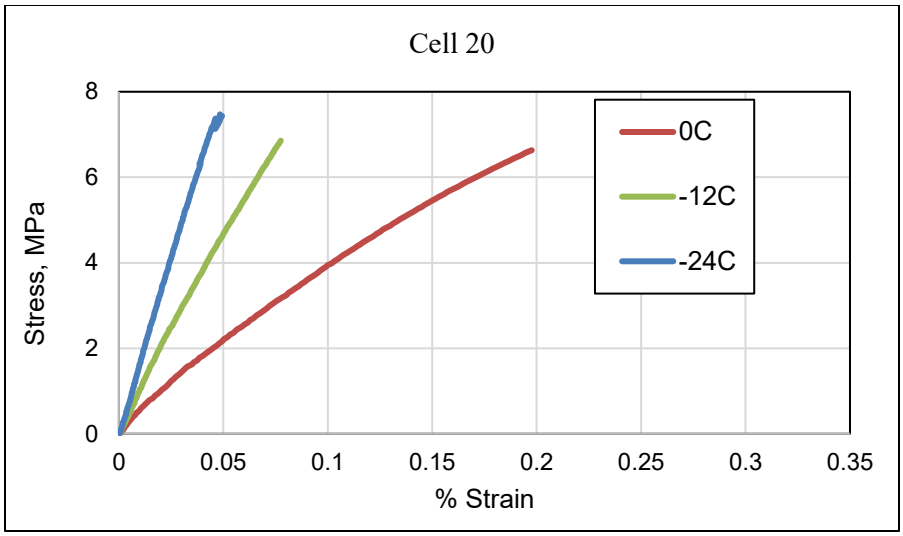

Figure 2.6: Stress vs Strain for Cell 20 at Different Temperatures.

The strength results of asphalt mixture from the seven test cells at three different temperatures are presented in Figure 2.7. Similar to the creep stiffness results, Cell 22 mixture had the highest strength, with a value above 10 MPa. Cells 17 and 19 mixtures had the lowest strength values. A summary of the BBR creep and strength properties of all asphalt mixture at three different temperatures is presented in Table 2.2.

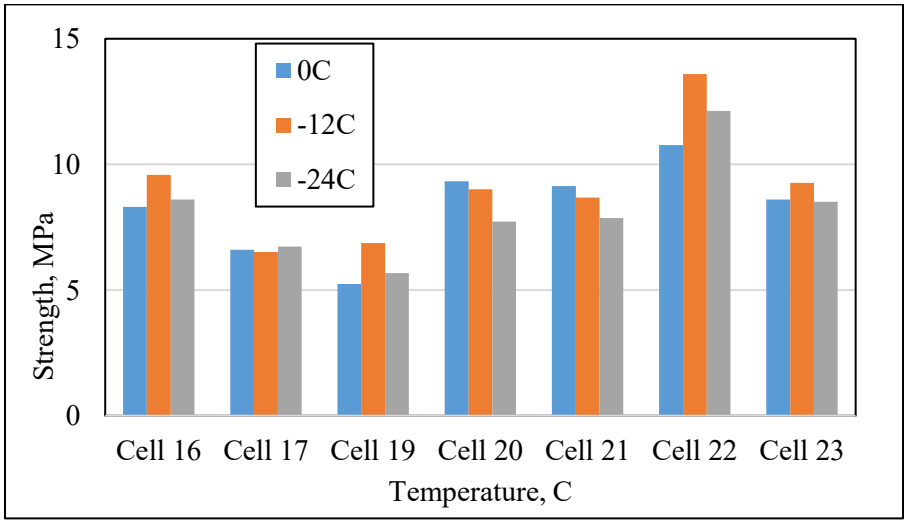

Figure 2.7: BBR Mixture Strength at 0C, -12C and -24C.

Table 2.2: BBR Creep Stiffness and Strength of Asphalt Mixtures.

Cell No.	Temp	Stiffness @ 60sec, MPa	m-value @ 60 sec	Max Deflection, mm	Stress Failure, MPa	Strain Failure, %	Load Failure, N	Time to fail, sec
16	0	1562	0.248	0.21	8.31	0.717	28.37	39.7
	-12	6341	0.170	0.08	9.59	0.156	32.48	44.8
	-24	10434	0.088	0.06	8.60	0.065	29.60	40.9
17	0	1242	0.277	0.25	6.60	0.782	24.74	34.8
	-12	3839	0.144	0.16	6.52	0.172	24.03	33.3
	-24	7057	0.070	0.08	6.73	0.067	25.28	35.0
19	0	1407	0.304	0.23	5.25	0.588	19.69	27.9
	-12	4080	0.153	0.17	6.87	0.172	24.09	33.4
	-24	8469	0.065	0.06	5.68	0.153	20.96	29.1
20	0	2600	0.252	0.11	9.33	0.405	34.58	48.3
	-12	5541	0.126	0.08	9.01	0.108	33.63	46.2
	-24	11045	0.055	0.05	7.73	0.052	28.19	39.0
21	0	2415	0.255	0.13	9.13	0.428	34.17	47.6
	-12	4754	0.108	0.09	8.68	0.122	32.86	45.3
	-24	6793	0.034	0.09	7.86	0.075	29.88	41.0
22	0	2290	0.341	0.22	10.77	0.695	31.70	44.2
	-12	7452	0.181	0.09	13.59	0.176	40.79	56.2
	-24	14478	0.080	0.05	12.13	0.150	36.35	50.2
23	0	1518	0.280	0.30	8.60	0.672	27.67	38.8
	-12	5002	0.155	0.10	9.27	0.171	33.04	45.6
	-24	10894	0.074	0.06	8.51	0.063	29.03	40.1

2.2 DYNAMIC MODULUS TEST

This test was selected to determine complex modulus of asphalt mixture over a wide range of temperature and frequencies. Complex modulus is typically measured in compression on cylinders 100 mm in diameter and 170 mm tall. This geometry severely limits the possibility of testing field cores. In this preliminary testing, an alternative method based on the indirect tension (IDT) loading configuration was used. In this test, the load is applied along the diameter of the test specimen, which is 150 mm in diameter and 38 mm thick.

Frequency sweeps were performed on each replicate at 3 temperatures, -12°C, 12°C, and 36°C, and eight frequencies: 25, 10, 5, 1, 0.5, 0.1, 0.05, 0.01 Hz. Two replicates were tested at each temperature and |E*| values were calculated for each of the temperature and frequency combinations. Average |E*| values were then used to construct master curves using time-temperature superposition principle by fitting the data to the following equation (Rowe, et al. 2009):

$$\log|E^*| = \delta + \frac{\alpha - \delta}{1 + e^{\beta+\gamma(log\omega+\log(a(T)))}} \qquad [2.1]$$

where: ω = frequency of load

a(T) = temperature shift parameter

δ, α, β and γ are fitting parameters.

Table 2.3 shows the fitting parameters and shift factor values

Table 2.3: |E*| master curve fitting parameters.

	cell 16	cell 17	cell 18	cell 19	cell 20	cell 21	cell 22	cell 23
alpha	2.06E+10	2.06E+10	1.18E+10	2.50E+10	2.04E+10	2.36E+10	2.87E+10	1.24E+10
delta	2.77E+07	2.77E+07	3.74E+07	2.18E+06	1.40E+06	8.14E+04	5.94E+02	3.22E+07
beta	-1.30	-1.30	-1.37	-1.26	-1.56	-1.49	-1.68	-1.35
gama	-0.41	-0.41	-0.55	-0.32	-0.42	-0.32	-0.27	-0.65
log at(-12)	3.50	2.06	3.50	3.80	3.86	3.60	3.00	3.00
log at(+36)	-3.50	-3.61	-3.50	-3.60	-2.77	-3.50	-3.00	-3.50

As expected, |E*| decreases with decrease in temperature and frequency. Fitted master curves for all cells are shown in Figure 2.8 and summaries of results obtained at 25 Hz are presented in figure 2.9. Table 2.4 summarizes all |E*| values.

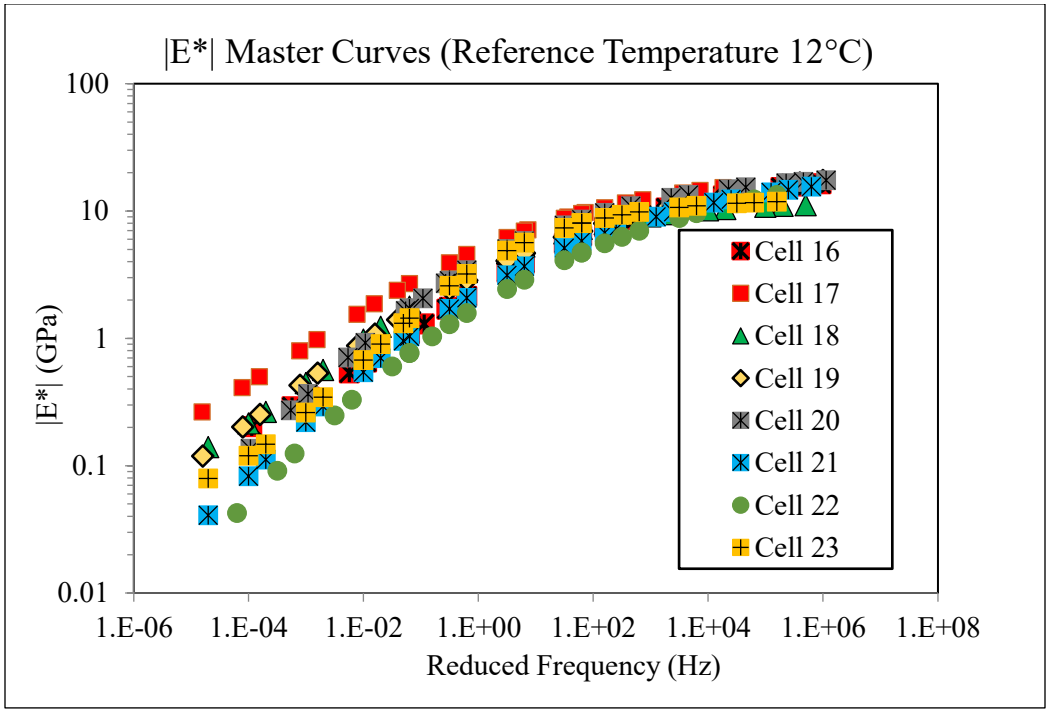

Figure 2.8: Fitted dynamic modulus master curves for all Cells of MnROAD.

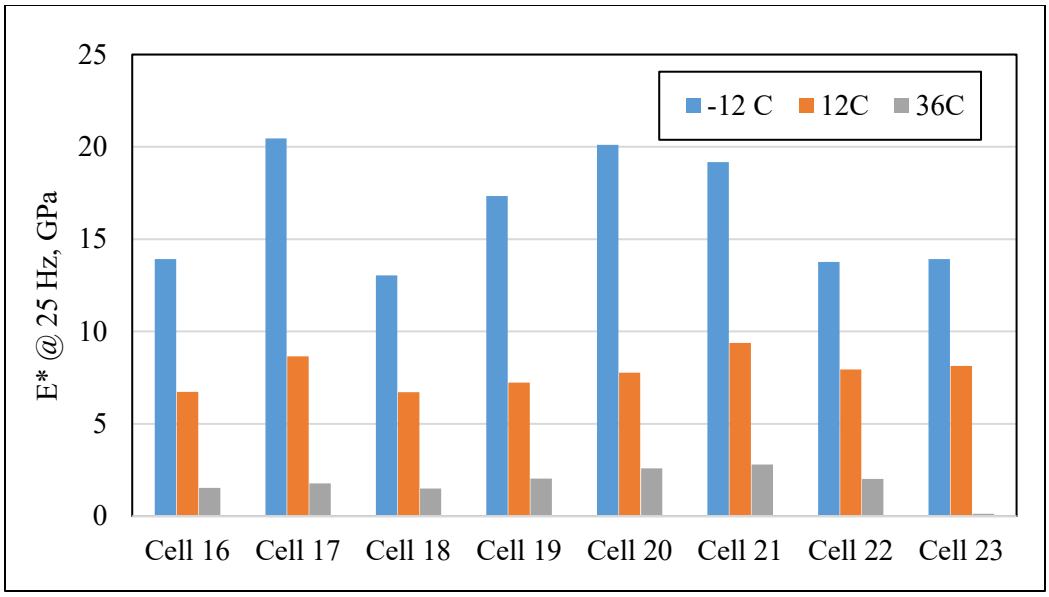

Figure 2.9: |E*| values at 25 Hz for all Cells.

Table 2.4: Calculated values for |E*| [GPa].

Cell (2008)	T °C	25 Hz	10 Hz	5 Hz	1 Hz	0.5 Hz	0.1 Hz	0.05 Hz	0.01 Hz
16	-12	13.91	16.09	15.50	13.63	12.99	11.83	10.94	9.10
	12	6.73	6.18	5.31	4.12	3.53	2.28	1.80	0.92
	36	1.53	1.34	1.03	0.63	0.50	0.31	0.26	0.16
17	-12	20.46	14.81	12.54	11.09	9.84	9.40	8.98	7.85
	12	8.66	9.59	8.44	7.64	6.59	4.87	4.10	2.42
	36	1.78	1.62	1.30	0.96	0.78	0.53	0.41	0.25
18	-12	13.04	10.27	8.83	7.99	6.97	6.60	6.23	5.54
	12	6.71	7.44	6.66	5.40	4.72	3.40	2.86	1.73
	36	1.50	1.21	1.00	0.63	0.52	0.30	0.25	0.14
19	-12	17.34	18.60	18.17	15.96	15.57	13.87	12.96	9.95
	12	7.23	6.86	5.92	4.74	4.08	2.97	2.46	1.63
	36	2.02	1.05	0.85	0.51	0.42	0.27	0.23	0.29
20	-12	20.10	16.76	16.60	15.03	13.97	13.43	12.40	11.08
	12	7.77	7.50	8.13	6.24	5.80	3.97	3.03	1.40

	36	2.59	2.16	1.68	0.86	0.70	0.36	0.28	0.14
21	-12	19.17	14.21	12.25	11.21	9.72	9.30	8.95	7.97
	12	9.38	4.92	4.25	3.42	3.02	2.14	1.84	1.04
	36	2.80	2.26	1.74	1.03	0.78	0.45	0.37	0.21
22	-12	13.77	8.38	6.77	5.72	4.64	4.29	3.89	3.27
	12	7.93	4.39	3.84	2.77	2.40	1.59	1.23	0.74
	36	2.01	1.56	1.26	0.83	0.70	0.52	0.18	0.15
23	-12	13.93	11.24	9.80	8.27	7.26	6.88	6.40	5.65
	12	8.13	8.65	7.11	5.53	5.21	3.57	2.60	1.28
	36	0.12	0.10	0.08	0.06	0.06	0.05	0.04	0.03

2.3 SEMI CIRCULAR BEND (SCB) TEST

SCB testing followed the existing provisional AASHTO procedure: AASHTO TP 105-2013 Standard Method of Test for Determining the Fracture Energy of Asphalt Mixtures Using the Semicircular Bend Geometry (SCB), 2013.

The fracture energy G_f was calculated according to RILEM TC 50-FMC specification that has been extensively used in the study of concrete. The work of fracture is the area under the loading-deflection (P-u) curve and the fracture energy (G_f) can then be obtained by dividing the work of fracture with the ligament area, which is the product of the ligament length and the thickness of the specimen. W_f is the work of fracture and A_{lig} is the area of the ligament:

$$\mathrm{G_f} = \frac{W_f}{A_{lig}} \qquad [2.2]$$

The tail part of the P-u curve is obtained by fitting the data curve in the post peak region.

$$W_f = \int P du \qquad [2.3]$$

Two fracture properties, fracture toughness, K_{IC} (MPa*m0.5), and fracture energy, G_f (kJ/m2), were calculated and compared. The results are presented in Table 2.5. Figure 2.10 presents the fracture energy values and Figure 2.11 presents the fracture toughness for the eight cells.

Table 2.5: Fracture Energy and Fracture Toughness at -12°C and -24°C.

Cell (2008)	Fracture Energy G_f (kJ/m^2)		Fracture Toughness, K_{IC} ($MPa*m^{0.5}$)	
	-12°C	-24°C	-12°C	-24°C
16	0.616	0.287	0.612	0.719
17	0.475	0.345	0.704	0.711
18	0.319	0.275	0.600	0.644
19	0.404	0.288	0.618	0.719
20	0.291	0.299	0.661	0.770
21	0.316	0.286	0.685	0.814
22	0.705	0.405	0.628	0.878
23	0.679	0.453	0.777	0.834

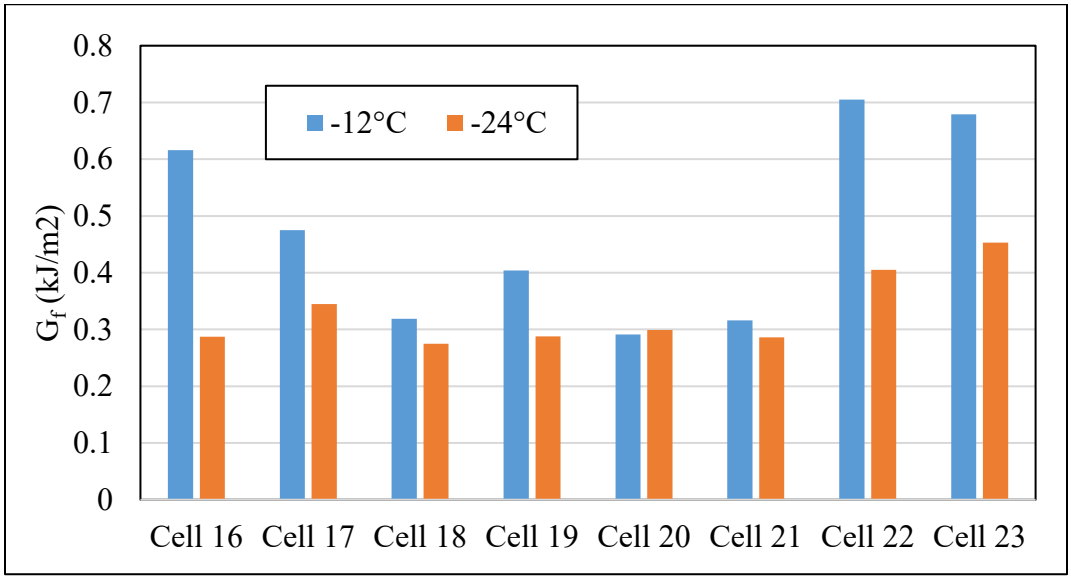

Figure 2.10: Fracture Energy for All Asphalt Mixtures.

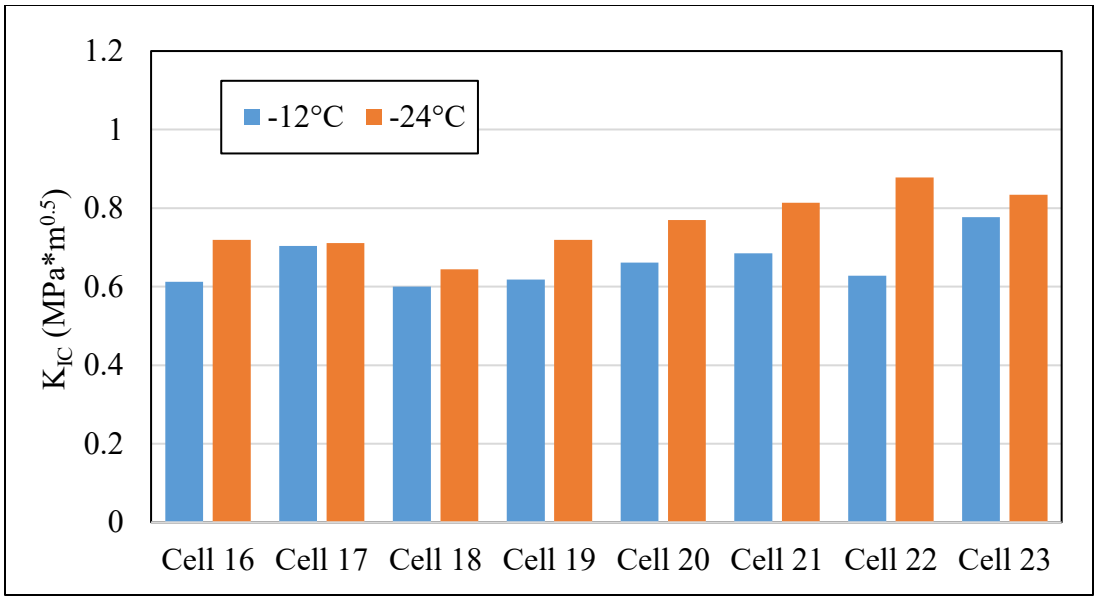

Figure 2.11: Fracture Toughness for All Asphalt Mixtures.

An example of the load vs. load line displacement curves for the three replicates obtained -12 for the asphalt mixtures on Cell 19 is presented in figure 2.12.

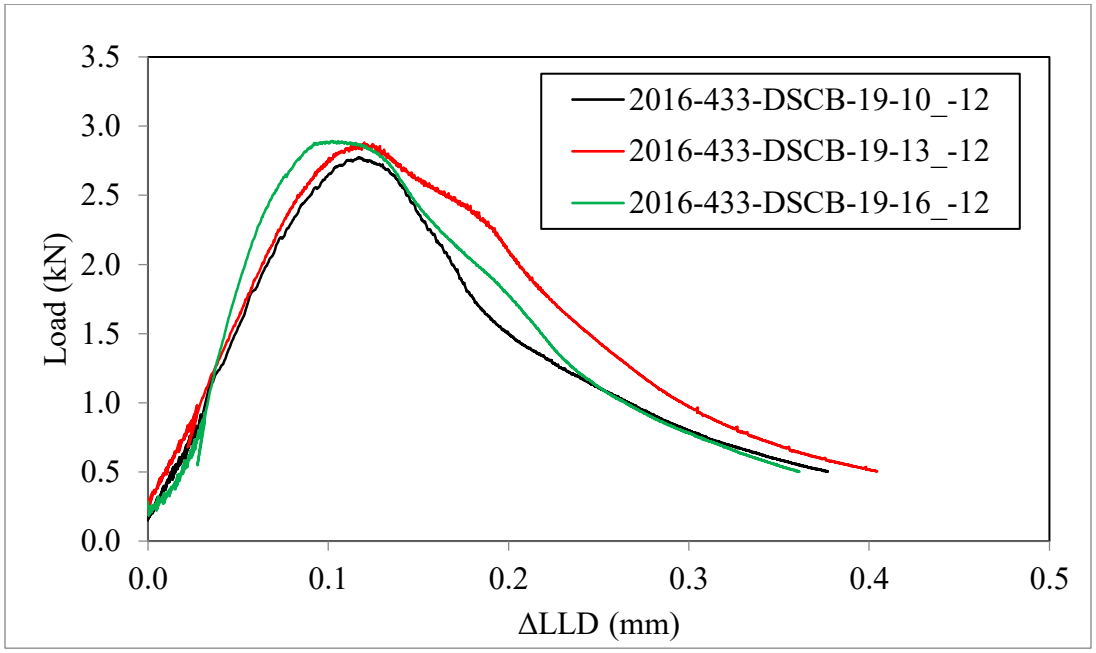

Figure 2.12: Cell 19 loading deflection curves at -12°C.

2.4 CONCLUSIONS

The preliminary results did not reveal any problems with the proposed testing methods. The results followed the expected trends for viscoelastic materials: an increase in stiffness, modulus and strength with decrease in temperature or an increase in frequency or decrease in loading time.

CHAPTER 3: MATERIAL SELECTION

In the beginning of the project, the research team collected the materials used in the experimental plan that supplements the planned testing under the MnROAD/NCAT partnership. The CG test matrix includes three types of asphalt mixture materials, as shown in Table 3.1. In this investigation, only the field-mixed, lab-compacted (FMLC) materials were investigated. These materials represent loose asphalt mixtures collected from cells 16 through 23 at the time of construction of these cells during the summer of 2016. A summary of the loose mix and original binders collected is presented in Table 3.2.

Table 3.1: Asphalt Mixture Samples for CG Study.

Sample Source	Sample Type
CG mix design	LMLC
CG production	FMLC
CG cores	Cores

LMLC = lab-mixed, lab-compacted; FMLC = field-mixed, lab-compacted.

Table 3.2: Inventory of Materials Received.

Summer 2016 Construction			
Cell and Mixture Type	Binder Type	Loose Mix	Binder
1616 BM xxx* SPWEB 540L 1716 BM xxx* SPWEB 540L 1816 BM xxx* SPWEB 540L 1916 BM xxx* SPWEB 530L	PG 64S-22	5 Buckets	1 Quart (in two cans)
2016 BM xxx* SPWEB 540A 2116 BM xxx* SPWEB 540C 2216 BM xxx* SPWEB 540C 2316 BM xxx* SPWEB 540E	PG 52S-34 PG 58H-34 PG 58H-34 PG 64E-34	5 Buckets	1 Quart (in two cans)

xxx*= bucket ID

Table 3.3 shows the summary designs for the eight mixtures used in the MnROAD cracking group experiment and Figure 3.1 shows their gradation curves.

Table 3.3: Gradation and asphalt content of 2016 mixtures.

Cell No.	Mix Design	Binder	RAP %	RAS %	Total AC %	Virgin AC %	NCAT Mix ID	N_{des}
16	SPWEB540L	PG 64S-22	20	5	5.27	3.17	30-40% ABR with RAS	80
17	SPWEB540L	PG 64S-22	10	5	5.43	3.94	20-30% ABR with RAS	80
18	SPWEB540L	PG 64S-22	20	0	5.43	4.20	20% ABR	80
19	SPWEB530L	PG 64S-22	20	0	5.70	4.46	20% ABR 100 gyration, 3.0% Va	100
20	SPWEB540A	PG 52S-34	30	0	5.32	3.47	35% ABR with PG 52S-34	80
21	SPWEB540C	PG 58H-34	20	0	5.38	4.15	20% ABR with PG 58H-34	80
22	SPWEB540C	PG 58H-34	20	0	5.73	4.5	20% ABR with LMS	80
23	SPWEB540I	PG 64E-34	15	0	5.23	4.31	20% ABR with PG 64E-34	80

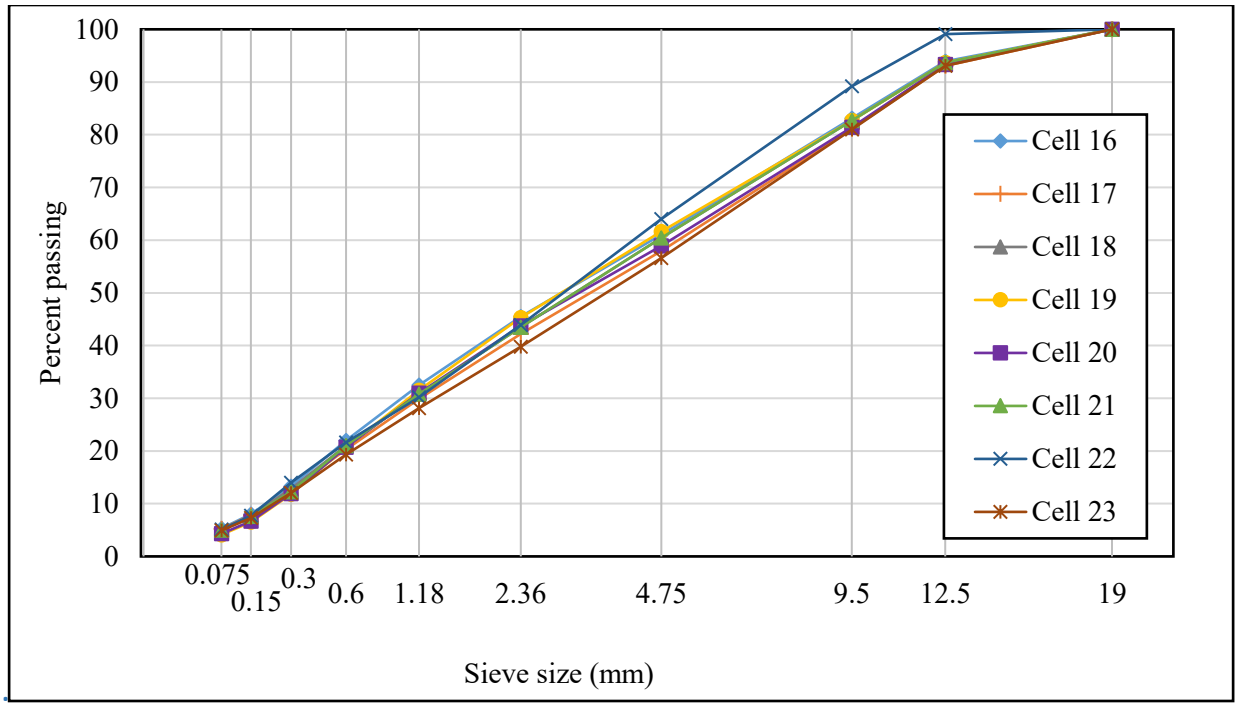

Figure 3.1: Gradation curve of the eight mixtures on the 0.45 power chart.

The gradation of all mixtures are close to the 0.45 power line and, therefore, can be classified as well graded. The total and effective asphalt content is shown in figure 3.2. Cells 19 and 22 have the highest percentage of total asphalt content, while cells 16, 20 and 22 have the lowest. Regarding the effective asphalt content, cell 19 has the highest percentage, and cells 22 and 23 have the lowest.

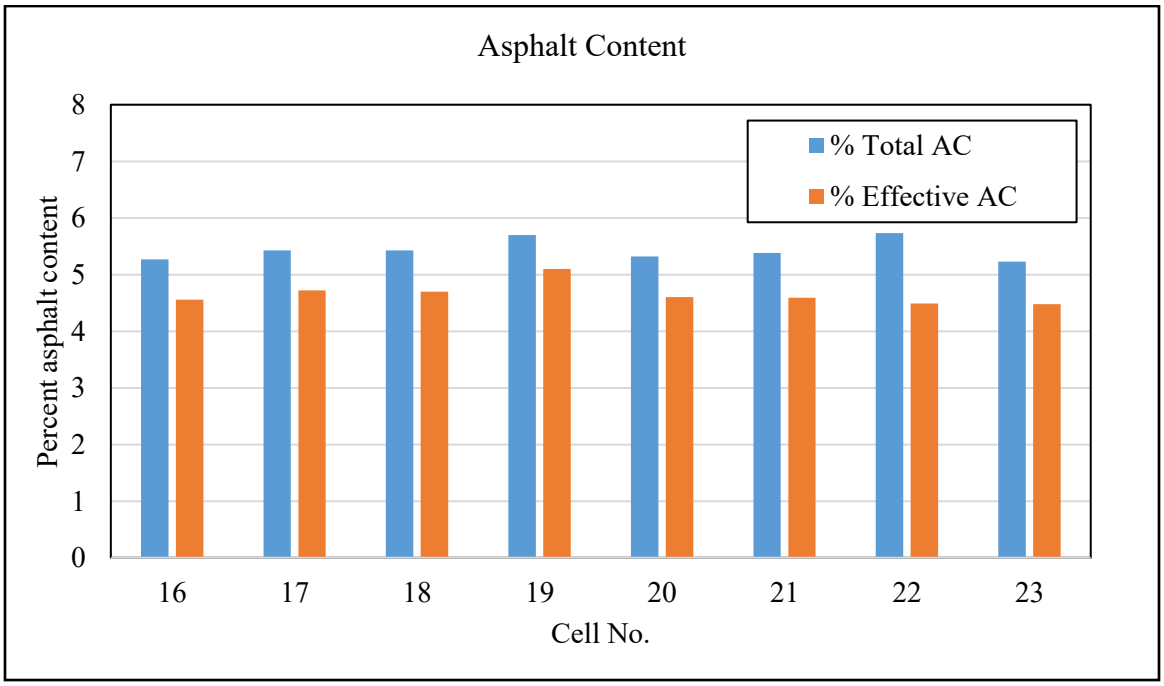

Figure 3.2: Percentage of total and effective asphalt content.

Figure 3.3 shows the percentage of Reclaimed Asphalt Pavement (RAP) and Recycled Asphalt Shingles (RAS). Cell 20 has the highest percentage of RAP and Cell 17 has the lowest. Only cells 16 and 17 received RAS. Both have the same amount. Note that none of the mixtures have 0% RAP, and therefore, there is no control mixture for the statistical analysis.

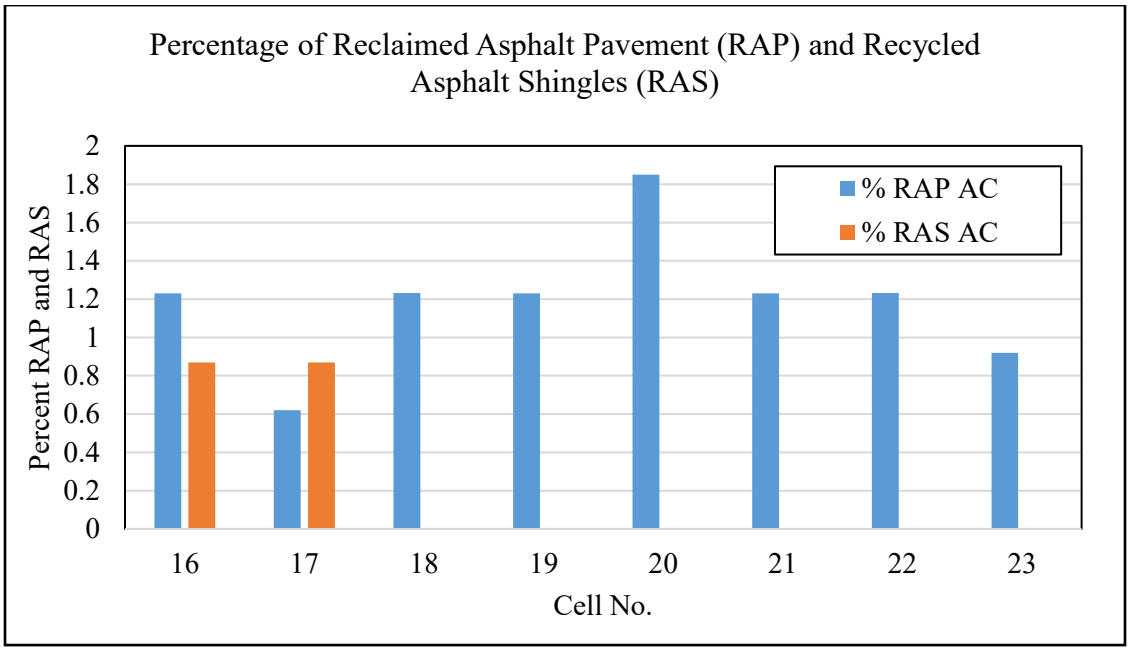

Figure 3.3: Percentage of RAP and RAS

Figure 3.4 shows the voids in the mineral aggregate (VMA) values. Cell 17 has the highest percentage of VMA and cells 22 and 23 have the lowest.

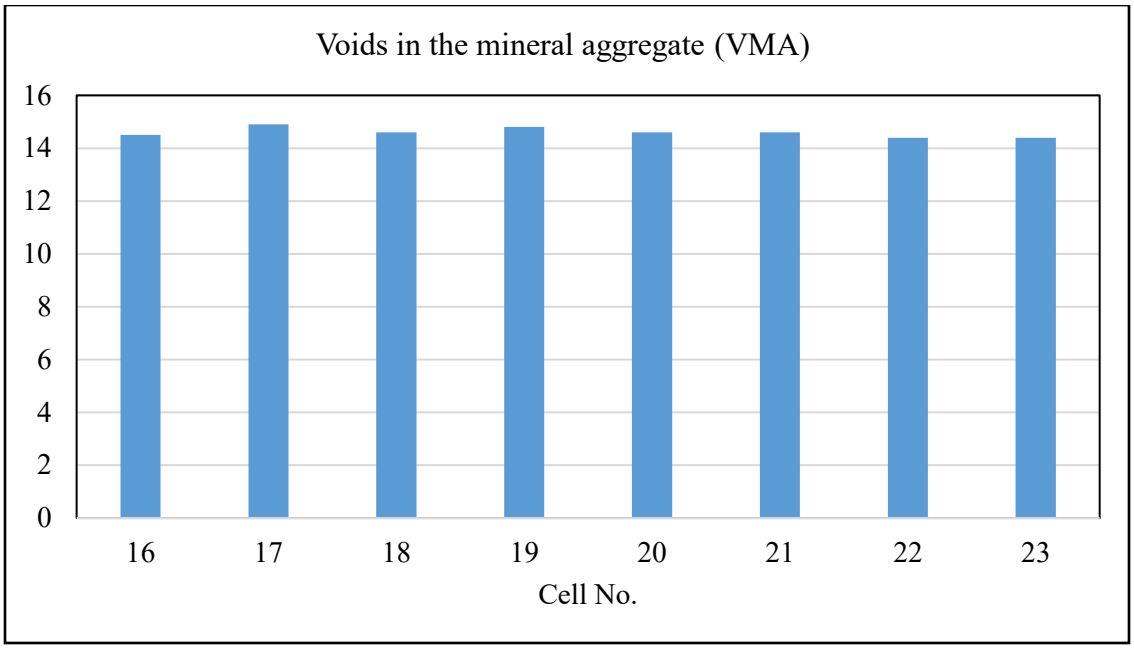

Figure 3.4: Voids in the mineral aggregate (VMA).

The adjusted values of Asphalt Film Thickness (AFT) for each of the eight cells were plotted and presented in figure 3.5 and table 3.4.

Table 3.4: Adjusted AFT for cells 16 to 23.

Cell No.	Effective Asphalt Content %	Percent Total Asphalt Cement	Percent Aggregate in Mixture/100	Adjusted AFT
16	4.56	5.27	0.9473	8.3
17	4.72	5.43	0.9457	9.4
18	4.70	5.43	0.9457	7.9
19	5.1	5.70	0.943	10.1
20	4.6	5.32	0.9468	8.7
21	4.59	5.38	0.9462	8.4
22	4.49	5.73	0.9427	8.2
23	4.48	5.23	0.9477	8.9

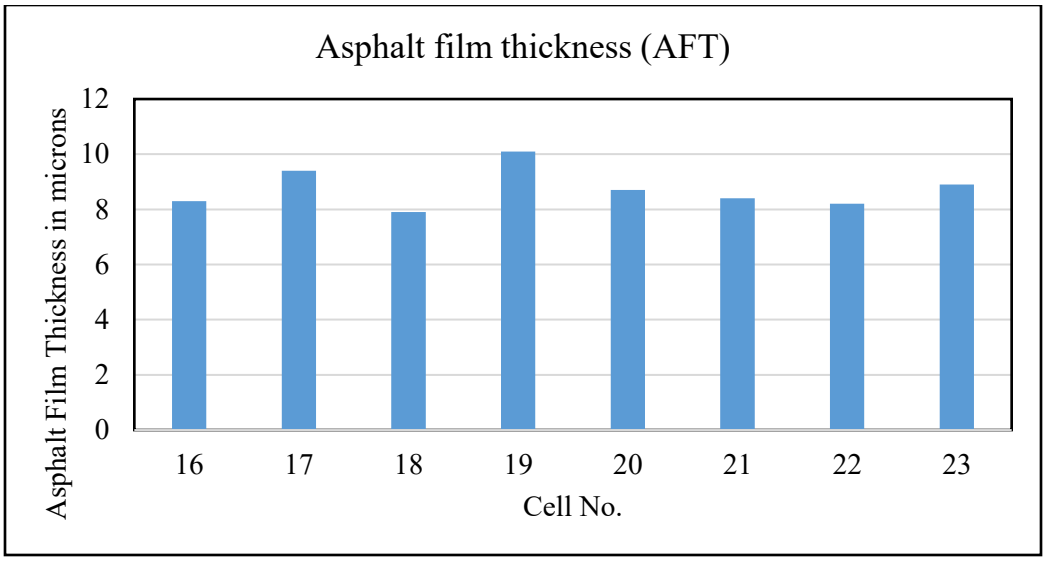

Figure 3.5: Adjusted Asphalt Film Thickness (AFT).

The mixture in cell 19 has the largest value of film thickness and cell 22 has the lowest value. Note that cell 19 also has the highest percentage of effective asphalt content and cells 22 and 23 have the lowest.

CHAPTER 4: BBR TESTING OF ASPHALT BINDERS

BBR creep and strength testing was performed on the five binders that correspond to MnROAD Cells 16-19, 20, 21, 22 and 23, constructed in 2016. The binders were short and then long-term aged using RTFO and PAV procedures, respectively. Note that binders in cells 21 and 22 are the same, except that cell 22 binder contains antistripping agent. All testing was performed using a Bending Beam Rheometer Pro at PGLT+10C and PGLT+6C and using air as cooling medium. Six replicates were tested for each type of binder at each temperature. Table 4.1 summarizes the binder test matrix.

Table 4.1: Asphalt Binder Testing Matrix.

Cell No.	Binder Type	Replicates	Temperature	Test Method	Properties Obtained
16-19	PG 64S-22	6	-12C and -18C	Creep and Strength Test	Creep Stiffness m-value Strength Strain at Failure
20	PG 52S-34	6	-24C and -30C		
21	PG 58H-34	6	-24C and -30C		
22	PG 58H-34	6	-24C and -30C		
23	PG 64E-34 (highly modified)	6	-24C and -30C		

4.1 PREVIOUS EFFORTS

In previous work, the authors have proposed a new strength testing method using a modified BBR device, called BBR-Pro. In their investigation, the authors demonstrated that, by taking into account the size effect and the cooling medium effect, the DTT and the BBR strength testing methods result in strength values that are similar (Marasteanu et al., 2012b).

By imposing constraints related to the duration of the test (1 minute for practical reasons, similar to the criterion used for establishing the strain rate for DTT), and knowing that, based on hundreds of tests performed, the failure stress does not exceed 12MPa, a loading rate of 0.65N/s was proposed for routine testing (Marasteanu et al., 2017). The tests are performed at PGLT+10ºC and at PGLT+4ºC, similar to current BBR and DTT specifications. PGLT stands for performance grade low temperature limit. The strength tests can be performed after a 240s recovery period immediately after BBR creep testing, or they can be performed as a separate test on new binder specimens. The first method is much

shorter and requires less asphalt binder, since the creep and strength tests are performed on the same beam of asphalt binder.

Unlike DTT experiments, in which the strain rate was not constant, in the BBR stress-controlled test the stress rate remains constant for the entire duration of the test. An example is shown in Figure 4.1.

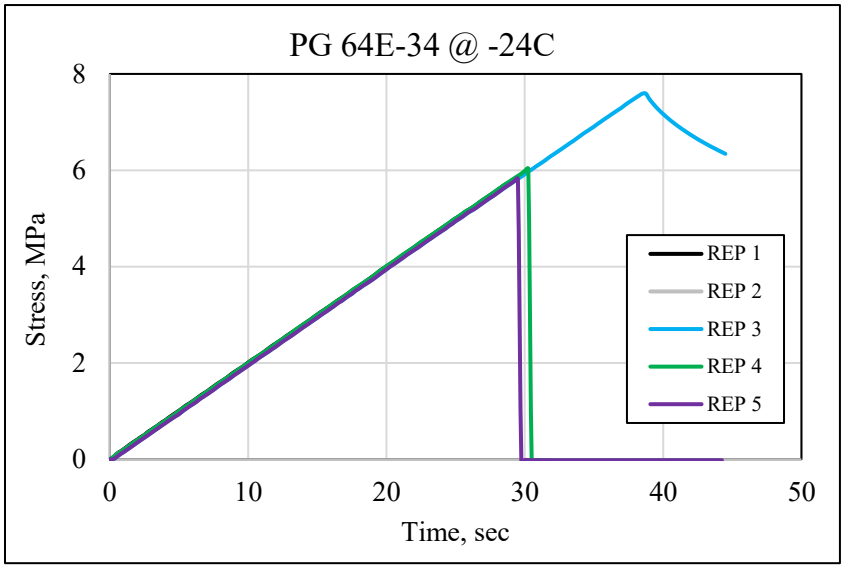

Figure 4.1: Loading rate for strength test performed at -24ºC on Cell 23 asphalt binder.

This also means that, unlike DTT experiments, in which the stress-strain data could not be related to relaxation modulus due to changes in strain rate during the test, the BBR strength data can be related to creep compliance. This is demonstrated below.

In a test in which the stress is increased linearly starting from zero, the resulting strain will reflect the superposition of a series of retarded compliances (*9*). If $\dot{\sigma} = \mathrm{d}\sigma/\mathrm{d}t$ is the rate of stress increase, then:

$$\gamma = \dot{\sigma} t J_g + \dot{\sigma} \int_0^t \int_{-\infty}^{\infty} L(1 - e^{-u/\tau}) d \ln \tau \, du + \frac{\dot{\sigma} t^2}{2\eta_o} \qquad [4.1]$$

$$\gamma = \dot{\sigma} t J_g + \dot{\sigma} \int_{-\infty}^{\infty} L\left[t - \tau\left(1 - e^{-t/\tau}\right)\right] d \ln \tau + \frac{\dot{\sigma} t^2}{2\eta_o} \qquad [4.2]$$

When the stress-strain curve under this condition is differentiated, the result is the creep compliance:

$$\frac{d\gamma}{d\sigma} = (1/\dot{\sigma}) \frac{d\gamma}{dt} = J_g + \int_{-\infty}^{\infty} L\left(1 - e^{-t/\tau}\right) d \ln \tau + t/\eta_o = J(t) \qquad [4.3]$$

Therefore, if creep compliance is known, the variation of strain with stress is known for a constant loading rate test. If this loading rate is known, then the entire stress-strain curve can be determined.

Previously, the authors used a simple approximation to predict stress-strain curve, for a given loading rate, from creep compliance. First, we assume that the BBR strength test is performed at a constant stress rate $\dot{\sigma}$. The stress at any time can be simply calculated as

$$\sigma(t) = \dot{\sigma} * t \qquad [4.4]$$

By making the assumption that the creep compliance *J(t)* obtained in the creep test follows a power law of the stress in the strength test, we obtain:

$$J(t) = a * \{\sigma(t)\}^b \qquad [4.5]$$

Coefficients *a* and *b* can be simply calculated by fitting equation 5 to the creep compliance vs. stress curve, for an assumed loading rate. The loading rate value is required to match the times for the creep compliance (obtained in the creep test) and the stress (in the strength test).

From equation 4.5, the first derivative of the strain-stress curve is the creep compliance, $J(t)$, and, therefore, we can rewrite equation 4.5 as:

$$J(t) = \mathrm{d}\varepsilon(t)/\mathrm{d}\sigma(t) = a * \{\sigma(t)\}^b \quad [4.6]$$

The strain can then be obtained as:

$$\varepsilon(t) = \frac{a*\{\sigma(t)\}^{b+1}}{b+1} + c \quad [4.7]$$

Constant *c* is zero since the plot starts in origin.

An example is presented in Figure 4.2.

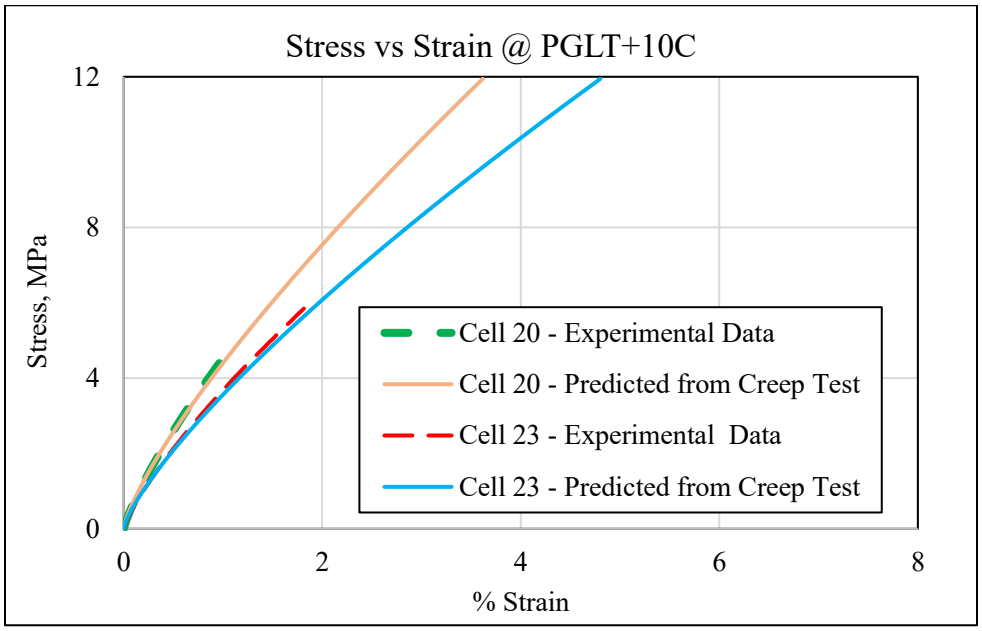

Figure 4.2: Predicted and experimentally determined stress-strain curves for two binders.

An alternative method is to use the Burgers model commonly used to analyse the linear viscoelastic behaviour of asphalt binders. The model in shown in Figure 4.3.

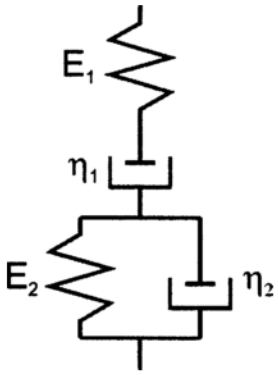

Figure 4.3: Burgers model.

The expression for creep compliance is:

$$J(t) = \frac{1}{E_1} + \frac{t}{\eta_1} + \frac{1}{E_2}\left(1 - e^{-\frac{tE_2}{\eta_2}}\right) \qquad [4.8]$$

The stress history for the creep and recovery test is written as:

$$\sigma(t) = \begin{cases} \sigma_0 H(t) \\ \sigma_0 H(t) - \sigma_0 H(t - t_0) \end{cases} \qquad [4.9]$$

Based on the linear superposition principle of viscoelasticity, the corresponding deflection can be calculated as follows:

$$\varepsilon(t) = \begin{cases} \sigma_0 J(t) & 0 < t < t_0 \\ \sigma_0 J(t) - \sigma_0 J(t - t_0) & t > t_0 \end{cases} \qquad [4.10]$$

where $H(t)$ is the Heaviside step function, t_0 is the time when creep test ends and recovery test begins.

Substituting equation 4.8 into equation 4.9, we obtain the strain history for creep and recovery.

When $0 < t < t_0$

$$\varepsilon(t) = \sigma_0\left(\frac{1}{E_1} + \frac{t}{\eta_1} + \frac{1}{E_2}\left(1 - e^{-\frac{tE_2}{\eta_2}}\right)\right) \qquad [4.11]$$

When $t > t_0$

$$\varepsilon(t) = \sigma_0\left(\frac{t_0}{\eta_1} + \frac{1}{E_2} e^{-\frac{tE_2}{\eta_2}}\left(e^{\frac{t_0 E_2}{\eta_2}} - 1\right)\right) \qquad [4.12]$$

The loading expression for the strength test is

$$\sigma(t) = \alpha t \qquad [4.13]$$

where α is the loading rate.

Based on linear viscoelasticity, strain history can be calculated as the following convolution:

$$\varepsilon(t) = \int_{-\infty}^{t} J(t - \xi)\, \dot{\sigma}(\xi) d\xi \qquad [4.14]$$

Substituting equaion 4.13 into equation 4.14 and changing the integration variable to $\zeta = t - \xi$, we obtain

$$\varepsilon(t) = \alpha \int_0^{\infty} J(\zeta) d\zeta \qquad [4.15]$$

Substituting equation 4.8 into equation 4.15 and integrating, we obtain

$$\varepsilon(t) = \alpha \left(\frac{t}{E_1} + \frac{t^2}{2\eta_1} + \frac{1}{E_2} \left(t - \frac{\eta_2}{E_2} (1 - e^{-\frac{tE_2}{\eta_2}}) \right) \right) \qquad [4.16]$$

Equations 4.11, 4.12, and 14.6 represent the expressions for creep, recovery and strength tests respectively. These three equations can be used to predict stress-strain curves from creep and recovery experimental data.

An example is shown below for the binders used in Cells 20 and 21 at MnROAD. First, equations 4.11 and 4.12 are used to fit the creep and recovery experimental data. As shown in Figure 4.4, the model fits very well with the experimental data.

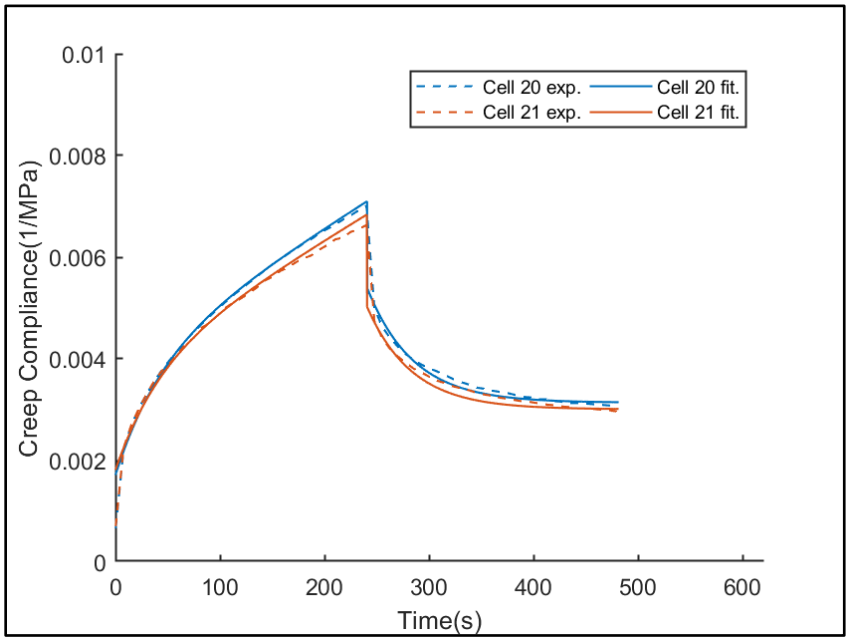

Figure 4.4: Using Burgers model to fit creep and recovery experimental data.

The strain history for strength test can be predicted using equation 4.16. As seen in Figure 4.5, the prediction matches very well the experimental data, which indicates that the experimental strength data is obtained under linear viscoelastic condition in a constant stress test.

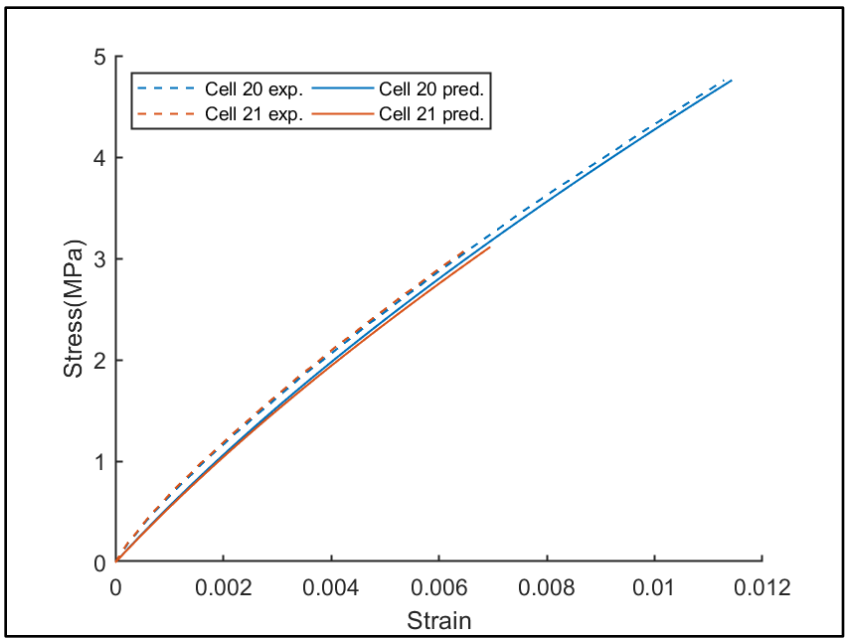

Figure 4.5: Prediction of strength test using Burgers model.

4.2 TESTING OF MNROAD ASPHALT BINDERS

The procedure previously described was used to test the binders used in MnROAD cells 16-19, 20, 21, 22, 23 constructed in summer of 2016. The first binder was a PG -22 and the remaining four binders were PG -34. The binder used in cell 23 was highly modified. The binders in cell 21 and 22 were the same, except that the binder in cell 22 contained an antistrip agent.

Tables 4.2 and 4.3 show the creep and strength test results, representing the average of six replicates. Figures 4.6 to 4.9 show plots of the creep stiffness at 60 sec, m-value at 60 sec, strength and strain at failure. All binders pass the stiffness criterion of being below 300 MPa at PGLT+10C, as well as having a minimum m-value of 0.300. The strength results, however, show clear differences between the binders: Cell 16 and 23 binders have similar stiffness values; however, Cell 16 binder has the lowest strength, whereas Cell 23 binder has the highest strength. The difference in creep and strength properties of the binders can also be seen in Figures 4.10 and 4.11. A less obvious difference is observed for cell 20 and 21 binders that have almost the same creep stiffness and m-value. However, stress-strain curves indicate that cell 21 binder may perform better than cell 20 binder.

Table 4.2: Creep Stiffness and m-value of Asphalt Binder.

Cell No.	Binder	Creep Stiffness, S(60) MPa				m-value, m(60)			
		PGLT + 10C		PGLT + 4C		PGLT + 10C		PGLT + 4C	
		Avg.	CV	Avg.	CV	Avg.	CV	Avg.	CV
16	PG 64S-22	172	4%	433	10%	0.372	2%	0.298	7%
20	PG 52S-34	252	10%	495	14%	0.338	2%	0.266	6%
21	PG 58H-34	241	9%	435	7%	0.328	1%	0.266	6%
22	PG 58H-34	221	9%	432	5%	0.335	5%	0.271	4%
23	PG 64E-34	190	4%	407	10%	0.344	4%	0.290	6%

Table 4.3: Strength and Strain at Failure of Asphalt Binder.

Cell No.	Binder	Strength MPa				Strain at Failure %			
		PGLT + 10C		PGLT + 4C		PGLT + 10C		PGLT + 4C	
		Avg.	CV	Avg.	CV	Avg.	CV	Avg.	CV
16	PG 64S-22	4.30	18%	3.69	17%	1.47	22%	0.54	23%
20	PG 52S-34	5.23	22%	3.92	25%	1.23	30%	0.51	29%
21	PG 58H-34	5.96	32%	5.68	22%	1.56	43%	0.81	27%
22	PG 58H-34	5.01	13%	6.03	23%	1.33	14%	0.92	24%
23	PG 64E-34	6.79	12%	5.53	10%	2.20	15%	0.91	14%

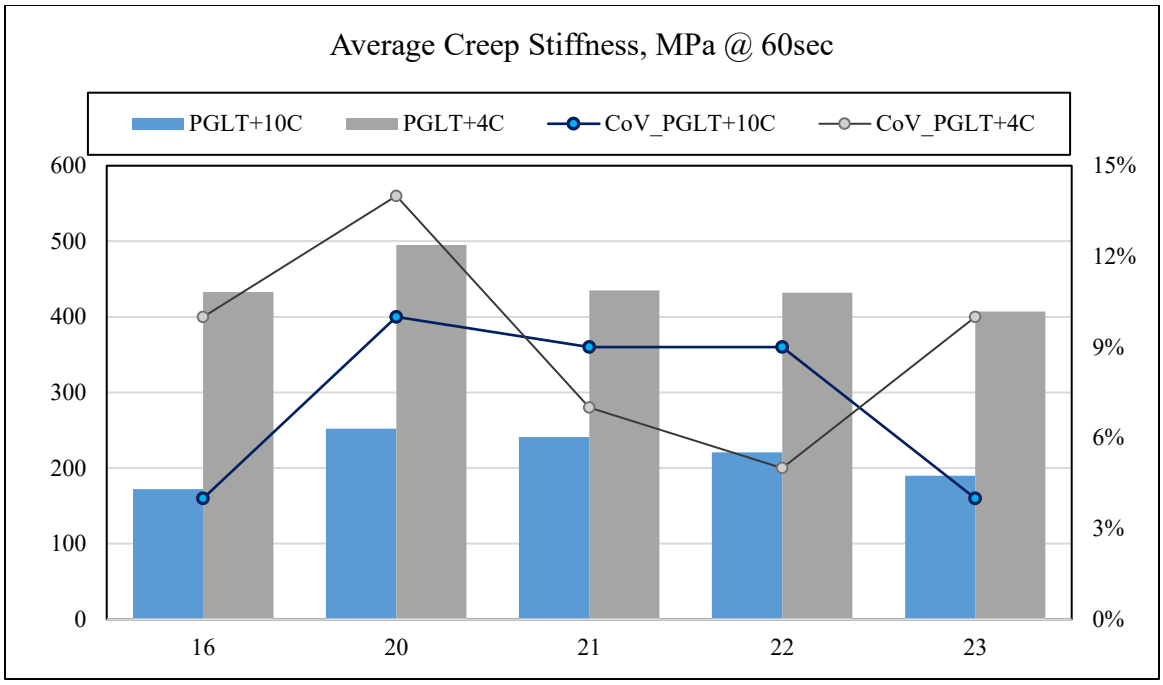

Figure 4.6: Creep Stiffness at 60 sec for binders from Cell 16, 20-23.

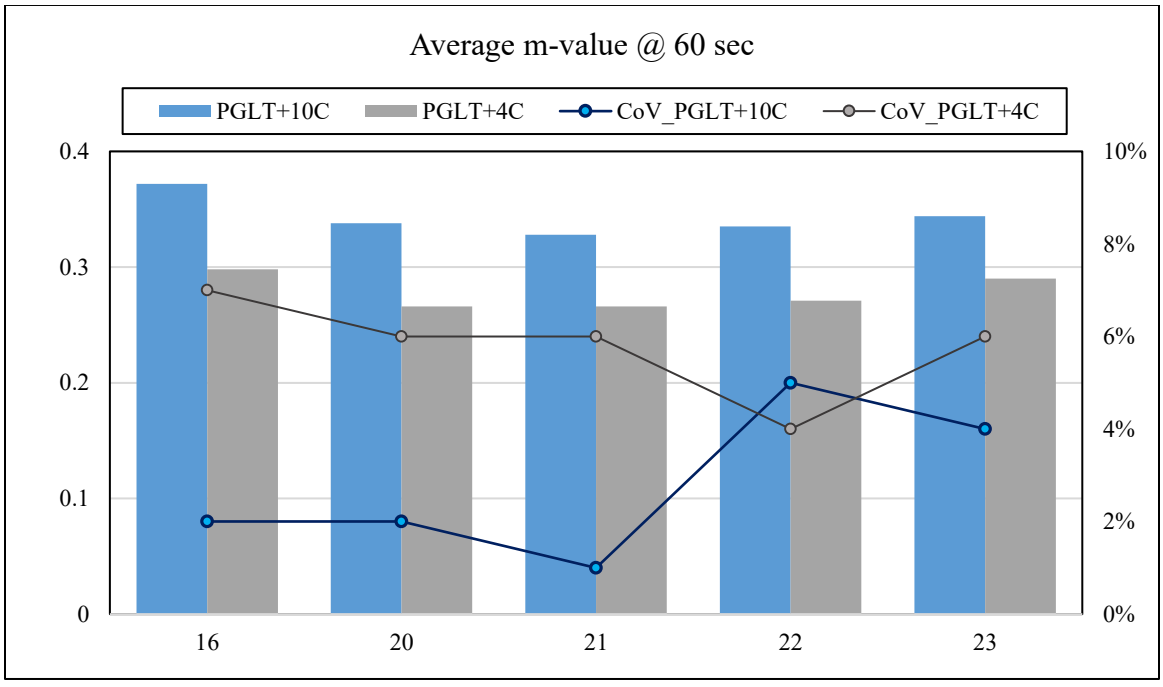

Figure 4.7: m-value at 60 sec for binders from Cell 16, 20-23.

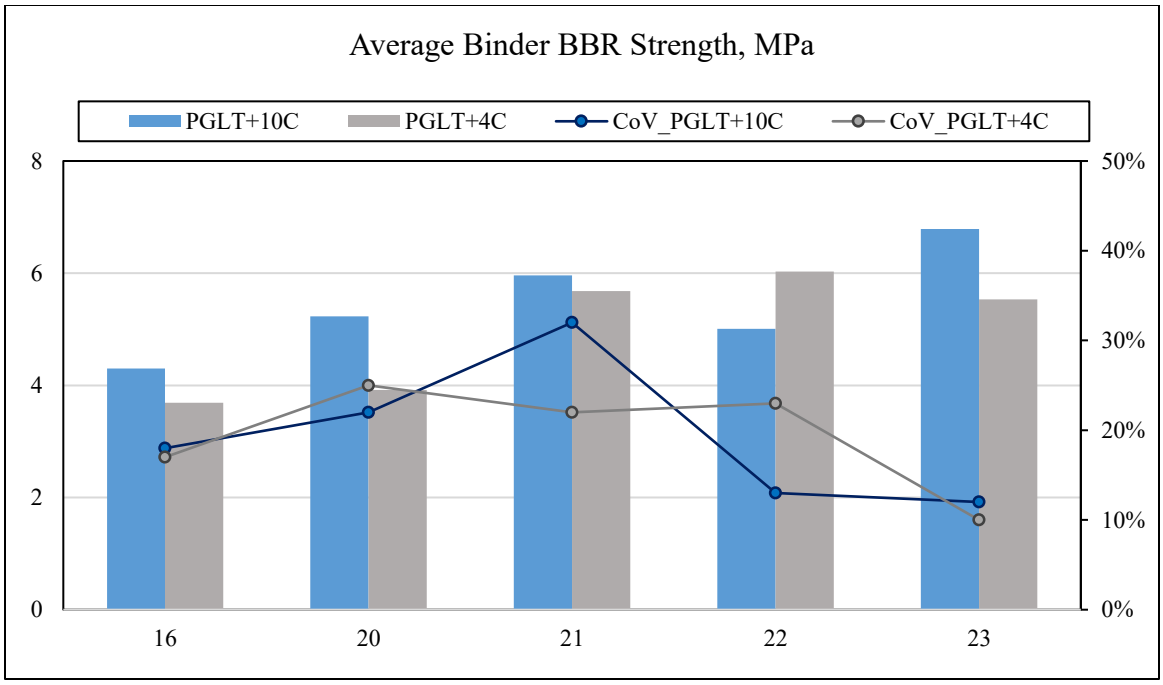

Figure 4.8: BBR Strength of Binders from Cell 16, 20-23.

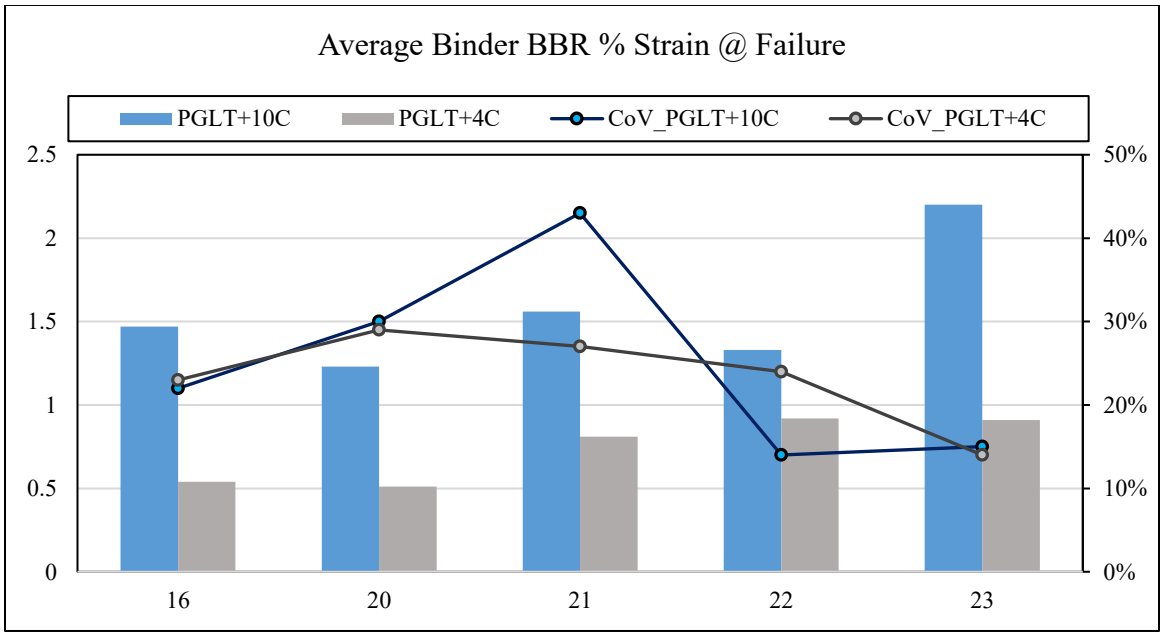

Figure 4.9: Strain at Failure of Binders from Cell 16, 20-23.

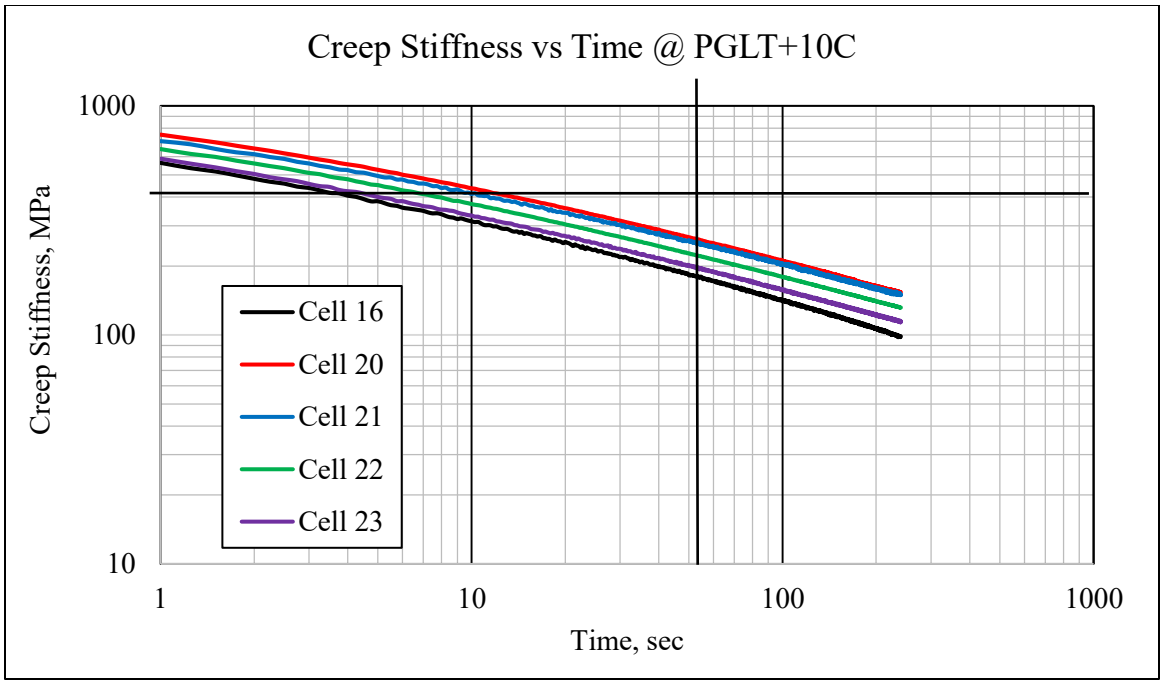

Figure 4.10: Creep Stiffness vs Time of Binders from Cell 16-23 at PGLT+10C.

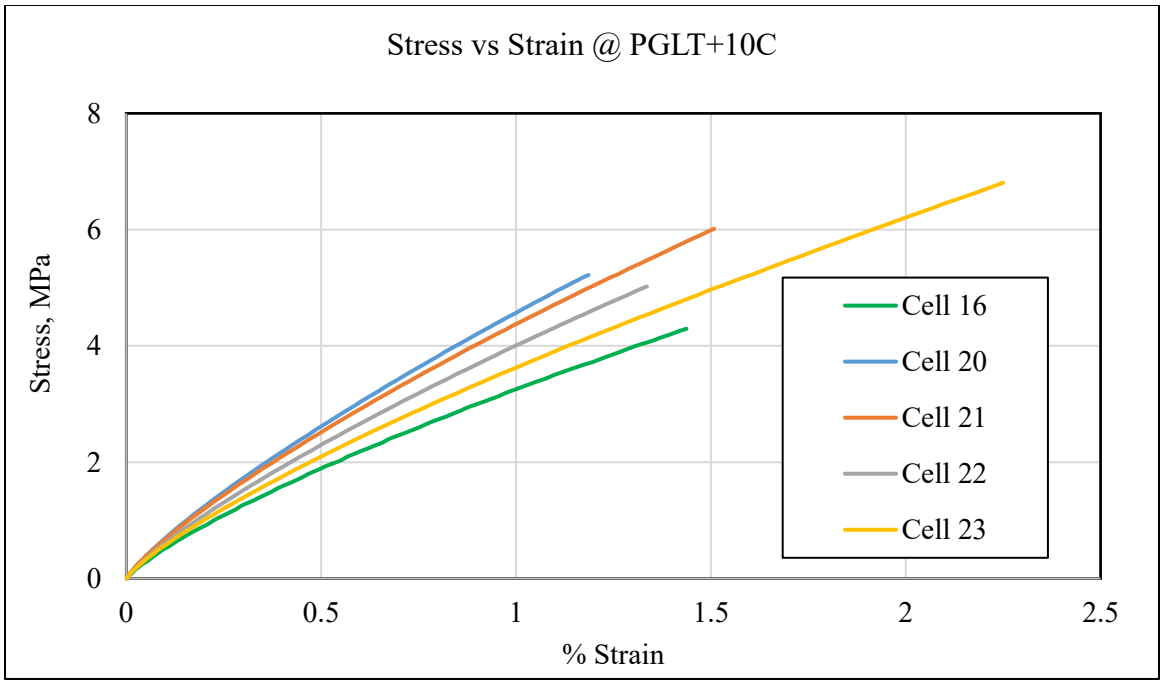

Figure 4.11: Stress-Strain Curve of Binders from Cell 16-23 @ PGLT+10C.

CHAPTER 5: BBR TESTING OF ASPHALT MIXTURES

In this chapter, the experimental work performed to obtain the creep stiffness and strength of the asphalt mixtures used in the reconstruction of cells 16 to 23 that took place in fall 2016 is presented.

5.1 SPECIMEN PREPARATION

Loose mix from the eight cells were used to prepare gyratory specimens. To keep the heating time as uniform as possible during specimen preparation, the process started by heating the bucket in the oven at 140°C for five hours. Then, 7000 grams of loose mix were stored in a covered pan and kept for another hour in the oven to better control the material temperature. Finally, the mixture was poured into the gyratory compactor mold and compacted. Six cylinders were compacted for each mixture. All cylinders were compacted at N_{des} number of gyrations, which resulted in air voids values within 1% of the reported mix design values. The cylinders were then cut to prepare testing specimens, as shown in Table 5.1.

Table 5.1: Testing Matrix for Asphalt Mixtures.

Test	Number of specimens	Testing Temperatures and Number of Replicates
BBR Mixture	18 beams	(-24°C creep, recovery, strength) x 6 (-12°C creep, recovery, strength) x 6 (0°C creep, recovery, strength) x 6
E* IDT geometry	2 slices	(-12°C, 12°C and 36°C) x 2
SCB	6 semicircular slices	(-12°C) x 3 (-24°C) x 3
Creep and strength IDT	6 slices	(-24°C creep, -24°C strength) x 3 (-12°C creep, -12°C strength) x 3

For BBR testing, the specimen preparation method includes several cutting steps, starting with a gyratory compacted (GC) cylinder, and ending with the actual BBR beams. Each layer was cut into ten

beams with the dimensions of approximately l =125.0mm, b=12.5mm, h=6.25mm. After the preparation, the beams were kept on a flat surface to avoid any deflections.

5.2 TESTING PROCEDURE

Each mixture beam was tested under a combined procedure that included an initial BBR creep test (AASHTO TP125-16), followed by a recovery period and a strength test that is described elsewhere (NCHRP Idea 151, 2012) without removing the beam from the testing frame. The creep test had a duration of 500 seconds selected to ensure that the individual temperature results overlap when shifted to create master curves. Creep tests followed by recovery and strength tests were performed at three temperatures for each cell: 0°C, -12°C and -24°C. Six replicates were tested: the two lowest values were discarded and the average was calculated using 4 specimens.

The creep loading was chosen to be 2N, 4N and 6N for testing at 0°C, -12°C and -24°C, respectively, to be able to measure the small deflection values obtained in mixture testing. The creep test was followed by a recovery of 500 seconds, using a very small seating load that allowed measuring the recovery deflection. At the end of the recovery period, a strength test was performed using a constant loading rate that was selected such that a load of 44N was obtained in 60 sec. The test ended when the beam broke. A summary of the BBR creep results at 60s of loading time is shown in Figures 5.1 and 5.2. The results are also presented in Table 5.2.

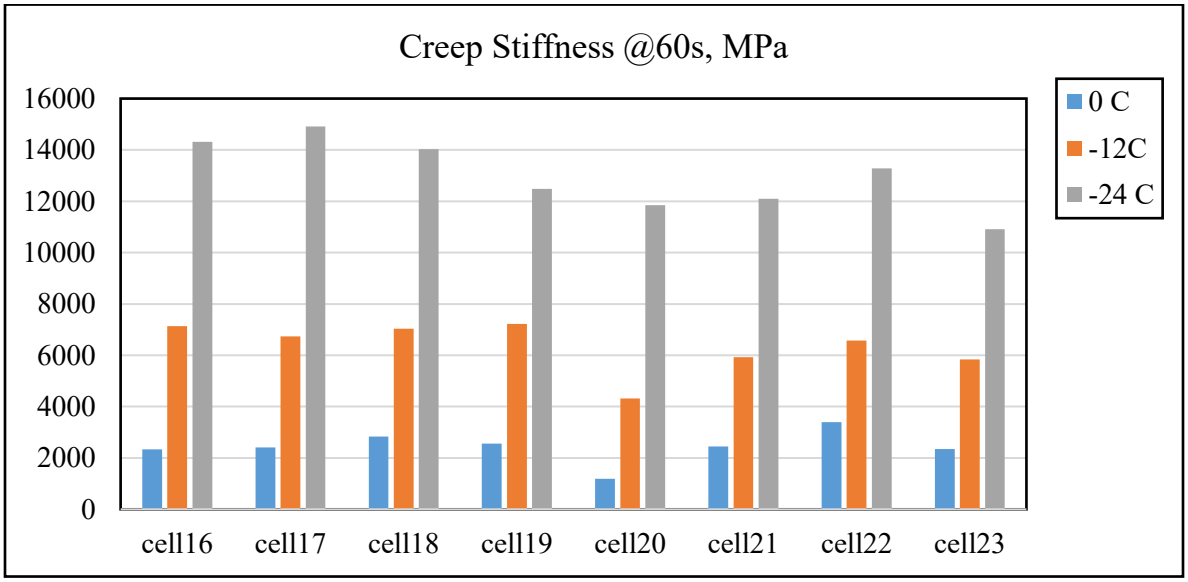

Figure 5.1: BBR Mixture Creep Stiffness at 60 seconds.

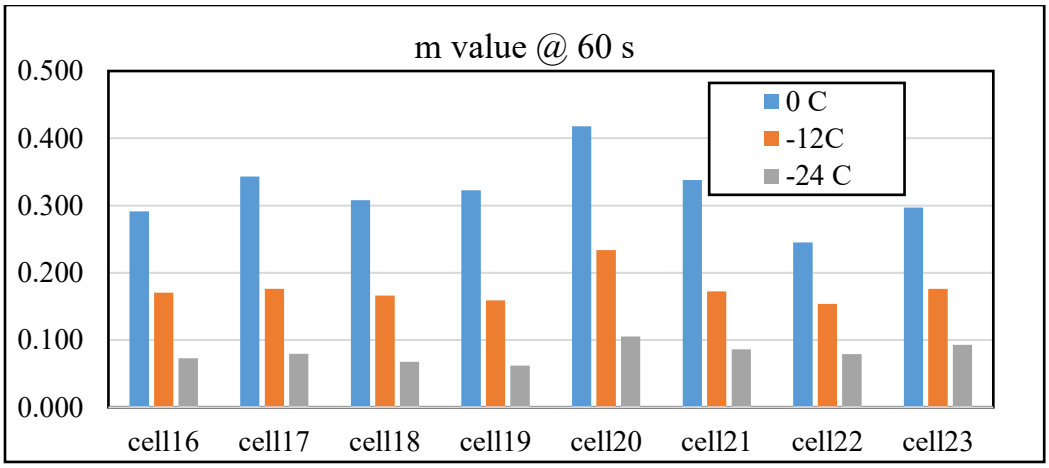

Figure 5.2: BBR m-values at 60 seconds.

Table 5.2: BBR Creep Stiffness and m-value Results.

Cell Number	Temperature °C	S(60s) MPa	CV %	m(60s)	CV %	Max. Defl., mm	CV %
16	0	2330	15	0.291	17	0.120	3
	-12	7131	5	0.170	4	0.059	10
	-24	14311	9	0.073	12	0.033	8
17	0	2412	12	0.343	6	0.129	14
	-12	6737	8	0.176	7	0.065	11
	-24	14916	7	0.080	6	0.034	7
18	0	2831	17	0.308	7	0.108	7
	-12	7039	13	0.166	11	0.060	11
	-24	14028	10	0.068	6	0.033	5

19	0	2559	12	0.323	4	0.089	16
	-12	7224	7	0.159	2	0.053	13
	-24	12486	11	0.062	21	0.033	8
20	0	1190	10	0.418	6	0.268	10
	-12	4318	9	0.234	17	0.103	11
	-24	11849	18	0.105	7	0.045	10
21	0	2448	22	0.338	2	0.152	20
	-12	5922	11	0.172	11	0.087	5
	-24	12100	6	0.086	13	0.053	2
22	0	3398	4	0.245	6	0.084	4
	-12	6573	4	0.154	6	0.075	4
	-24	13282	4	0.079	11	0.039	6
23	0	2349	8	0.297	7	0.130	11
	-12	5843	5	0.176	5	0.087	7
	-24	10917	8	0.093	6	0.056	10

Cells 16, 17, 18 and 19 have similar creep stiffness values, since they share the same PG binder, 64S-22. Cell 20, constructed with the PG 52S-34 binder, has the lowest creep stiffness at all three temperatures. Cell 23, constructed with the PG 64E-34 binder, has the lowest creep stiffness variation with temperatures. Cells 21 and 22, although they share the same binder, have different results because the aggregates are different, granite and limestone, respectively. Similar trends are seen for m-value. Cells 16 to 19 have values that are not very different. Cell 20 mixture with PG 52S-34 binder has the highest

m-values for all temperatures, and cell 23 mixture has the lowest m-value variation with temperature. Cell 22, the limestone asphalt mixture, has lower m-values than Cell 21 with granite.

BBR strength and failure strain results are shown in Figures 5.3 and 5.4 and table 5.3. For cells 16 to 18 and 23, the strength at failure decreases with decrease in temperature. For the other mixtures, the trend is not that clear. For all mixtures, strain at failure decreases with decrease in temperature. Cell 20 has the highest strain at failure at all temperatures.

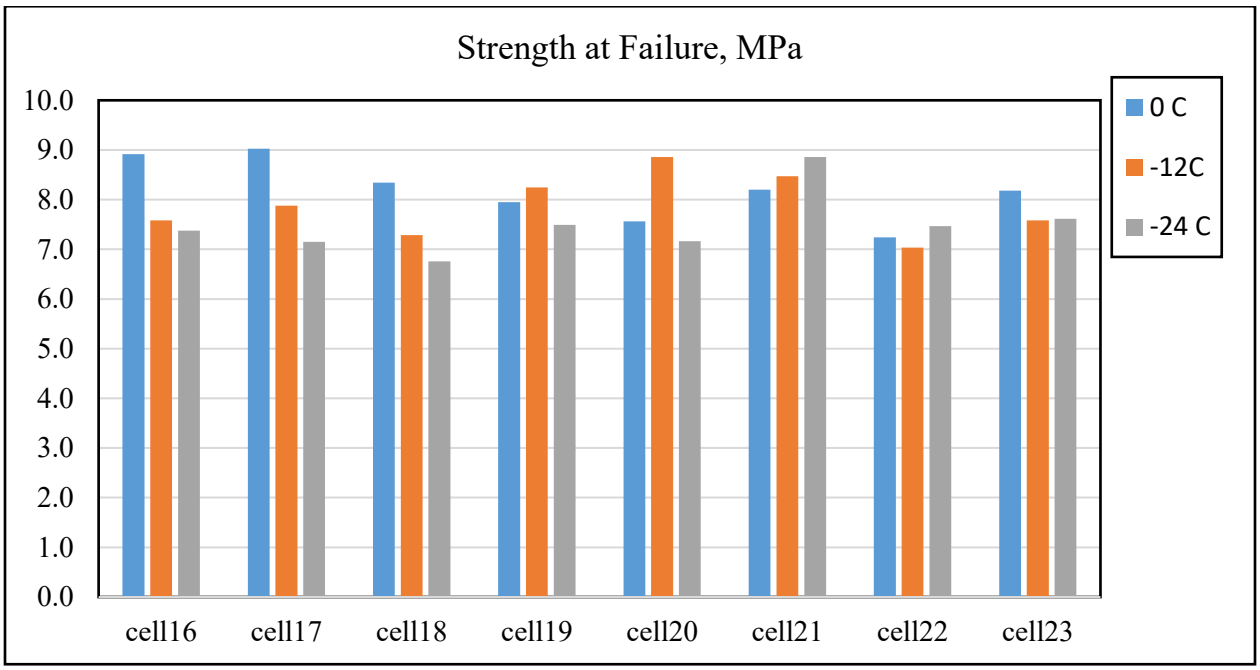

Figure 5.3: BBR Mixture Strength.

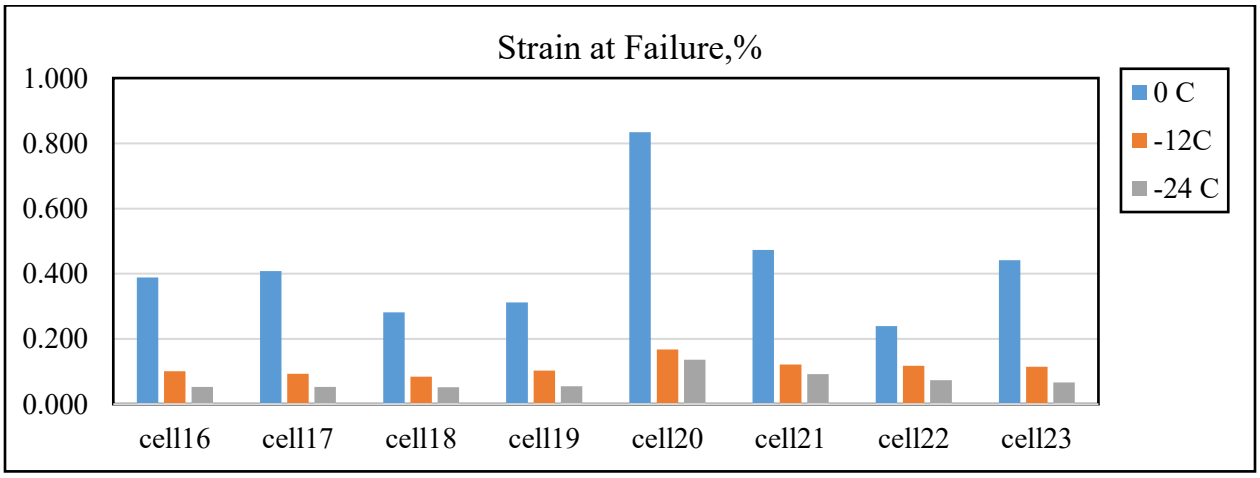

Figure 5.4: BBR Mixture Strain at Failure.

Table 5.3: BBR Strength Results.

Cell	Temperature °C	Stress @ Failure, MPa	CV %	Strain @ Failure, %	CV %	Load @ Failure, N	CV %
16	0	8.917	5	0.389	9	33.214	7
	-12	7.582	3	0.101	20	29.283	6
	-24	7.374	13	0.052	14	29.153	11
17	0	9.025	10	0.408	27	33.675	8
	-12	7.876	11	0.093	15	29.925	9
	-24	7.149	8	0.053	22	27.718	7
18	0	8.345	11	0.281	20	32.339	10
	-12	7.283	10	0.085	8	28.657	10
	-24	6.755	9	0.051	22	27.145	10
19	0	7.951	11	0.312	25	36.347	16
	-12	8.248	15	0.103	16	34.453	18
	-24	7.490	10	0.055	8	32.557	6
20	0	7.565	11	0.834	29	31.651	11
	-12	8.857	9	0.168	8	36.332	10
	-24	7.164	8	0.136	18	28.853	14

21	0	8.202	15	0.473	25	27.923	17
	-12	8.469	4	0.122	9	28.836	9
	-24	8.858	11	0.092	24	29.592	13
22	0	7.241	11	0.239	19	24.958	11
	-12	7.036	6	0.118	18	23.670	6
	-24	7.465	4	0.073	8	29.187	6
23	0	8.184	17	0.422	26	29.329	18
	-12	7.581	9	0.114	7	26.754	11
	-24	7.615	6	0.067	7	26.926	10

Examples of test result over the entire duration of the testing procedures are presented in the following four figures. Figure 5.5 and Figure 5.6 presents creep results for Cell 17 at 0°C and Figure 5.7 and Figure 5.8 present the strength results for Cell 17 and 23.

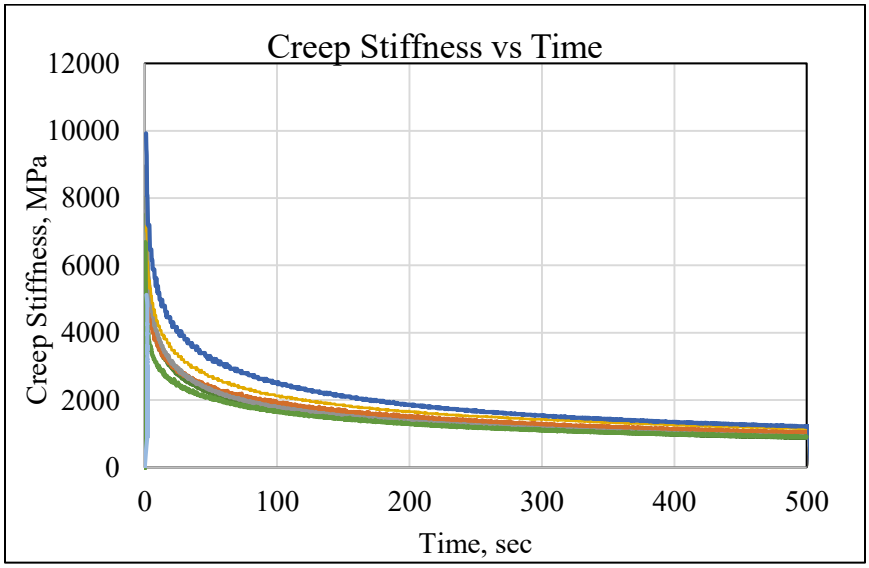

Figure 5.5: Creep Stiffness for Cell 17 at 0°C.

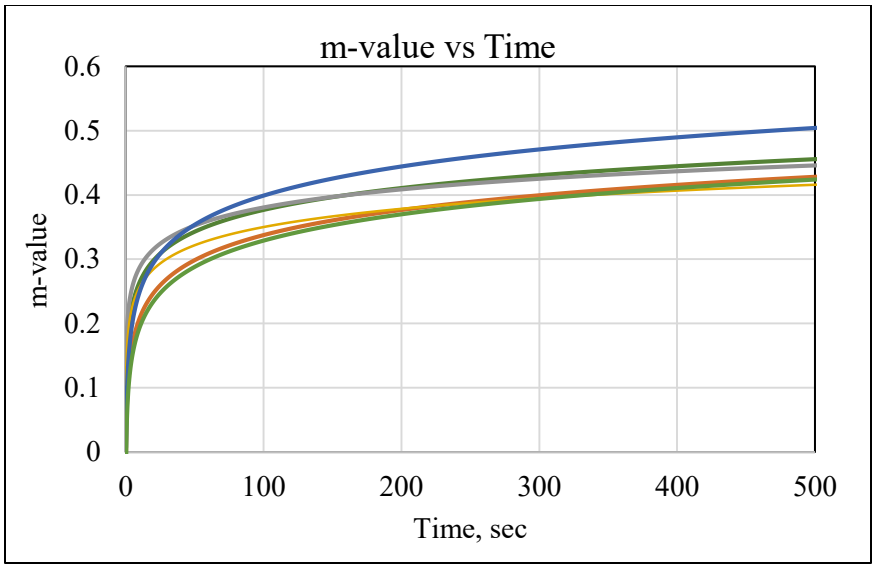

Figure 5.6: m-value for Cell 17 at 0°C.

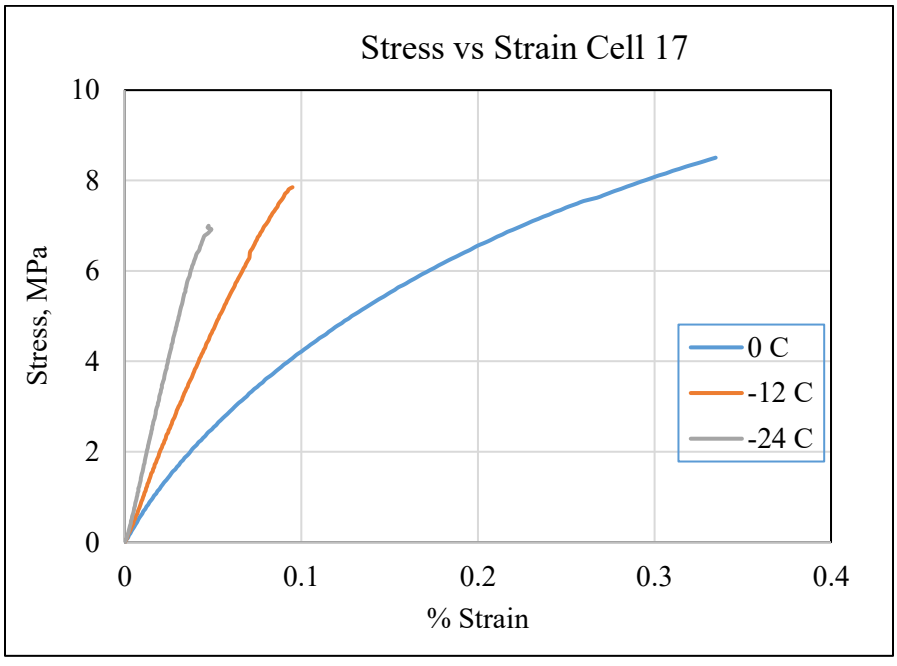

Figure 5.7: Stress Strain curve for Cell 17.

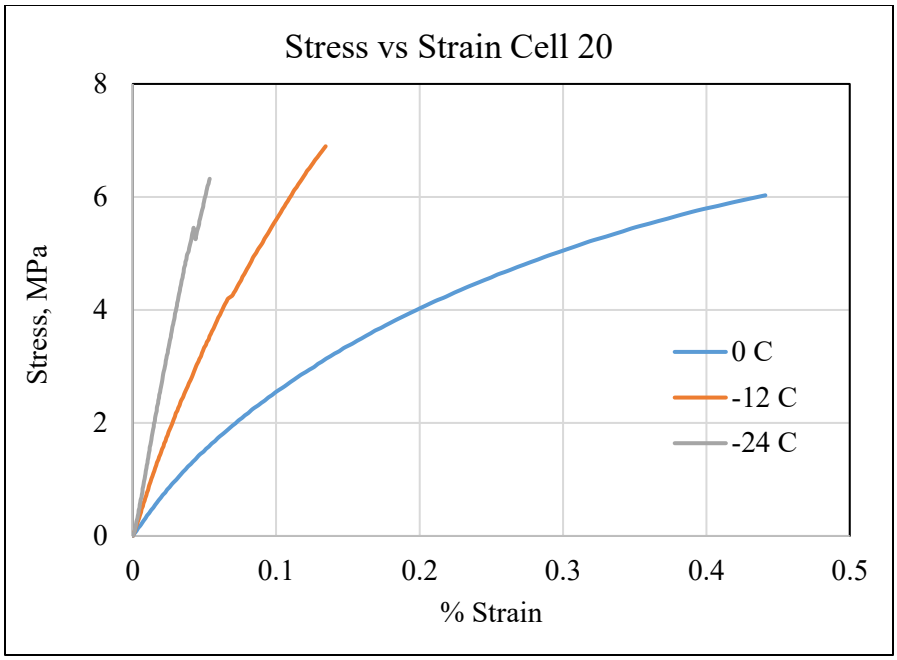

Figure 5.8: Stress Strain curve for Cell 20.

5.3 GUIDELINES FOR LIMITING CREEP AND STRENGTH CRITERIA FOR ASPHALT MIXTURES

A number of approaches are proposed to develop asphalt mixtures selection criteria based on creep and strength results at low temperature.

5.3.1 Limiting criteria for BBR creep stiffness of asphalt mixtures

This approach was previously developed by the authors as part of a previous pooled fund study (Marasteanu et al., 2012). A summary is presented below.

The development of the SHRP asphalt binder criterion for low temperature cracking was based on the assumption that the 2-hour mixture stiffness correlated well with the severity of thermal cracking in the field (Readshaw, 1972). This assumption was extended to asphalt binder stiffness obtained in low-temperature creep tests. N. W. McLeod (Burgess et al., 1971) tentatively concluded that the critical low temperature pavement modulus of stiffness, at which transverse pavement cracking is likely to occur is 1,000,000 psi or 7GPa. A value twice as high was proposed by Readshaw.

As previously shown by the authors (Cannone Falcheto et al., 2011), mixture creep stiffness can be predicted using binder creep stiffness data. One interesting application is to predict the creep stiffness value of the mixture corresponding to a creep stiffness value of 300MPa for the binder, which represents the current PG specification limit. The challenge is to match the aging condition of the two materials. Since it is generally accepted that binder RTFOT matches the aging condition of the mixture after short-term aging (or loose mix sampled behind the paver), it was decided to first determine the corresponding creep stiffness limit for binders in RTFOT condition and then use Hirsch model to predict mixture creep stiffness. Asphalt binders tested in the first phase of the low temperature pooled fund

study (Marasteanu et al., 2007) were used because BBR data was obtained for both PAV and RTFOT conditions.

The BBR binder PAV data was used to calculate the critical temperature at which S(60s) is equal to 300MPa. This was done by assuming a linear relation between log S(60s) and test temperature and interpolating to obtain the critical temperature, as shown in Figure 5.9 (left side). Based on the same linearity variation of RTFOT log S(60s) and temperature, a corresponding stiffness value at the critical temperature is obtained, as seen in Figure 5.9 (right side).

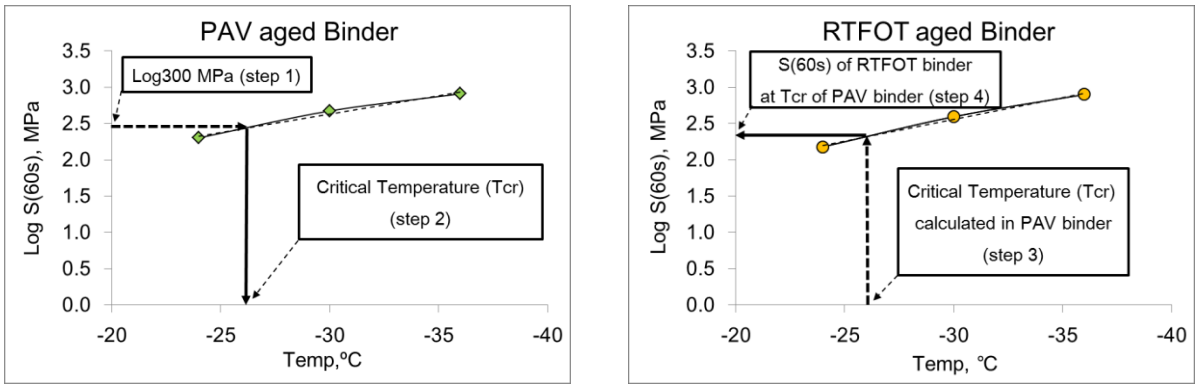

Figure 5.9: Predicting RTFOT Binder S(60s) at PAV Binder Critical Temperature, TCR.

Next, the creep stiffness of asphalt mixture was predicted from RTFOT binder creep stiffness by means of Hirsch model. Table 5.4 summarizes the results. It can be observed that the values range from 9.5GPa to approximately 12.2GPa.

Table 5.4: Predicted Mixture S(60) at PAV Binder Critical Temperature.

Mix ID	$S(60s)T_{cr}$ [MPa]	Mix ID	$S(60s)T_{cr}$ [MPa]
B: G	10864	B: L	10873
C: G	12146	C: L	12156
D: G	11310	D: L	11319
E: G	10644	E: L	10654
F: G	10814	F: L	10823
G: G	12204	G: L	12214
H: G	11647	H: L	11657
I: G	11854	I: L	11864
J: G	9521	J: L	9530

*: G: Granite, L: Limestone

By using this approach and the values for creep stiffness at -24°C from Figure 5.1, it appears that mixtures 16, 17, 18, and 22 exceed these limits and may be more prone to cracking at -24°C.

5.3.2 Limiting cracking temperature from BBR creep and strength of asphalt mixtures

The creep compliance results can be used to calculate thermal stresses and determine critical cracking temperatures using the intersection point with the BBR strength master curve. A lower critical temperature is an indication of better thermal cracking performance. A summary of the method used is given below.

Thermal stress that develops as the temperature drops in a restrained uniaxial viscoelastic beam can be calculated using Equation 5.1:

$$\sigma(t) = \int_{-\infty}^{t} \dot{\varepsilon}(t') \cdot E(t-t')dt' \qquad [5.1]$$

Where:

$\sigma(t)$ = time dependent stress

$$\dot{\varepsilon}(t') = \frac{d\varepsilon(t')}{dt'}$$

$E(t-t')$ = relaxation modulus

Taking into consideration that the strain is expresses as:

$$\varepsilon = \alpha \cdot \Delta T \qquad [5.2]$$

where

α = coefficient of thermal expansion or contraction;

ΔT = temperature change

and that the reduced time (ζ) expressed as:

$$\xi = \frac{t}{a_T} \qquad [5.3]$$

Where:

t = time, sec;

a_T = shift factor

then equation [1] can be written as:

$$\sigma(\xi) = \int_{-\infty}^{\xi} \frac{d\varepsilon(\xi')}{d\xi'} \cdot E(\xi-\xi')d\xi' = \int_{-\infty}^{t} \frac{d(\alpha\Delta T)}{dt'} \cdot E(\xi(t)-\xi'(t))dt' \qquad [5.4]$$

Where:

$E(\xi - \xi')$ = relaxation modulus;

$\varepsilon(\xi')$ = strain

To calculate thermal stress, the following procedure is used:

1. Creep compliance is obtained from BB experiments, as previously described.
2. Relaxation modulus E(t) is calculated from BBR creep compliance using Hopkins and Hamming numerical algorithm (1957).
3. Relaxation modulus E(t) master curve is obtained using CAM model (Marasteanu and Anderson, 1999):

$$E(t) = E_g \cdot \left[1 + \left(\frac{t}{t_c}\right)^v\right]^{-w/v} \quad [5.5]$$

Where:

E_g = Glassy modulus;

T_c, v and w = parameters in the model

The shift factor expression is:

$$a_T = 10^{C_1 + C_2 \cdot T} \quad [5.6]$$

Where:

C_1 and C_2 = parameters;

T = reference temperature, ^oC

4. The one-dimensional hereditary integral equation (Equation [5.4]) is solved numerically using Gaussian quadrature with 24 Gauss points.
5. The BBR strength at all three temperatures is plotted and the intersection of the strength vs. temperature curve and thermal stress curve gives the critical cracking temperature.

Example are shown in figures 5.10 and 5.11. A summary of critical temperatures obtained using a coefficient of thermal contraction al = $5*10^{-5}$ (Marasteanu et al., 2012) and an assumed cooling rate of 10ºC per hour is presented in Table 5.5.

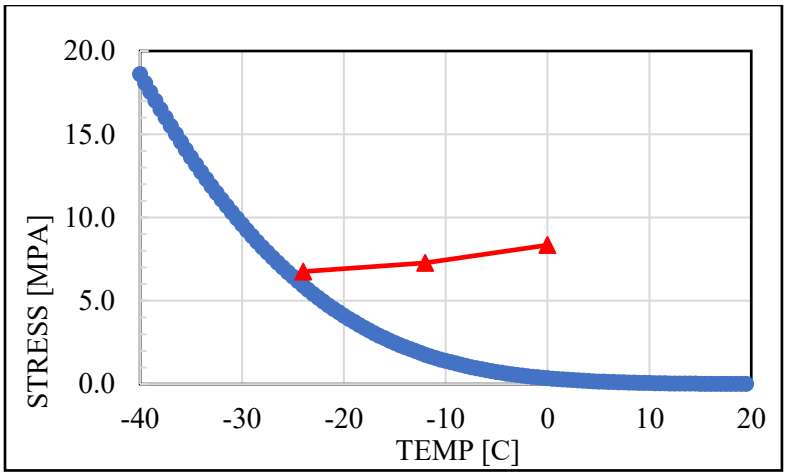

Figure 5.10: Cell 18 thermal stress and strength obtained from BBR creep and strength tests.

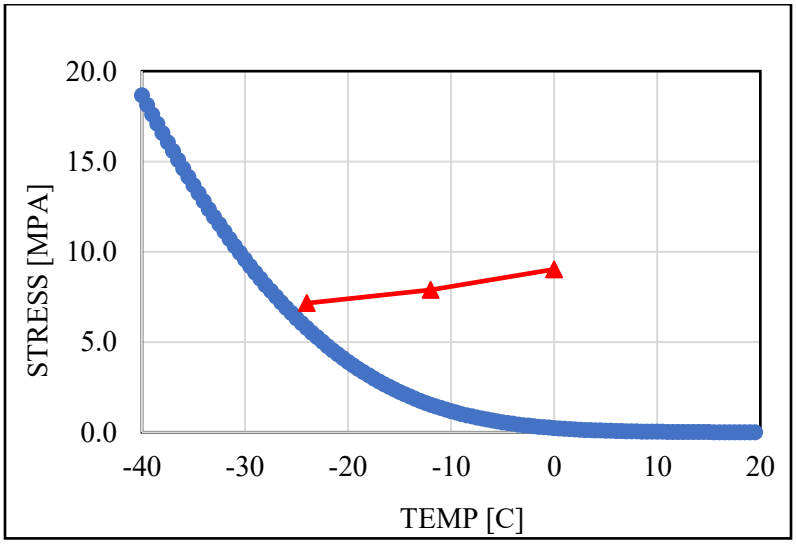

Figure 5.11: Cell 17 thermal stress and strength obtained from BBR creep and strength tests.

Table 5.5: Critical Temperature for all Cells.

Cell	16	17	18	19	20	21	22	23
T critical, ºC	-20.98	-22.57	-22.82	-18.99	-25.47	-22.51	-19.93	-21.48

5.3.3 Limiting criteria for BBR creep stiffness and m-value of asphalt mixtures

This approach was previously developed by University of Utah and Utah DOT (Romero et al., 2016 & Romero, 2017). Based on extensive laboratory work and field observations, the authors concluded that a true performance-based specification can be developed at the mix design stage using BBR mixture S and

m-value. An example is shown below for a low design temperature of -22ºC. Note that the contours shown were developed on a large data set of field performance data from test sites in Utah.

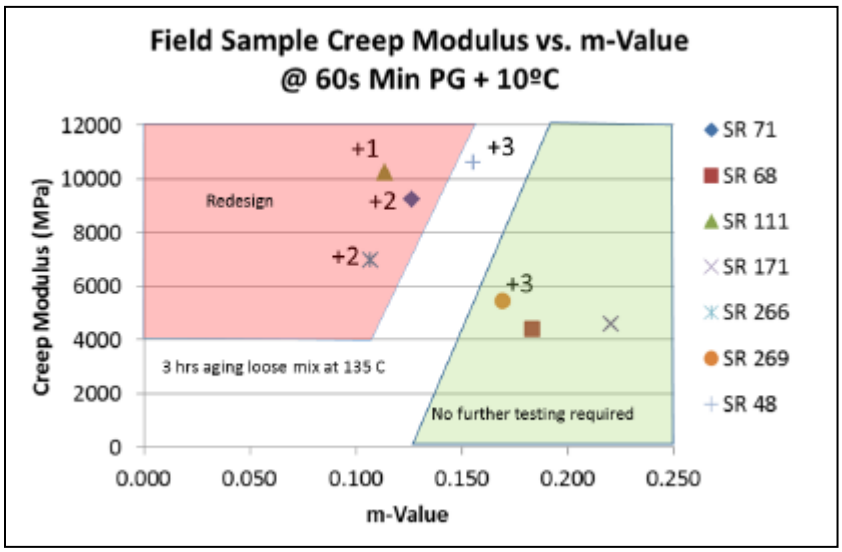

Figure 5.12: Example of diagram used for a design temperature of -22ºC.

In this example, if the proposed mixture results in low modulus and high m-value, no further testing is required. If the proposed mixture results in high modulus and low m-value, the mixture is rejected and must be redesigned. Finally, if the modulus and m-value fall within a transition zone, 3 hours of loose mixture aging at 135ºC is required prior to compaction. If, after aging, the proposed mixture is still below the allowed modulus and above the minimum m-value, then the mixture would be acceptable; otherwise, it must be redesigned.

Using the BBR mixture data obtained at -12ºC and at -24ºC, and assuming the performance contours are valid for MnROAD test sections, hypothetical designs are generated at -22ºC and at -34ºC and are presented in Figures 5.13 and 5.14. Most mixtures pass at -12ºC and no mixtures need to be redesigned. However, at -24ºC, none of the mixtures pass the design.

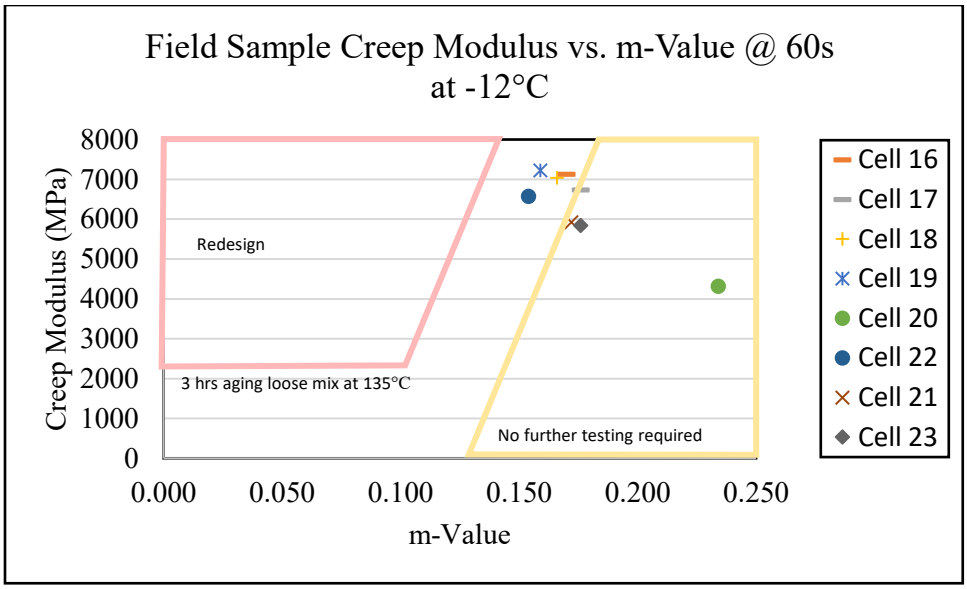

Figure 5.13: Hypothetical diagram for a design temperature of -22ºC.

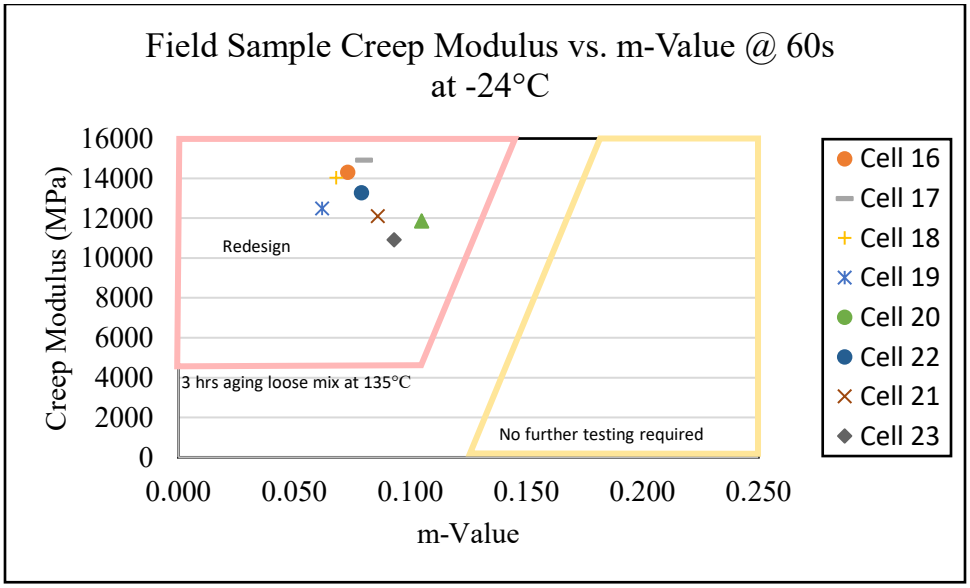

Figure 5.14: Hypothetical diagram for a design temperature of -34ºC.

CHAPTER 6: SCB AND E* TESTING OF ASPHALT MIXTURES

Fracture testing, using the SCB testing method, and E* complex modulus testing, using diametral compression loading, were conducted on the asphalt mixtures investigated. Although not part of the work plan, IDT creep and tensile strength were also conducted to compare IDT and BBR test results. The comparison is included in the data analysis in Chapter 7.

6.1 SPECIMEN PREPARATION

As mentioned in Chapter 5, six cylinders were compacted for each of the mixtures. Four cylinders were used for preparing the SCB and E* test specimens. Each cylinder was cut into two circular 38 mm and one 32 mm thick slices for testing. The 32 mm thick slice was later cut into two semicircular shapes and a 15mm long, 1 mm wide notch, perpendicular to the diameter, in the center of it, was cut.

6.2 SEMI CIRCULAR BENDING (SCB) TEST

The Semi-Circular Bending (SCB) fracture tests was performed according to AASHTO TP-105 (AASHTO TP105, 2013). Testing procedure was performed on all mixtures at two temperatures, -24°C, and -12°C using three replicates. The loading head used was a rigid cylinder with a radius of 25.4 mm connected to the actuator, as shown on the left side of Figure 6.1. The mixtures from cells 21 and 22 were also tested using a new loading head provided by Test Quip, which consists of a half cylinder with the same 25.4 mm radius, with an articulation that offers a degree of freedom, and can rotate freely in order to accommodate a small difference in the height of the sample between the two sides, as shown on the right side of Figure 6.1. The reason for this fixture is to provide the same loading on both sides, and this is supposed to be noticed with the two extensometers applied on both sides of the specimen. For Cell 21 and 22 sawing of specimens was done in a different way. Two cylinders per cell were used, and from each cylinder, six semicircular specimens were obtained. Three of them, coming from three different layers were tested with one fixture, and the other three with the other fixture, at the same temperature.

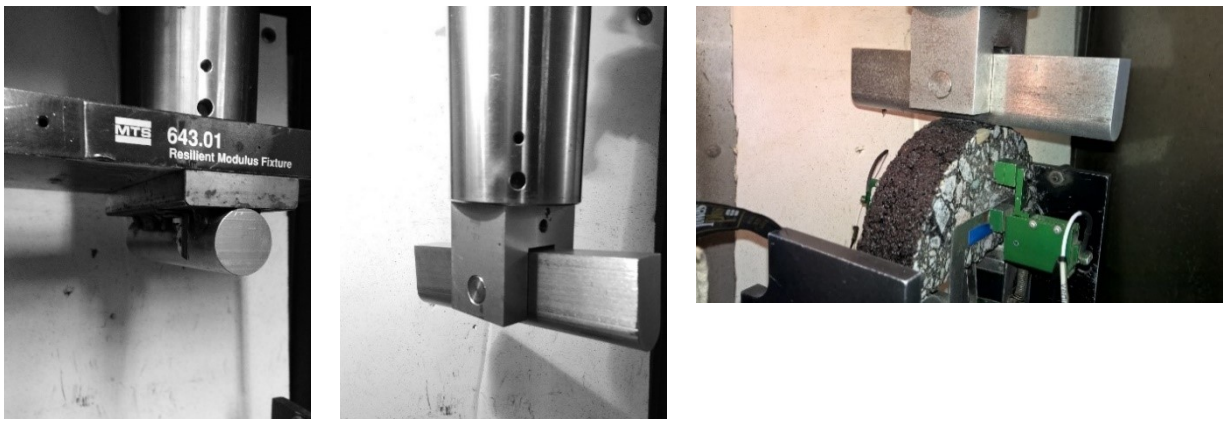

Figure 6.1: The original (left) and the the new loading fixture (right two photos).

The fracture energy measured by the SCB test is a material property that directly represents the fracture resistance under mode-I loading (tensile fracture). The work of fracture is determined as the area under

the loading-deflection (*P-u*) curve. The fracture energy G_f can then be obtained by dividing the work of fracture with the ligament area:

$$G_f = \frac{\int P\,\mathrm{d}u}{A_l} \qquad [6.1]$$

where: $\int P\,\mathrm{d}u$ = total work done by the external force *P*, and A_l = ligament area. Eq. 6.1 assumes that the external work is all spent in crack propagation and the rest part of the specimen behaves elastically. This assumption is reasonable for asphalt mixture specimens at low temperatures, which generally exhibit a damage localization mechanism.

The apparent fracture toughness can also be calculated from the measured peak load of the specimen within the framework of linear elastic fracture mechanics (LEFM). The essential failure criterion of LEFM is that the stress intensity factor (SIF) of the specimen reaches a critical value (i.e. fracture toughness) as the peak load is attained. The SIF of the SCB specimen can be written as (6.2)

$$K = \frac{P}{2rt}\sqrt{\pi a}\left[4.782 + 1.219\left(\frac{a}{r}\right) + 0.063\exp\left(7.045\left(\frac{a}{r}\right)\right)\right] \qquad [6.2]$$

where *r* = radius of the SCB specimen, *t* = thickness of specimen, and *a* = notch depth. Considering the LEFM failure criterion, we can compute the fracture toughness K_{1c} based on Eq. 6.2 and the experimentally measured peak load. It should be emphasized here that the fracture toughness computed by Eq. 6.2 is strictly anchored by the assumption of LEFM. For SCB specimen, it has been shown that the LFEM limit may not be achieved since the fracture process zone at the crack tip is not necessarily negligible compared to the specimen size (Le at al., 2013, Lim at al., 1993 & Li at al., 2004). Therefore, we refer this calculated K_{1c} as to the apparent fracture toughness. The true fracture toughness is the value of K_{1c} for an infinite size specimen, which is a material property. By contrast, the apparent fracture toughness strongly depends on specimen geometry and size, and therefore it does not directly measure the actual fracture resistance of the material.

6.3 DIAMETRAL E* TEST

Dynamic modulus is typically measured in compression on cylinders 100 mm in diameter and 170 mm tall (AASHTO TP 62-03, 2006). This geometry severely limits the possibility of testing field cores. As a consequence, an alternative method based on the indirect tension (IDT) loading mode, described by Kim et al. (2004), was used. The same geometry used for IDT testing, 150 mm in diameter and 38 mm thick, was used to determine dynamic modulus. Frequency sweeps consisting of eight frequencies, ranging from 25 Hz to 0.01 Hz, were performed at 3 temperatures on each replicate: -12°C, 12°C, and 36°C. Two replicates from each material type were tested and |E*| were calculated for each of the 24 temperature and frequency combinations. Average |E*| values were calculated from the three replicates, which were then used to construct master curves using time-temperature superposition principle.

Dynamic modulus was calculated following the procedure described by Kim et al. (2004). First, four integrals were computed based on specimen geometry:

$$F = \int_{-l}^{l} \frac{(1 - x^2/R^2)sin2\alpha}{1 + 2\left(\frac{x^2}{R^2}\right)cos2\alpha + x^4/R^4} dx \quad [6.3]$$

$$G = \int_{-l}^{l} \tan^{-1}\left[\frac{1 - x^2/R^2}{1 + x^2/R^2} tan\alpha\right] dx \quad [6.4]$$

$$M = \int_{-l}^{l} \frac{(1 - y^2/R^2)sin2\alpha}{1 + 2\left(\frac{y^2}{R^2}\right)cos2\alpha + y^4/R^4} dy \quad [6.5]$$

$$N = \int_{-l}^{l} \tan^{-1}\left[\frac{1 + y^2/R^2}{1 - y^2/R^2} tan\alpha\right] dy \quad [6.6]$$

where x and y are along the horizontal and vertical axes of the specimen, respectively, and:

R = radius of specimen
a = width of load
d = thickness of specimen
l = half of gauge length
α = radial angle of loading $= \sin^{-1}\left(\frac{a/2}{R}\right)$

Dynamic modulus ($|E^*|$) and Poisson's ratio (v) were then computed for each of the 24 temperature and frequency combinations for each of the specimens using the following equations:

$$|E^*| = 2\frac{P_0}{\pi ad}\frac{\beta_1 U_0 - \gamma_1 V_0}{-\beta_2 U_0 + \gamma_2 V_0}$$

$$v = \frac{\beta_1 U_0 - \gamma_1 V_0}{-\beta_2 U_0 + \gamma_2 V_0}$$

where:

P_0 = amplitude of applied load
U_0 = amplitude of horizontal displacement (averaged between the two sides)
V_0 = amplitude of vertical displacement (averaged between the two sides)

P_0, U_0, and V_0 were taken as half of the distance between the smallest and largest values for the last five cycles of loading, and

β_1 = -N − M
β_2 = N − M
γ_1 = F − G
γ_2 = F + G

6.4 INDIRECT TENSILE TEST (IDT) CREEP COMPLIANCE AND TENSILE STRENGTH

Creep and tensile strength tests followed procedures outlined in "Standard Test Method for Determining the Creep Compliance and Strength of Hot Mix Asphalt (HMA) Using the Indirect Tensile Test Device," AASHTO T322 -07 (2007).

For creep compliance, specimens were loaded diametrically using a vertical constant load selected to keep horizontal strains in the linear elastic range that means below a horizontal strain of 500 x 10^{-6} mm/mm, during the creep test. Based on the 150 mm sample diameter the horizontal deformation was kept between 0.00125 mm and 0.019 mm. Horizontal and vertical deformation were measured using extensometers fixed near the center of the sample. Deformation measurements were then used to calculate creep stiffness. Three replicates were tested for each material at two temperatures, -24°C, and -12°C, for a total of six tests.

At the end of each creep test, indirect tensile strength tests were performed. Specimens were loaded with a constant rate of vertical deformation until sample failure. Specimen geometry and maximum load were then used to calculate tensile strength. The creep compliance is calculated using the following equations:

$$D(t) = \frac{\Delta X \times D \times b}{P \times GL} \times C \quad [6.9]$$

where:

D(t) = creep compliance at time t (kPa)

$\triangle X =$ horizontal deformation

P = average creep load applied to specimen

b = thickness of specimen (38 mm for all specimens)

D = diameter of specimen (150 mm for all specimens)

GL = gage length

Creep stiffness (S) is the inverse of creep compliance:

$$S = \frac{1}{D(t)} \quad [6.10]$$

Tensile strength is calculated by the following equation:

$$S = (2P)/(\pi bD) \quad [6.11]$$

where:

S = tensile stress of specimen

P = failure load for specimen

b = thickness of specimen (38 mm for all specimens)

D = diameter of specimen (150 mm for all specimens)

6.5 SCB TEST RESULTS

Table 6.1 summarizes the calculated fracture energy and apparent fracture toughness for all cells. Figure 6.2 presents the fracture energy plot and Figure 6.3 the apparent fracture toughness. The results obtained with the new fixture are labeled as Cell 21 NF and Cell 22 NF.

Table 6.1: Fracture energy and apparent fracture toughness.

Specimen	Fracture Energy G_f (kJ/m^2)		Fracture Toughness, K_{IC} (MPa*m$^{0.5}$)	
	-12°C	-24°C	-12°C	-24°C
Cell 16	0.335	0.246	0.576	0.674
Cell 17	0.486	0.237	0.599	0.646
Cell 18	0.392	0.277	0.599	0.644
Cell 19	0.339	0.263	0.604	0.659
Cell 20	0.613	0.299	0.602	0.711
Cell 21	0.561	0.296	0.703	0.715
Cell 21 NF	0.541	0.321	0.692	0.699
Cell 22	0.307	0.198	0.566	0.542
Cell 22 NF	0.276	0.176	0.518	0.565
Cell 23	0.416	0.315	0.630	0.714

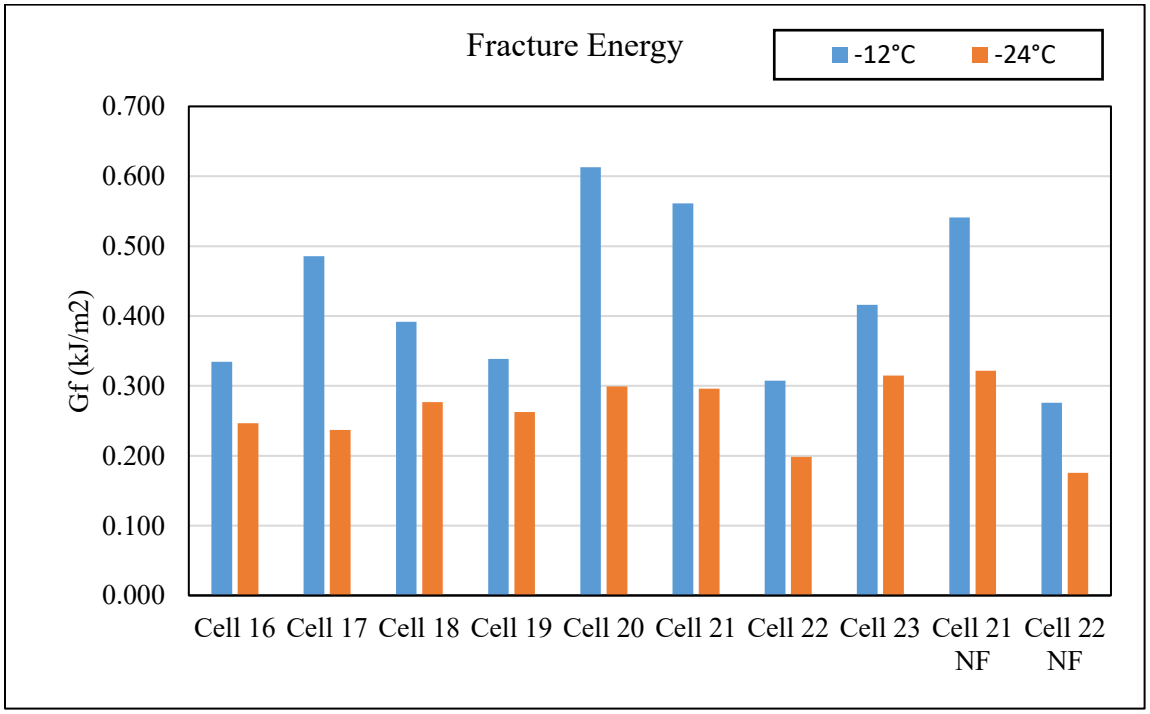

Figure 6.2: Fracture energy for all mixtures.

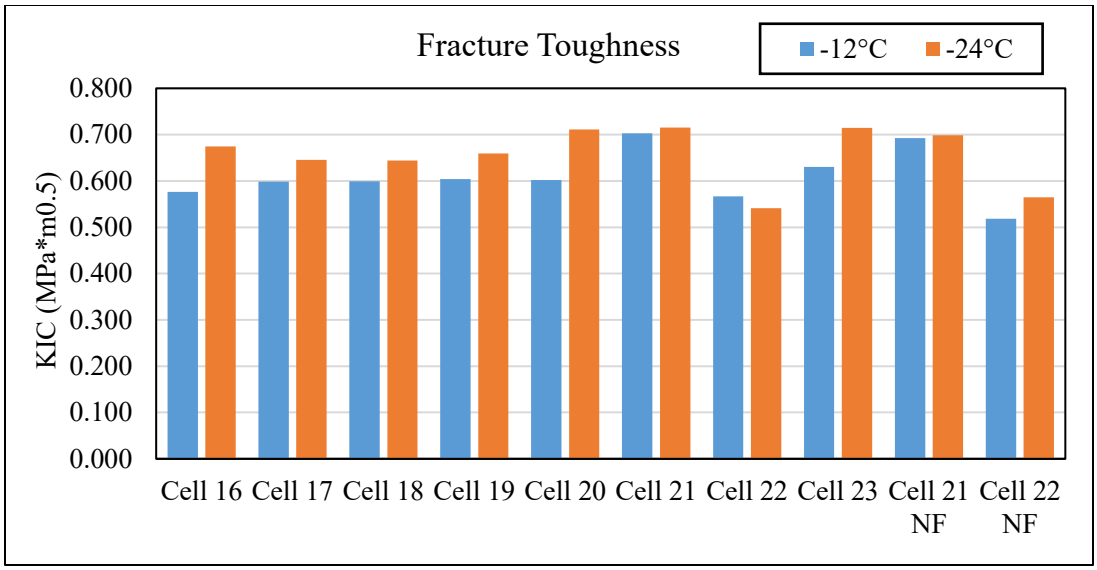

Figure 6.3: Fracture toughness for all mixtures.

A number of observations can be made based on the results. The highest fracture energy is observed for cells 20 and 21 at -12°C. At - 24°C, cells 23 and 21 mixtures have the highest fracture energy. The lowest values, for both test temperatures, are obtained for cell 22 mixture.

A comparison between the results obtained with the original and the new fixtures was performed for the mixtures from cells 21 and 22 and the results are presented in Table 6.2. A comparison between the upper loading fixtures is presented in figures 6.4 and 6.5. The left side of each figure was obtained using the regular fixture and the right side using the new one. They show the load line displacement (LLD) for each side of the sample, the average LLD and the actuator displacement. A small improvement, which means closer results for both sides, may be attributed to the new fixture.

Table 6.2: Comparison of the SCB results obtained with the two fixtures.

Sample	Fracture Energy G_f (kJ/m^2)		Fracture Toughness, K_{IC} (MPa*m$^{0.5}$)	
	-12°C	-24°C	-12°C	-24°C
Cell 21	0.561	0.296	0.703	0.715
Cell 21 NF	0.541	0.321	0.692	0.699
Difference %	3.70	-7.79	1.59	2.29
Cell 22	0.307	0.198	0.566	0.542
Cell 22 NF	0.276	0.176	0.518	0.565
Difference %	11.23	12.50	9.27	-4.07

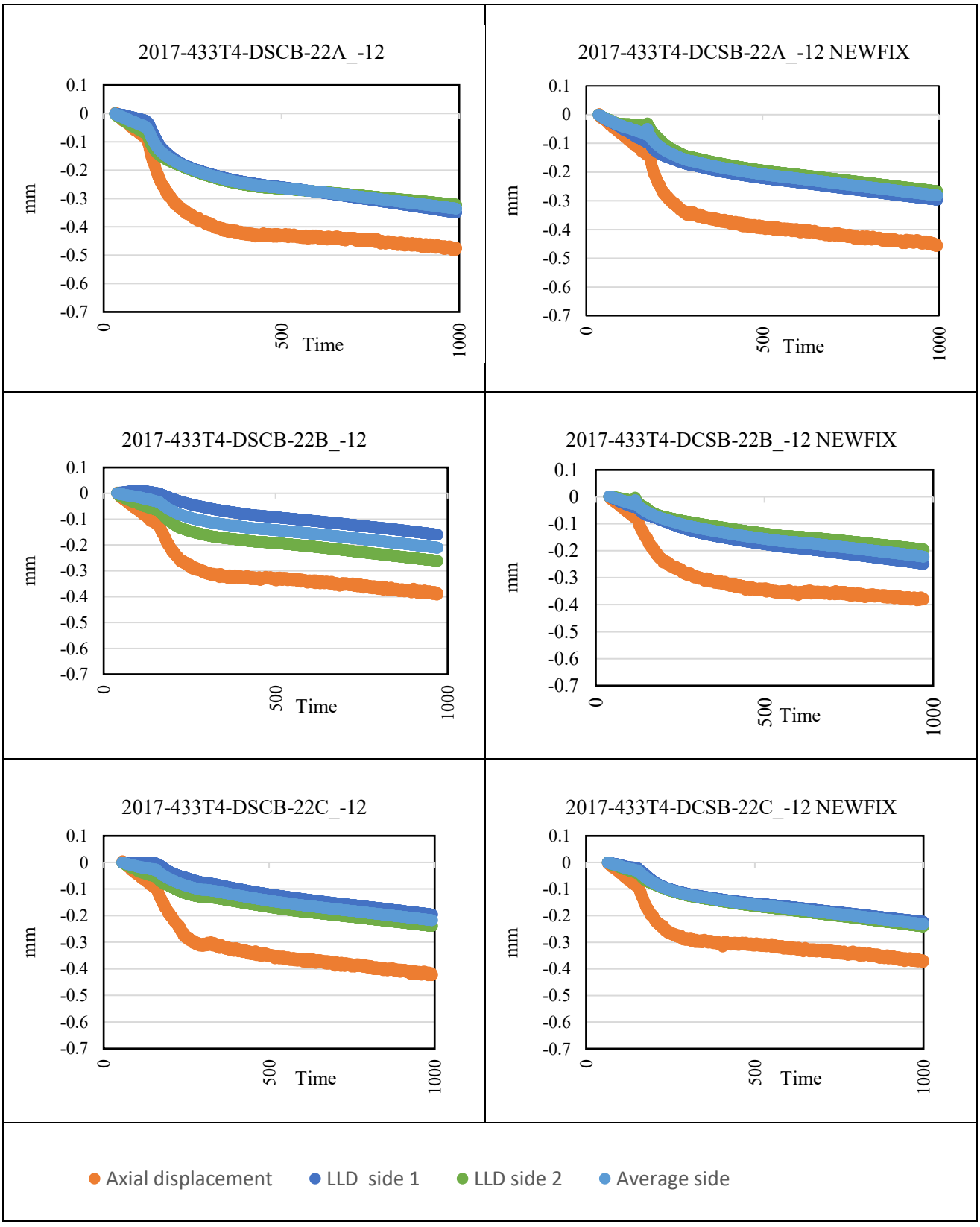

Figure 6.4: Cell 22 LLD and actuator displacement at -12°C.

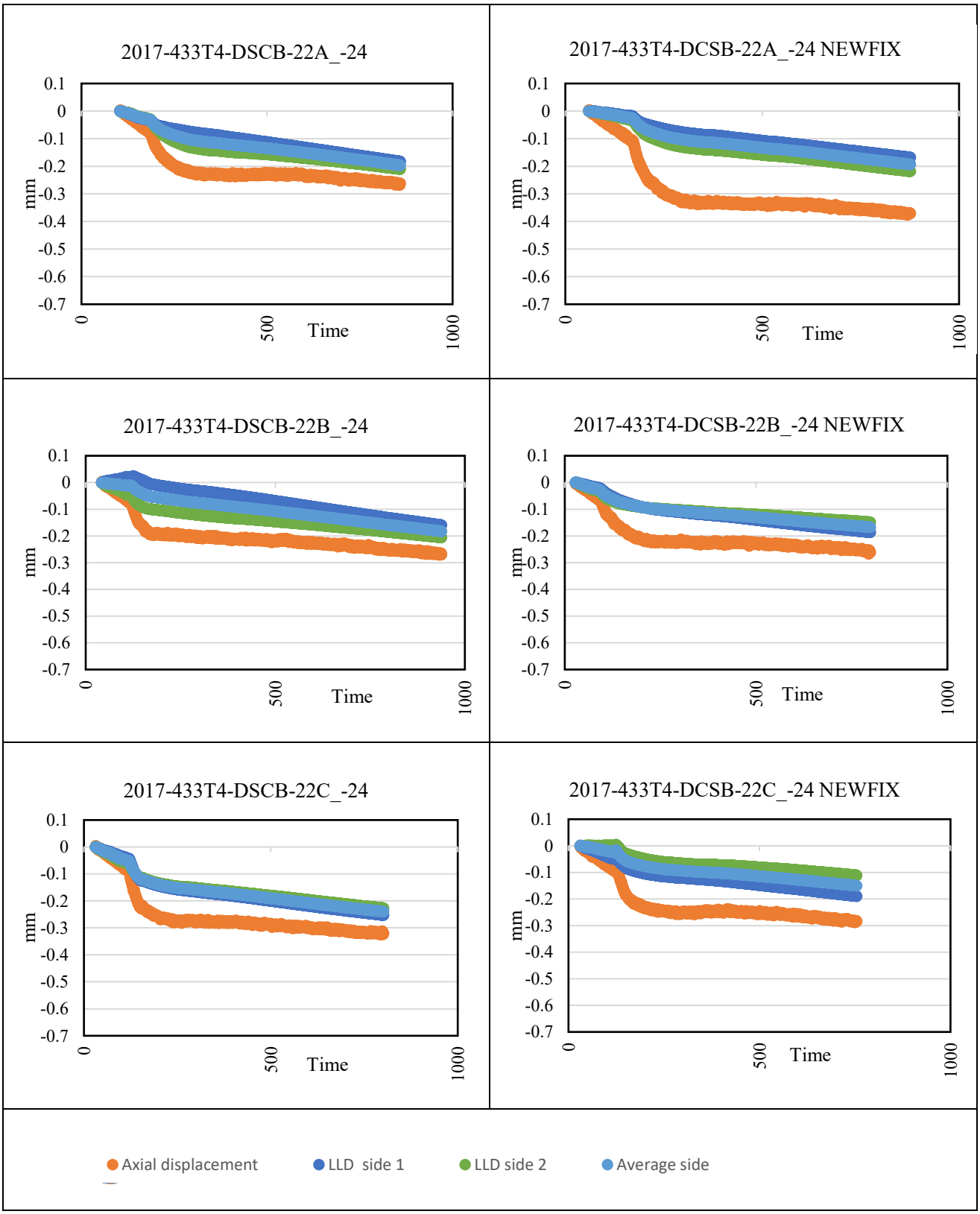

Figure 6.5: Cell 22 LLD and actuator displacement at -24°C.

6.6 DIAMETRAL E* RESULTS

Table 6.3 contains |E*| values for all eight cells as an average of two replicates at all 24 temperature/frequency combinations.

Table 6.3: |E*| values for all cells, average values.

Sample	Temp °C	25 Hz (GPa)	10 Hz (GPa)	5 Hz (GPa)	1 Hz (GPa)	0.5 Hz (GPa)	0.1 Hz (GPa)	0.05 Hz (GPa)	0.01 Hz (GPa)
Cell 16	-12	20.65	20.35	20.65	18.73	18.16	15.71	15.09	12.94
	12	8.74	7.91	6.94	5.42	4.65	2.58	2.01	0.75
	36	1.76	1.58	1.20	0.50	0.37	0.19	0.15	0.09
Cell 17	-12	15.52	11.83	10.41	9.49	9.00	8.19	7.90	6.99
	12	7.58	7.83	7.34	4.55	3.99	2.12	1.57	0.57
	36	1.66	1.35	1.07	0.42	0.30	0.16	0.13	0.04
Cell 18	-12	15.08	12.10	10.84	10.04	8.80	8.66	8.42	7.30
	12	7.35	5.96	5.63	3.97	3.55	2.35	1.86	0.61
	36	1.48	0.96	0.79	0.42	0.30	0.18	0.15	0.09
Cell 19	-12	19.79	20.59	19.89	19.48	17.89	16.78	15.41	13.15
	12	9.08	7.27	6.74	4.82	3.81	2.06	1.51	0.53
	36	1.70	1.43	1.08	0.44	0.33	0.18	0.15	0.08
Cell 20	-12	14.92	8.68	7.03	6.00	5.01	4.58	4.13	3.31
	12	7.57	6.03	5.48	3.16	2.46	1.13	0.82	0.30
	36	1.61	1.17	0.92	0.41	0.30	0.20	0.18	0.06
Cell 21	-12	15.21	13.92	12.79	11.43	10.46	9.31	9.10	7.70
	12	7.57	6.92	6.05	4.39	3.62	2.05	1.51	0.55
	36	1.39	1.10	0.84	0.37	0.28	0.17	0.15	0.09
Cell 22	-12	16.99	12.64	11.13	10.73	9.80	9.29	8.78	7.99
	12	9.53	8.46	6.46	4.57	3.25	2.98	2.05	1.58
	36	2.65	1.97	1.58	0.65	0.47	0.23	0.19	0.10
Cell 23	-12	14.17	10.71	9.22	8.41	7.07	6.70	6.37	5.07
	12	7.07	6.64	5.67	4.55	3.83	2.68	1.97	0.75
	36	1.71	1.40	1.17	0.67	0.43	0.24	0.22	0.13

The average values of |E*| were used to generate master curves for each of the cells mixtures at a reference temperature of 12°C. This was done by fitting the data to the following equation using a procedure proposed by Rowe, et al. (9):

$$\log|E^*| = \delta + \frac{\alpha - \delta}{1 + e^{\beta+\gamma(log\omega+\log(a(T)))}} \qquad [6.12]$$

where: ω = frequency of load

$a(T)$ = temperature shift parameter

δ, α, β and γ are fitting parameters.

Table 6.4 shows the fitting parameters and shift factor values.

Table 6.4: |E*| master curve fitting parameters.

	Cell 16	Cell 17	Cell 18	Cell 19	Cell 20	Cell 21	Cell 22	Cell 23
alpha	2.26E+10	1.23E+10	1.29E+10	2.14E+10	1.23E+10	1.42E+10	1.82E+10	1.26E+10
delta	9.28E+06	4.03E+07	3.76E+07	2.34E+07	2.54E+07	4.90E+07	5.87E+02	4.03E+07
beta	-1.00	-0.93	-0.88	-0.70	-0.62	-0.72	-2.19	-0.97
gama	-0.53	-0.80	-0.65	-0.61	-0.69	-0.72	-0.38	-0.62
log at(-12)	4.21	2.54	3.07	4.30	1.82	2.99	2.91	2.13
log at(+36)	-2.56	-2.41	-2.75	-2.33	-1.92	-2.57	-2.63	-2.58

|E*| master curves for each material, obtained from fitting average results to equation [6.12], are shown in Figure 6.6. Smooth master curves were obtained for all mixtures tested. The highest modulus value are observed for cells 16 and 19 at the highest frequencies (lowest temperatures) while the lowest values are observed for cell 20 and 19 at the lowest frequencies (highest temperatures). Cell 19 mixture appears to have the highest frequency (temperature) susceptibility of all mixtures.

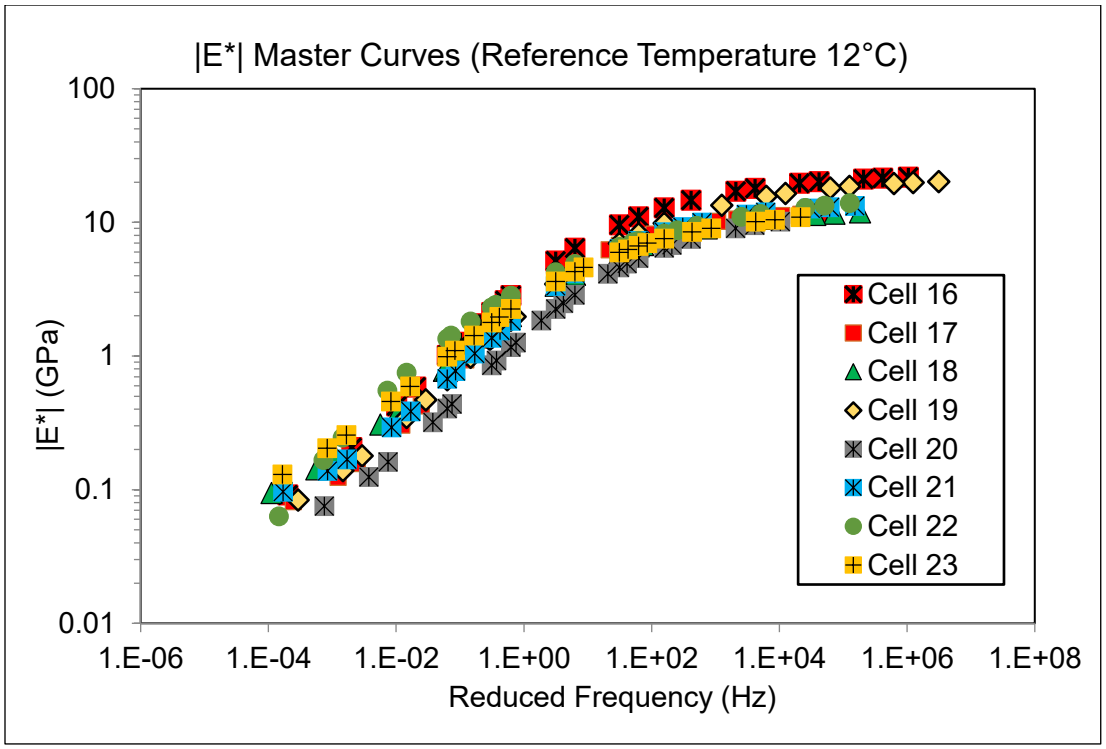

Figure 6.6: Fitted dynamic modulus master curves for all cells.

6.7 IDT CREEP COMPLIANCE AND TENSILE STRENGTH RESULTS

Average values for creep stiffness and tensile strength values are shown in Tables 6.5 and 6.6. Figures 6.7 and 6.8 present creep stiffness curves at -24 °C, and -12 °C, respectively, using average values. Figure 6.9 summarizes the tensile strength values for all materials.

Table 6.5: Creep stiffness and tensile strength at -12°C.

Testing temperature: -12°C	Cell 16	Cell 17	Cell 18	Cell 19	Cell 20	Cell 21	Cell 22	Cell 23
Stiffness S(60s) (GPa)	10.53	10.05	14.31	12.36	7.45	8.42	11.69	9.30
Stiffness S(500s) (GPa)	6.62	6.10	9.52	7.72	3.68	5.06	8.29	5.85
Tensile strength (MPa)	3.48	3.05	3.08	3.39	3.39	3.42	3.06	3.17

Table 6.6: Creep stiffness and tensile strength at -24°C.

Testing temperature: -24°C	Cell 16	Cell 17	Cell 18	Cell 19	Cell 20	Cell 21	Cell 22	Cell 23
Stiffness S(60s) (GPa)	18.24	16.33	25.44	17.32	15.78	17.50	15.97	14.04
Stiffness S(500s) (GPa)	15.72	13.88	21.54	16.22	11.89	13.37	13.34	12.50
Tensile strength (MPa)	3.22	2.84	2.84	3.32	3.60	3.17	3.32	3.46

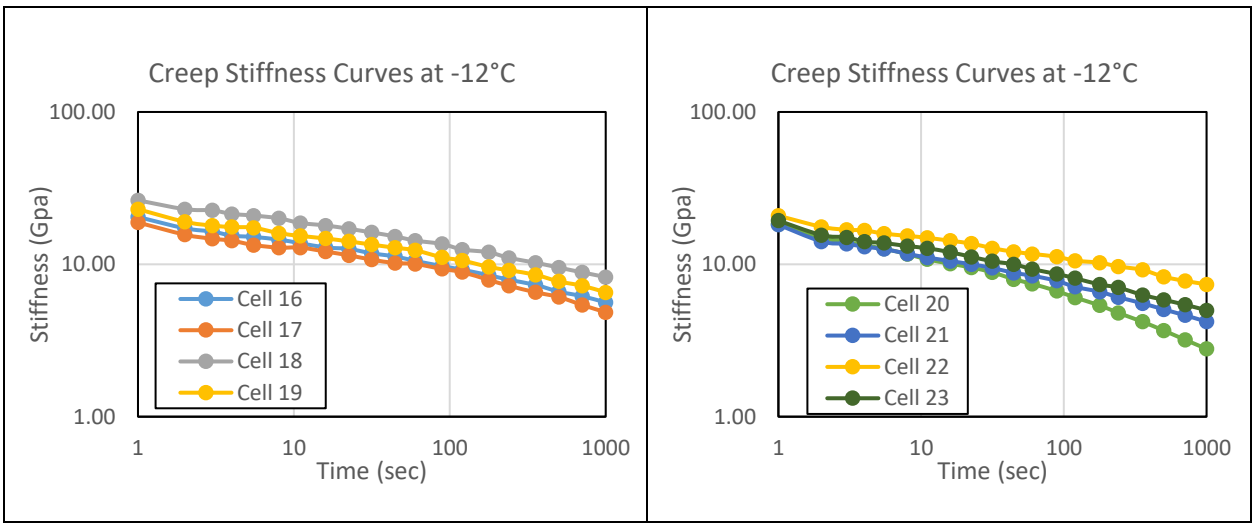

Figure 6.7: Creep stiffness curves at -12°C for all cells.

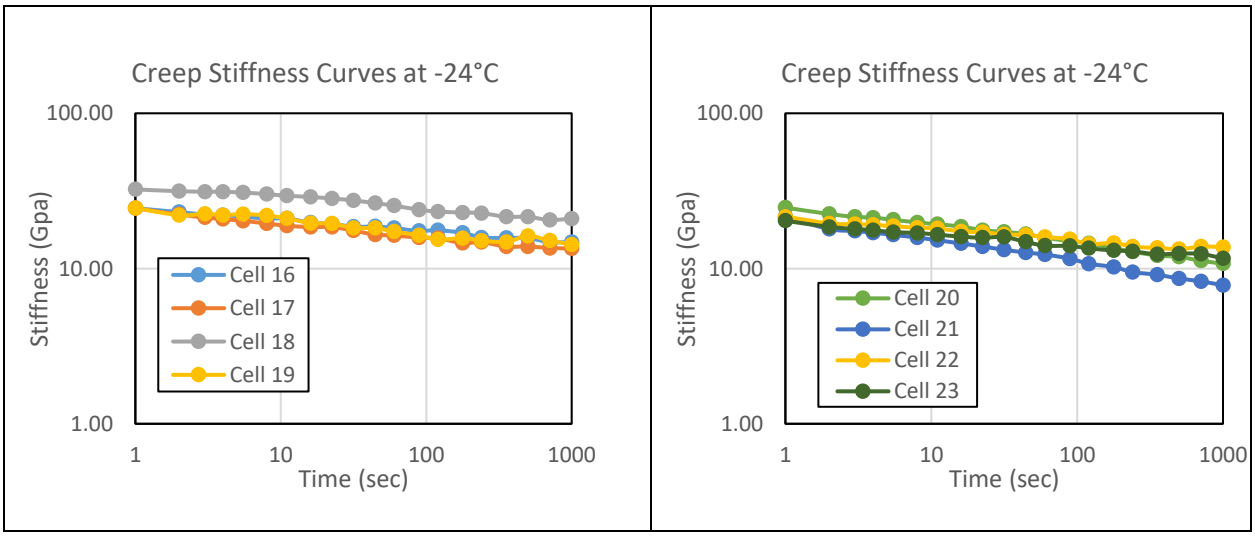

Figure 6.8: Creep stiffness curves at -24°C for all cells.

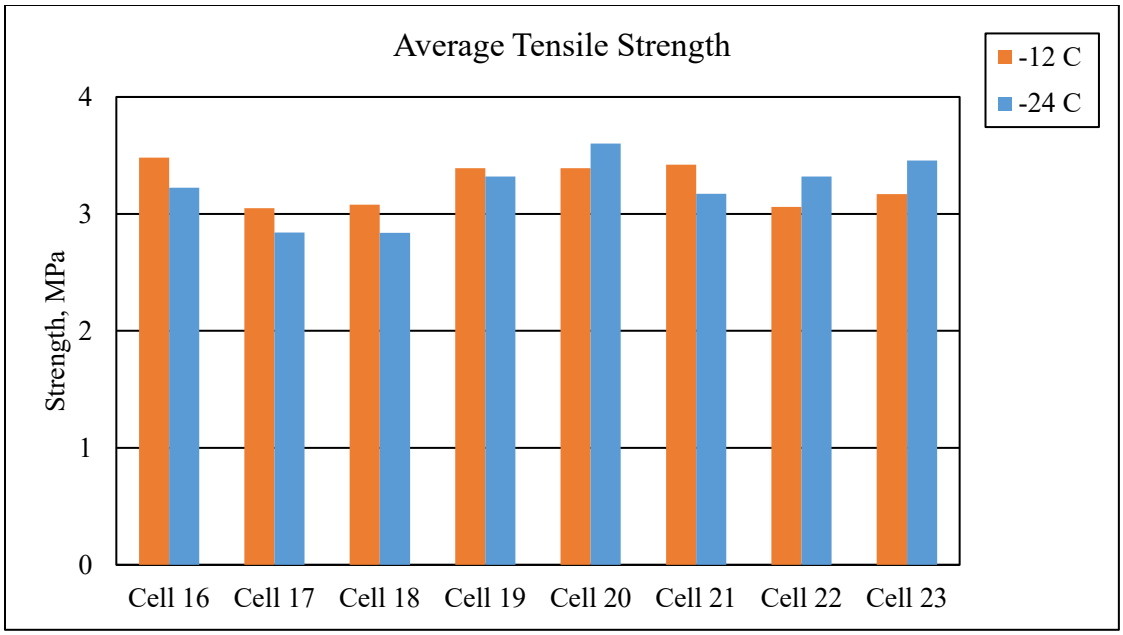

Figure 6.9: Average tensile strength at -24°C and -12°C.

At -12°C, cells 18 and 19 are the most stiff, while cell 20 is the less stiff. At -24°C, cell 18 mixture is clearly the stiffest one, while cell 21 is the less stiff mixture. Regarding the IDT strength, it is observed that for cells 16, 17, 18, 19 and 21, a decrease in temperature results in a decrease in strength, while for cells 20, 22, and 23, the strength increases with decrease in temperature.

CHAPTER 7: DATA ANALYSIS

In this chapter, statistical analyses are performed to identify significant factors. The tools used include analysis of variance (ANOVA), Tukey's method, which represents a pairwise comparison technique, and correlation matrices based on Pearson's correlation.

7.1 BINDERS ANOVA

In order to investigate differences in rheological and strength properties of binders, statistical analyses were performed on the binders used in cells 16, 20, 21, 22 and 23. The binder properties analyzed were BBR creep stiffness and m-value at 60 seconds, BBR strength and BBR strain at failure. Each property was obtained at two temperatures: PGLT+10°C and PGLT+4°C (tables 6.13 to 6.20). For the one-way analysis of variance (ANOVA), the significance level (α) was set at 0.05 and the null hypothesis (H_0) assumed that all the binder means were equal. The alternate hypothesis (H_a) was that at least one of the binder means was different.

PAV Binder BBR Creep Test

The ANOVA results for the PAV binder creep stiffness at 60 seconds at PGLT+10°C are presented in Table 7.1, and at PGLT+4°C are presented in Table 7.2. The results for the m-value at PGLT+10°C are presented in Table 7.3 and the results at PGLT+4°C are presented in Table 7.4.

Table 7.1: Summary and ANOVA: PAV binder BBR Creep Stiffness at PGLT+10°C.

SUMMARY

Groups	Count	Sum	Average	Variance
Cell 16	5	859.8016	171.9603	53.07403
Cell 20	4	1006.217	251.5542	74.94623
Cell 21	5	1203.323	240.6646	519.357
Cell 22	4	885.3054	221.3264	360.8912
Cell 23	5	948.5269	189.7054	65.00738

ANOVA

Source of Variation	SS	df	MS	F	P-value	F crit
Between Groups	21183.38	4	5295.845	24.71315	4.21E-07	2.927744
Within Groups	3857.266	18	214.2926			
Total	25040.65	22				

The F-value is greater than F-critical value and the p-value is smaller than the alpha level selected (0.05). We can conclude that there is enough evidence to reject the null hypothesis and say that at least one of the eight cells has significantly different means and belongs to a different population.

Table 7.2: Summary and ANOVA: PAV binder BBR Creep Stiffness at PGLT+4°C.

SUMMARY

Groups	Count	Sum	Average	Variance
Cell 16	4	885.3054	221.3264	360.8912
Cell 20	4	1978.327	494.5817	4614.2
Cell 21	5	2174.431	434.8861	822.4499
Cell 22	6	2594.663	432.4438	562.686
Cell 23	6	2440.085	406.6809	1585.523

ANOVA

Source of Variation	SS	df	MS	F	P-value	F crit
Between Groups	175936.5	4	43984.12	30.37984	3.05E-08	2.866081
Within Groups	28956.12	20	1447.806			
Total	204892.6	24				

The F-value is greater than F-critical value and p-value is smaller than alpha level selected (0.05). We can conclude that there is enough evidence to reject the null hypothesis and say that at least one of the eight cells has significantly different means and belongs to a different population.

Table 7.3: Summary and ANOVA: PAV binder BBR m-value at PGLT+10°C.

SUMMARY

Groups	Count	Sum	Average	Variance
Cell 16	5	1.859389	0.371878	3.53E-05
Cell 20	4	1006.217	251.5542	74.94623
Cell 21	5	1.640056	0.328011	1.63E-05
Cell 22	4	1.3391	0.334775	0.000238
Cell 23	5	1.720497	0.344099	0.000194

ANOVA

Source of Variation	SS	df	MS	F	P-value	F crit
Between Groups	208524	4	52131	4173.441	1.95E-26	2.927744
Within Groups	224.8404	18	12.49113			
Total	208748.8	22				

The F-value is greater than the F-critical value and the p-value is smaller than the alpha level selected (0.05). We can conclude that there is enough evidence to reject the null hypothesis and say that at least one of the eight cells has significantly different means and belongs to a different population.

Table 7.4: Summary and ANOVA: PAV binder BBR m-value at PGLT+4°C.

SUMMARY

Groups	Count	Sum	Average	Variance
Cell 16	6	1.790056	0.298343	0.000448
Cell 20	4	1.063236	0.265809	0.000282
Cell 21	5	1.330373	0.266075	0.000248
Cell 22	6	1.627688	0.271281	0.000145
Cell 23	6	1.73776	0.289627	0.000323

ANOVA

Source of Variation	SS	df	MS	F	P-value	F crit
Between Groups	0.004802	4	0.0012	4.114032	0.0122587	2.816708
Within Groups	0.006419	22	0.000292			
Total	0.011221	26				

The F-value is greater than the F-critical value and the p-value is smaller than the alpha level selected (0.05). We can conclude that there is enough evidence to reject the null hypothesis and say that at least one of the eight cells has significantly different means and belongs to a different population.

PAV BBR Strength Test

Table 7.5 shows the ANOVA results for the PAV binder BBR Strength at PGLT+10°C and the results at PGLT+4°C are presented in Table 7.6.

Table 7.5: Summary and ANOVA: PAV binder BBR Strength at PGLT+10°C.

SUMMARY

Groups	Count	Sum	Average	Variance
Cell 16	4	17.20389	4.300974	0.570435
Cell 20	4	20.93503	5.233757	0.408315
Cell 21	5	29.77435	5.954869	3.622129
Cell 22	5	25.05974	5.011948	0.405941
Cell 23	5	33.94714	6.789428	0.639027

ANOVA

Source of Variation	SS	df	MS	F	P-value	F crit
Between Groups	16.56515	4	4.141288	3.450332	0.0292524	2.927744
Within Groups	21.60464	18	1.200258			
Total	38.16979	22				

The F-value is greater than F-critical value and the p-value is smaller than the alpha level selected (0.05). We can conclude that there is enough evidence to reject the null hypothesis and say that at least one of the eight cells has significantly different means and belongs to a different population.

Table 7.6: Summary and ANOVA: PAV binder BBR Strength at PGLT+4°C.

SUMMARY

Groups	Count	Sum	Average	Variance
Cell 16	5	18.42504	3.685009	0.373872
Cell 20	4	15.68412	3.92103	0.979203
Cell 21	4	22.70106	5.675264	1.504765
Cell 22	5	30.16731	6.033461	1.901788
Cell 23	5	27.65671	5.531342	0.276216

ANOVA

Source of Variation	SS	df	MS	F	P-value	F crit
Between Groups	21.87265	4	5.468164	5.573625	0.0042356	2.927744
Within Groups	17.65941	18	0.981078			
Total	39.53207	22				

The F-value is greater than F-critical value and the p-value is smaller than the alpha level selected (0.05). We can conclude that there is enough evidence to reject the null hypothesis and say that at least one of the eight cells has significantly different means and belongs to a different population.

Table 7.7 shows the ANOVA results for the PAV binder BBR Strain at PGLT+10°C and the results at PGLT+4°C are presented in Table 7.8.

Table 7.7: Summary and ANOVA: PAV binder BBR Strain at PGLT+10°C.

SUMMARY

Groups	Count	Sum	Average	Variance
Cell 16	4	5.881521	1.47038	0.10569
Cell 20	4	4.912279	1.22807	0.045171
Cell 21	5	7.795276	1.559055	0.459527
Cell 22	5	6.64407	1.328814	0.036219
Cell 23	5	11.01267	2.202534	0.108252

ANOVA

Source of Variation	SS	df	MS	F	P-value	F crit
Between Groups	2.798512	4	0.699628	4.390087	0.011877	2.927744
Within Groups	2.868577	18	0.159365			
Total	5.667088	22				

The F-value is greater than F-critical value and the p-value is smaller than the alpha level selected (0.05). We can conclude that there is enough evidence to reject the null hypothesis and say that at least one of the eight cells has significantly different means and belongs to a different population.

Table 7.8: Summary and ANOVA: Single Factor for PAV binder BBR Strain at PGLT+4°C.

SUMMARY

Groups	Count	Sum	Average	Variance
Cell 16	5	2.689592	0.537918	0.014776
Cell 20	4	2.05438	0.513595	0.0215
Cell 21	4	3.24471	0.811177	0.047093
Cell 22	5	4.585261	0.917052	0.04739
Cell 23	5	4.54909	0.909818	0.015829

ANOVA

Source of Variation	SS	df	MS	F	P-value	F crit
Between Groups	0.729953	4	0.182488	6.344233	0.0022859	2.927744
Within Groups	0.51776	18	0.028764			
Total	1.247713	22				

The F-value is greater than F-critical value and the p-value is smaller than the alpha level selected (0.05). We can conclude that there is enough evidence to reject the null hypothesis and say that at least one of the eight cells has significantly different means and belongs to a different population.

From the results presented in tables 7.1 to 7.8, it can be concluded that the binders are significantly different with respect to all properties investigated.

7.2 BINDERS TUKEY ANALYSIS

Since ANOVA only indicates if one or more binders have different means, it is necessary to run an additional test to find out the specific differences. Tukey's method, a pairwise comparison technique, was chosen because it constructs simultaneous confidence intervals for differences of all pairs of means and controls the probability of making one or more Type I errors. (Oehlert, 2000)

The confidence intervals and boxplot were generated for all binders and corresponding properties. Figures 7.1 (a) to 7.8 (a) show the pairwise confidence intervals and Figures 7.1 (b) to 7.8 (b) show the boxplot for pairwise comparison. The boxplots provide a visual interpretation of the confidence intervals where cells are grouped according to their means. Cells with the same color and letter belong to the same group.

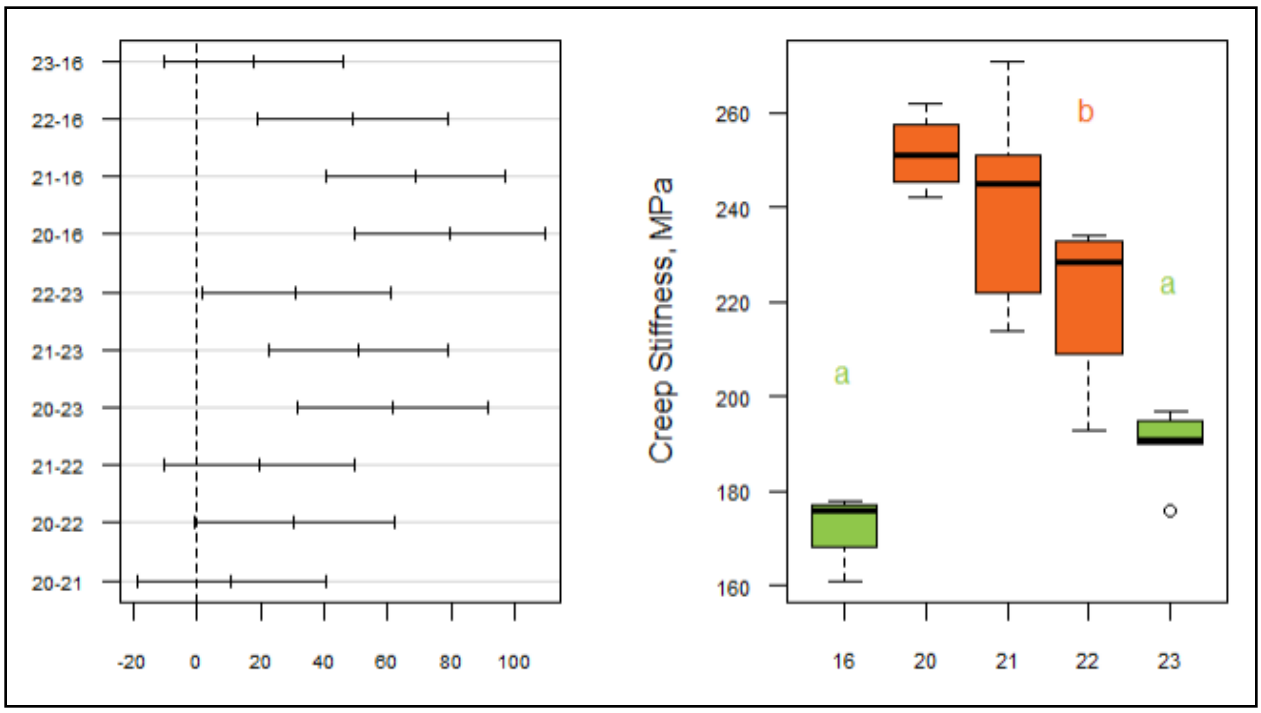

Figure 7.1: (a) Confidence intervals (Tukey) for PAV binder BBR Creep Stiffness at PGLT+10°C. (b) Boxplot for pairwise comparison.

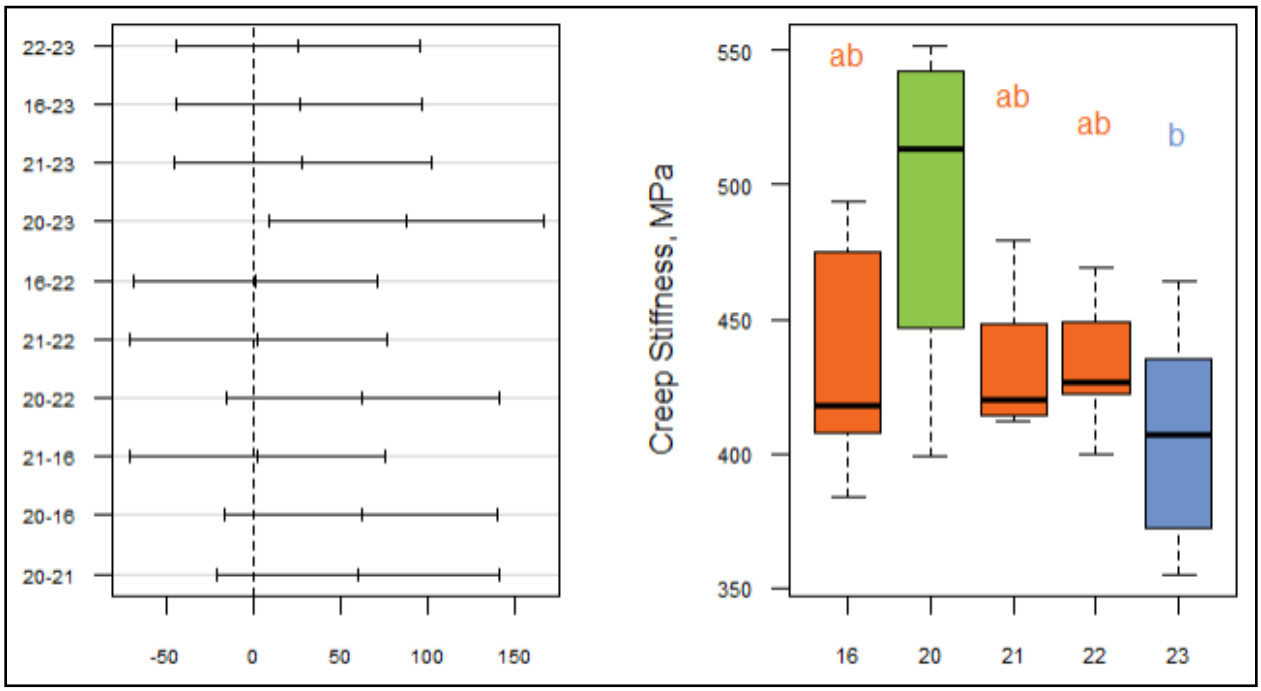

Figure 7.2: (a) Confidence intervals (Tukey) for PAV binder BBR Creep Stiffness at PGLT+4°C. (b) Boxplot for pairwise comparison.

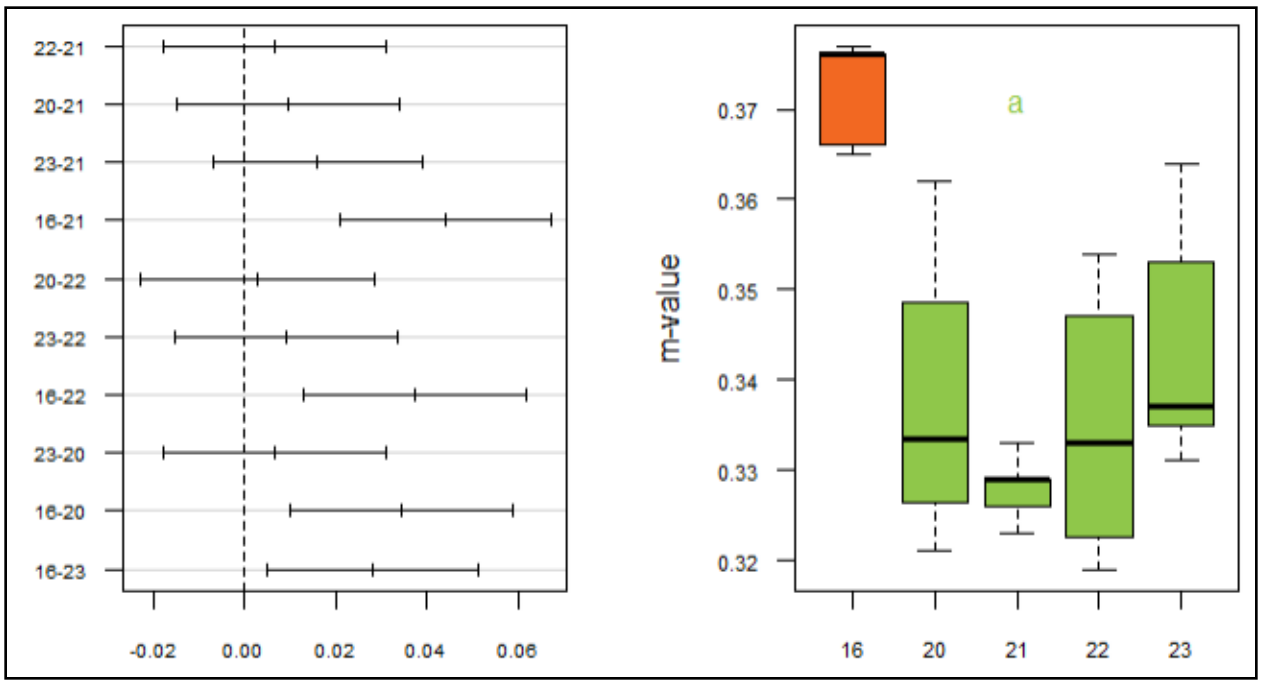

Figure 7.3: (a) Confidence intervals (Tukey) for PAV binder BBR m-value at PGLT+10°C. (b) Boxplot for pairwise comparison.

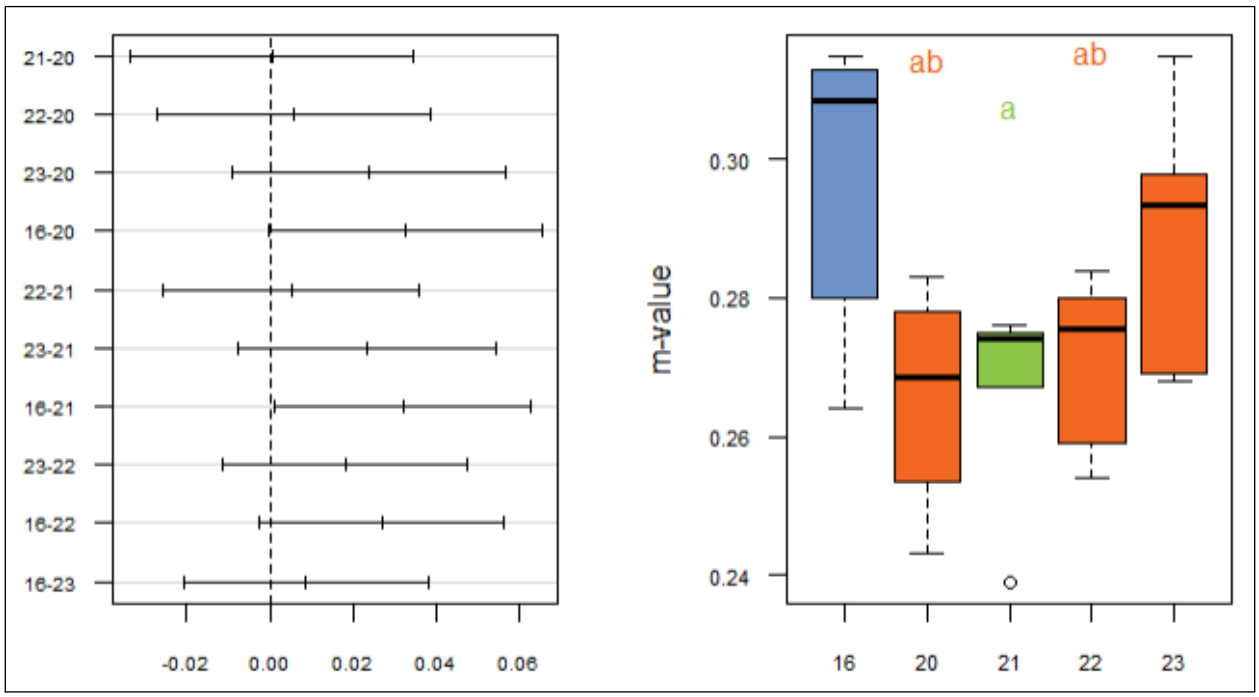

Figure 7.4: (a) Confidence intervals (Tukey) for PAV binder BBR m-value at PGLT+4°C. (b) Boxplot for pairwise comparison.

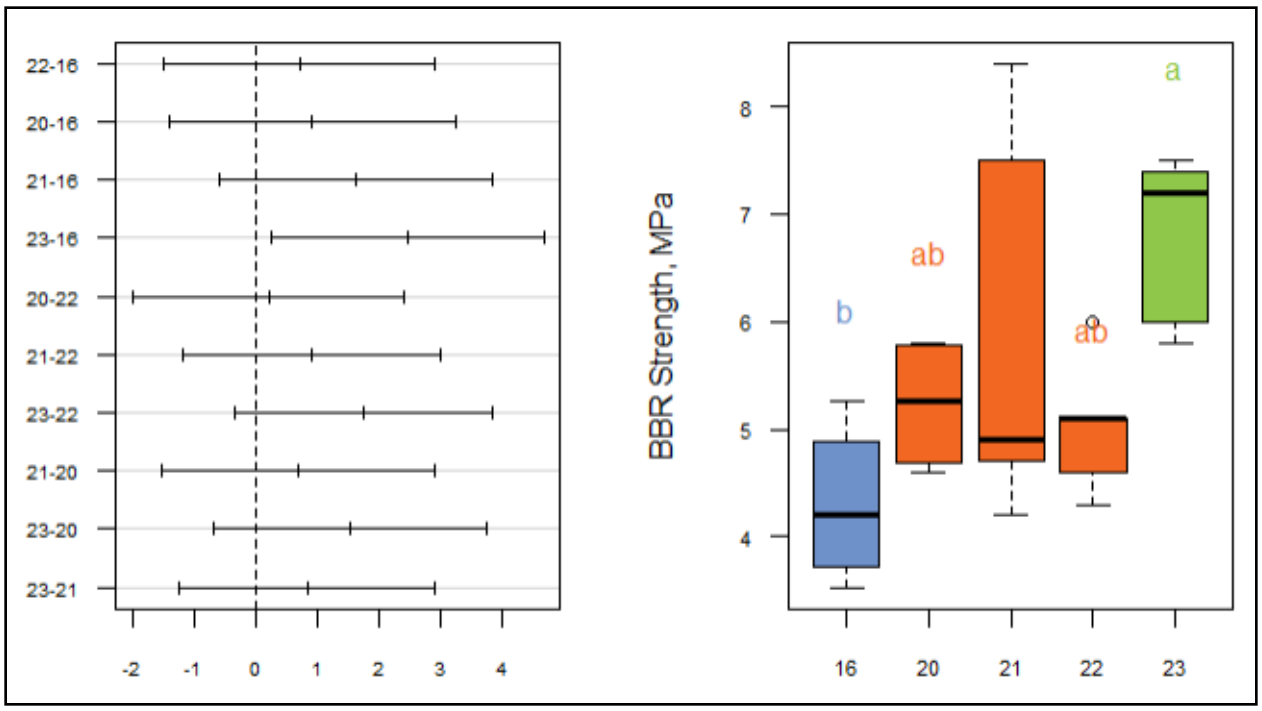

Figure 7.5: (a) Confidence intervals (Tukey) for PAV binder BBR Strength at PGLT+10°C. (b) Boxplot for pairwise comparison.

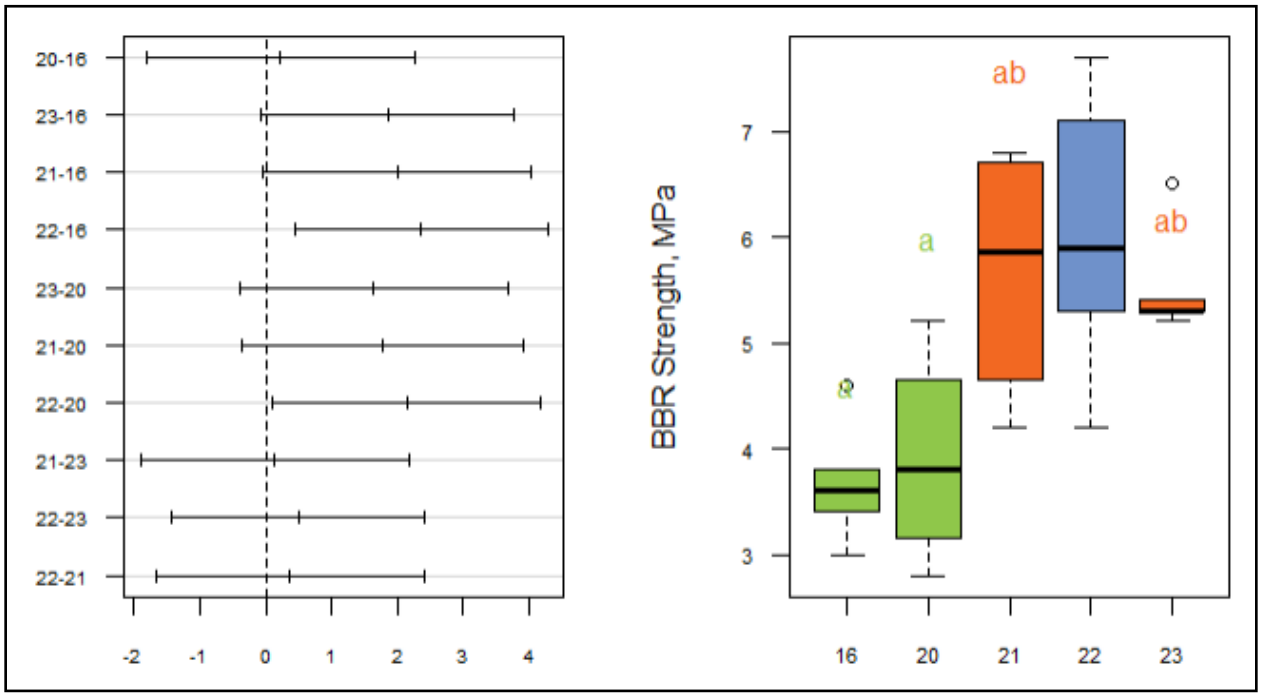

Figure 7.6: (a) Confidence intervals (Tukey) for PAV binder BBR Strength at PGLT+4°C. (b) Boxplot for pairwise comparison.

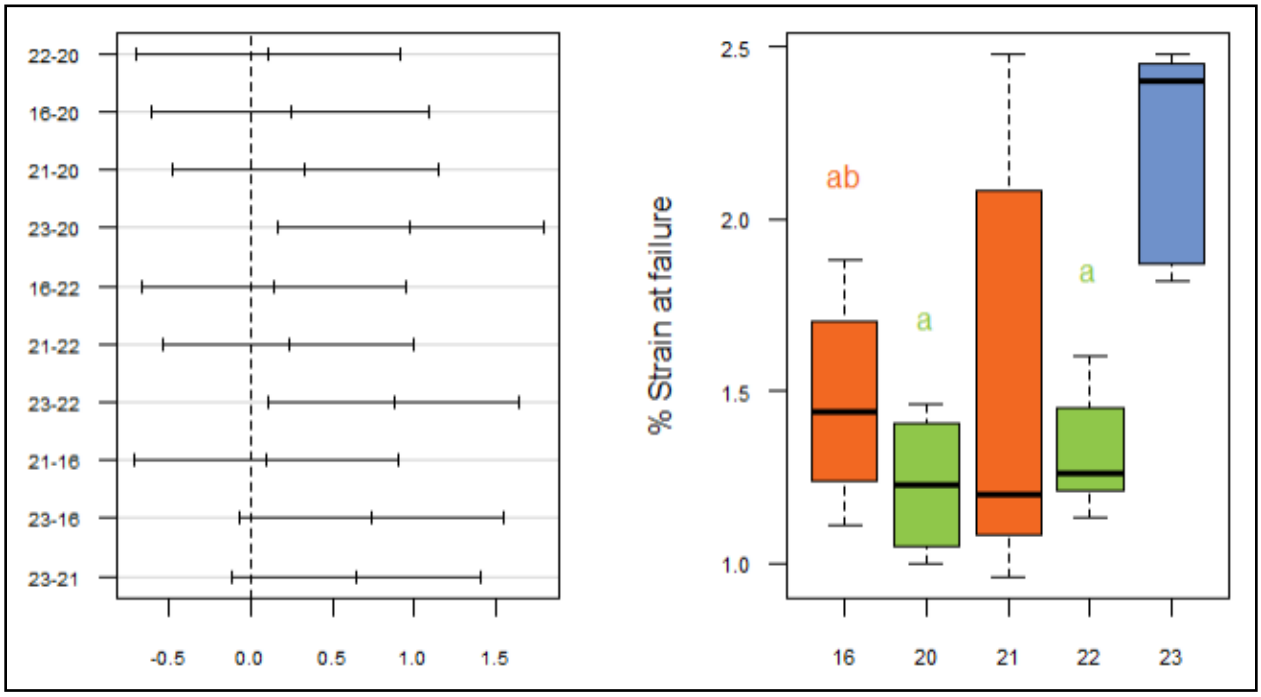

Figure 7.7: (a) Confidence intervals (Tukey) for PAV binder BBR Strain at failure at PGLT+10°C. (b) Boxplot for pairwise comparison.

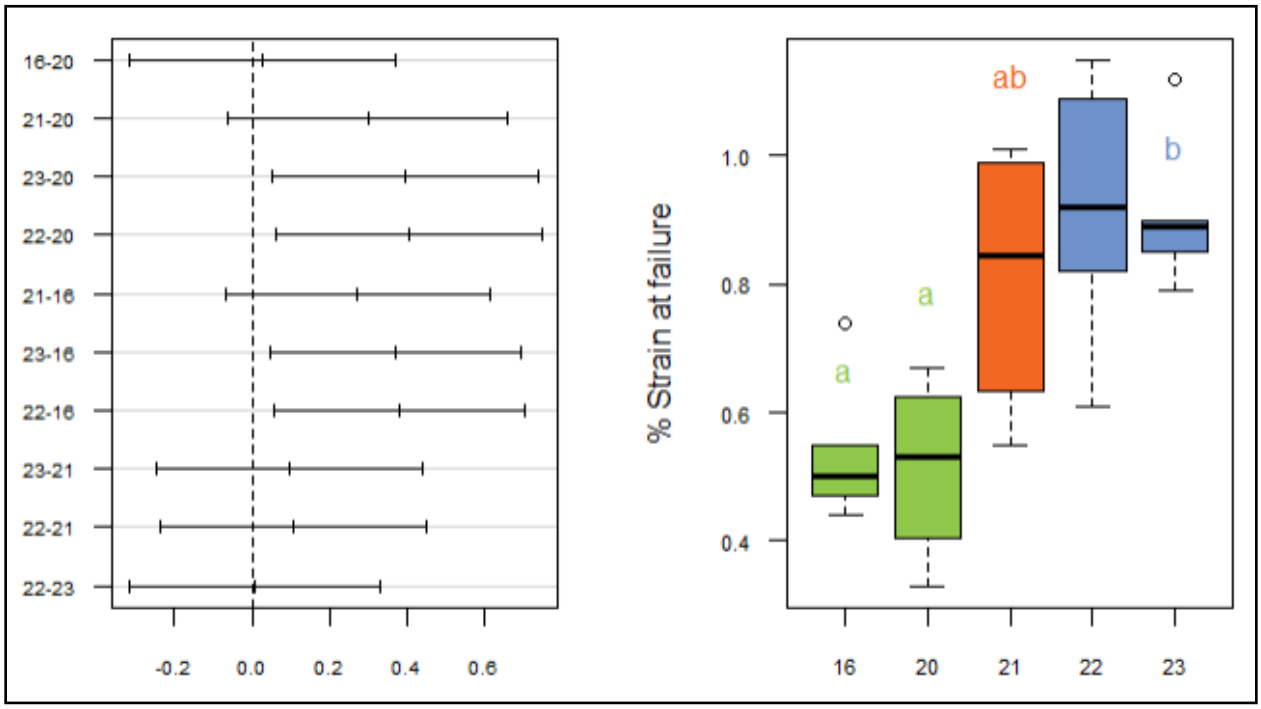

Figure 7.8: (a) Confidence intervals (Tukey) for PAV binder BBR Strain at failure at PGLT+4°C. (b) Boxplot for pairwise comparison

Conclusions

A summary of the boxplots results from figures 7.1 to 7.8 is presented in figure 7.9. For each of the properties investigated, the cells filled with the same pattern have means that belong to the same group.

	Temperature	Cells				
		16	20	21	22	23
Binder BBR Creep Stiffness (60s), MPa	PGLT+10C					
	PGLT+4C					
Binder m-value (60s)	PGLT+10C					
	PGLT+4C					
Binder BBR Strength, MPa	PGLT+10C					
	PGLT+4C					
Binder BBR Strain @ Failure, %	PGLT+10C					
	PGLT+4C					

Figure 7.9: Summary of boxplots for PAV binder results.

A number of important observations can be made. The grouping of binders based on similar rheological or strength characteristics changes with temperature. For example, in Figures 7.1 and 7.2, binders in cells 16 and 23 belong to one group and binders from cells 20, 21, and 22 belong to a different group, based on S(60s) results at PGLT+10°C. The grouping changes for PGLT+4°C.

From Figures 7.3 and 7.4, it is observed that the grouping based on m-value is different than the grouping based on S(60s). Binders in cells 21 and 22 are placed in the same group based on stiffness and m-value, except for m-value at PGLT+4°C. However, the two binders are grouped separately with respect to failure properties, except for BBR Strength at PGLT+10°C.

As mentioned before, the binder in cell 22 contains an antistripping agent. The most visible difference is observed in Figures 7.5 and 7.7 regarding the failure properties at PGLT+10°C. In both figures, the modified binder in cell 23 is grouped alone with the highest stress and strain at failure. The grouping changes at PGLT+4°C; based on strength, cell 21 and 23 binders are grouped together, and based on failure strain, cell 22 and 23 binders are grouped together.

Binders in cells 20 to 23 have the same PGLT of -34, however, the failure properties are significantly different based on the statistical analyses performed. In particular, the heavily modified asphalt binder used in cell 23 has significantly better failure stress and strain than the other binders at PGLT +10°C. It was also noticed that the addition of antistripping agent may significantly change failure properties.

7.3 MIXTURES ANOVA

Similar to binder analysis, one-way ANOVA was performed to determine the statistical significance of the mixture properties. The significance level (α) was set at 0.05. The null hypothesis (H_0) assumes that all the sample means are equal. The alternate hypothesis (H_a) states that at least one of the sample means is different.

Mixture BBR Creep Test

Table 7.9: shows the ANOVA results for the creep stiffness at 60 seconds at -12°C and Table 7.10 shows the results at -24°C.

Table 7.9: Summary and ANOVA: BBR Creep Stiffness at -12°C.

SUMMARY

Groups	Count	Sum	Average	Variance
Cell 16	6	40.08251	6.680419	0.519472
Cell 17	5	34.7625	6.952501	0.570816
Cell 18	5	35.19701	7.039402	1.194998
Cell 19	6	42.14436	7.024061	0.575539
Cell 20	5	22.49815	4.49963	0.562762
Cell 21	5	26.10168	5.220336	0.396015
Cell 22	5	32.7937	6.558741	0.122235
Cell 23	5	29.15639	5.831278	0.10331

ANOVA

Source of Variation	SS	df	MS	F	P-value	F crit
Between Groups	32.26184	7	4.608834	9.070614	2.82E-06	2.293832
Within Groups	17.2756	34	0.508106			
Total	49.53744	41				

The F-value is greater than the F-critical value and the p-value is smaller than the alpha level selected (0.05). We can conclude that there is enough evidence to reject the null hypothesis and say that at least one of the eight cells has significantly different means and belongs to a different population.

Table 7.10: Summary and ANOVA: BBR Creep Stiffness at -24°C.

SUMMARY

Groups	Count	Sum	Average	Variance
Cell 16	6	83.09406	13.84901	3.31136
Cell 17	6	85.94299	14.32383	2.880214
Cell 18	6	79.87011	13.31168	4.486247
Cell 19	6	67.40177	11.23363	5.167274
Cell 20	4	38.46447	9.616118	2.096874
Cell 21	5	56.10079	11.22016	1.994548
Cell 22	5	55.60792	11.12158	1.015567
Cell 23	6	55.35543	9.225906	6.617964

ANOVA

Source of Variation	SS	df	MS	F	P-value	F crit
Between Groups	141.7022	7	20.24317	5.578065	0.000208	2.277143
Within Groups	130.6464	36	3.629066			
Total	272.3485	43				

The F-value is greater than F-critical value and the p-value is smaller than the alpha level selected (0.05). We can conclude that there is enough evidence to reject the null hypothesis and say that at least one of the eight cells has significantly different means and belongs to a different population.

Table 7.11 shows the ANOVA results for the m-value at 60 seconds at -12°C and Table 7.12 shows the results at -24°C.

Table 7.11: Summary and ANOVA: BBR m-value at -12°C.

SUMMARY

Groups	Count	Sum	Average	Variance
Cell 16	6	0.991384	0.165231	6.94E-05
Cell 17	5	0.847218	0.169444	0.000341
Cell 18	5	0.831543	0.166309	0.000547
Cell 19	6	0.916513	0.152752	0.000313
Cell 20	5	1.147023	0.229405	0.001471
Cell 21	5	0.787838	0.157568	0.000555
Cell 22	5	0.739767	0.147953	9.86E-05
Cell 23	5	0.900643	0.180129	0.000159

ANOVA

Source of Variation	SS	df	MS	F	P-value	F crit
Between Groups	0.02334	7	0.003334	7.767326	1.31E-05	2.293832
Within Groups	0.014595	34	0.000429			
Total	0.037936	41				

The F-value is greater than F-critical value and the p-value is smaller than the alpha level selected (0.05). We can conclude that there is enough evidence to reject the null hypothesis and say that at least one of the eight cells has significantly different means and belongs to a different population.

Table 24 shows the ANOVA results for the m-value at 60 seconds at -24°C.

Table 7.12: Summary and ANOVA: BBR m-value at -24°C.

SUMMARY

Groups	Count	Sum	Average	Variance
Cell 16	6	0.439436	0.073239	0.000194
Cell 17	6	0.42558	0.07093	0.000134
Cell 18	6	0.404354	0.067392	3.17E-05
Cell 19	6	0.360941	0.060157	0.000182
Cell 20	4	0.420792	0.105198	0.000208
Cell 21	5	0.446598	0.08932	0.000164
Cell 22	5	0.422087	0.084417	0.000104
Cell 23	6	0.635542	0.105924	0.001613

ANOVA

Source of Variation	SS	df	MS	F	P-value	F crit
Between Groups	0.01116	7	0.001594	4.602886	0.000932	2.277143
Within Groups	0.012469	36	0.000346			
Total	0.023628	43				

The F-value is greater than F-critical value and the p-value is smaller than the alpha level selected (0.05). We can conclude that there is enough evidence to reject the null hypothesis and say that at least one of the eight cells has significantly different means and belongs to a different population.

Mixture BBR Strength Test

Table 7.13 shows the ANOVA results for BBR Strength at -12°C and Table 7.14 shows the results at -24°C. Table 7.15 shows the ANOVA results for BBR Strain at failure at -12°C and Table 7.16 shows the results at -24°C.

Table 7.13: Summary and ANOVA: BBR Strength at -12°C.

SUMMARY

Groups	Count	Sum	Average	Variance
Cell 16	6	44.0017	7.333617	0.912385
Cell 17	5	39.38142	7.876284	1.032498
Cell 18	5	36.41527	7.283053	0.739151
Cell 19	6	45.23467	7.539111	2.867397
Cell 20	5	44.16813	8.833626	0.865144
Cell 21	5	40.33591	8.067182	0.663624
Cell 22	5	34.54996	6.909992	0.329096
Cell 23	5	37.00941	7.401883	0.767537

ANOVA

Source of Variation	SS	df	MS	F	P-value	F crit
Between Groups	12.52358	7	1.789083	1.667132	0.150505	2.293832
Within Groups	36.48711	34	1.07315			
Total	49.01069	41				

The F-value is smaller than the F-critical value and the p-value is greater than the alpha level selected (0.05). We fail to reject the null hypothesis and conclude that all samples belong to the same population.

Table 7.14: Summary and ANOVA: BBR Strength at -24°C.

SUMMARY

Groups	Count	Sum	Average	Variance
Cell 16	6	44.94035	7.490058	1.175196
Cell 17	6	42.77968	7.129946	0.39847
Cell 18	6	41.1805	6.863417	0.409845
Cell 19	6	42.70459	7.117432	0.959679
Cell 20	4	31.56955	7.892388	0.65469
Cell 21	5	42.43565	8.48713	1.263511
Cell 22	5	31.60383	6.320765	0.08775
Cell 23	6	43.57851	7.263085	1.905921

ANOVA

Source of Variation	SS	df	MS	F	P-value	F crit
Between Groups	14.98285	7	2.140407	2.437307	0.037503	2.277143
Within Groups	31.61467	36	0.878185			
Total	46.59752	43				

The F-value is greater than the F-critical value and the p-value is smaller than the alpha level selected (0.05). We can conclude that there is enough evidence to reject the null hypothesis and say that at least one of the eight cells has significantly different means and belongs to a different population.

Table 7.15: Summary and ANOVA: BBR strain at failure at -12°C.

SUMMARY

Groups	Count	Sum	Average	Variance
Cell 16	6	0.559789	0.093298	0.000653
Cell 17	5	0.465868	0.093174	0.000305
Cell 18	5	0.423679	0.084736	7.45E-05
Cell 19	6	0.557169	0.092862	0.000598
Cell 20	5	0.952075	0.190415	0.002734
Cell 21	5	0.643318	0.128664	3.29E-06
Cell 22	5	0.576388	0.115278	0.000593
Cell 23	5	0.654667	0.130933	0.001433

ANOVA

Source of Variation	SS	df	MS	F	P-value	F crit
Between Groups	0.043368	7	0.006195	7.851663	1.18E-05	2.293832
Within Groups	0.026828	34	0.000789			
Total	0.070196	41				

The F-value is greater than F-critical value and the p-value is smaller than the alpha level selected (0.05). We can conclude that there is enough evidence to reject the null hypothesis and say that at least one of the eight cells has significantly different means and belongs to a different population.

Table 7.16: Summary and ANOVA: BBR strain at failure at -24°C.

SUMMARY

Groups	Count	Sum	Average	Variance
Cell 16	6	0.315864	0.052644	6.54E-05
Cell 17	6	0.326389	0.054398	0.000182
Cell 18	6	0.30703	0.051172	0.000131
Cell 19	6	0.332629	0.055438	0.000162
Cell 20	4	0.732814	0.183203	0.054309
Cell 21	5	0.430993	0.086199	0.000572
Cell 22	5	0.299483	0.059897	3.21E-05
Cell 23	6	0.433834	0.072306	0.000208

ANOVA

Source of Variation	SS	df	MS	F	P-value	F crit
Between Groups	0.059559	7	0.008508	1.811557	0.115081	2.277143
Within Groups	0.169082	36	0.004697			
Total	0.228641	43				

The F-value is smaller than F-critical and the p-value is greater than the alpha level selected (0.05). We fail to reject the null hypothesis and conclude that all samples belong to the same population.

Mixture SCB Fracture Energy

Table 7.17 shows the ANOVA results for SCB Fracture Energy at -12°C and Table 7.18 shows the results at -24°C.

Table 7.17: Summary and ANOVA: SCB Fracture Energy at -12°C.

SUMMARY

Groups	Count	Sum	Average	Variance
Cell 16	3	1.003823	0.334608	0.004947
Cell 17	3	1.456573	0.485524	0.009754
Cell 18	3	1.174952	0.391651	0.00965
Cell 19	3	1.016278	0.338759	0.00276
Cell 20	3	1.83921	0.61307	0.012798
Cell 21	3	1.682961	0.560987	0.00172
Cell 22	3	0.922232	0.307411	0.011394
Cell 23	3	1.248463	0.416154	0.001139

ANOVA

Source of Variation	SS	df	MS	F	P-value	F crit
Between Groups	0.263586	7	0.037655	5.561874	0.002181	2.657197
Within Groups	0.108323	16	0.00677			
Total	0.371909	23				

The F-value is greater than F-critical and the p-value is smaller than the alpha level selected (0.05). We can conclude that there is enough evidence to reject the null hypothesis and say that at least one of the eight cells has significantly different means and belongs to a different population.

Table 7.18: Summary and ANOVA: SCB Fracture Energy at -24°C.

SUMMARY

Groups	Count	Sum	Average	Variance
Cell 16	2	0.492638	0.246319	0.000132
Cell 17	3	0.710202	0.236734	0.002438
Cell 18	3	0.830685	0.276895	0.010503
Cell 19	3	0.787809	0.262603	0.003534
Cell 20	3	0.897585	0.299195	0.00064
Cell 21	3	0.888231	0.296077	0.003807
Cell 22	3	0.594989	0.19833	0.002021
Cell 23	3	0.944716	0.314905	0.003406

ANOVA

Source of Variation	SS	df	MS	F	P-value	F crit
Between Groups	0.030631	7	0.004376	1.242466	0.34058	2.706627
Within Groups	0.052829	15	0.003522			
Total	0.083461	22				

The F-value is smaller than F-critical and the p-value is greater than the alpha level selected (0.05). We fail to reject the null hypothesis and conclude that all samples belong to the same population.

Mixture IDT Creep Stiffness

Table 7.19 shows the ANOVA results for IDT Creep Stiffness at -12°C and Table 7.20 shows the results at -24°C.

Table 7.19: Summary and ANOVA: IDT Creep Stiffness at -12°C.

SUMMARY

Groups	Count	Sum	Average	Variance
Cell 16	3	31.58793	10.52931	2.416582
Cell 17	3	30.15939	10.05313	8.151594
Cell 18	3	42.94082	14.31361	10.55296
Cell 19	3	37.09468	12.36489	0.108503
Cell 20	3	22.34644	7.448814	2.190468
Cell 21	3	25.26369	8.421228	9.861322
Cell 22	3	35.07929	11.6931	5.940764
Cell 23	3	27.89484	9.298279	6.992166

ANOVA

Source of Variation	SS	df	MS	F	P-value	F crit
Between Groups	104.1562	7	14.87946	2.57573	0.055492	2.657197
Within Groups	92.42871	16	5.776794			
Total	196.585	23				

The F-value is smaller than F-critical and the p-value is greater than the alpha level selected (0.05). We fail to reject the null hypothesis and conclude that all samples belong to the same population.

Table 7.20: Summary and ANOVA: IDT Creep Stiffness at -24°C.

SUMMARY

Groups	Count	Sum	Average	Variance
Cell 16	3	54.72349	18.24116	30.13118
Cell 17	3	48.97575	16.32525	3.209443
Cell 18	3	76.32289	25.44096	86.15953
Cell 19	3	51.95776	17.31925	6.344415
Cell 20	3	47.33985	15.77995	2.549091
Cell 21	3	52.50076	17.50025	7.51289
Cell 22	3	47.9055	15.9685	2.971263
Cell 23	3	42.12068	14.04023	0.327909

ANOVA

Source of Variation	SS	df	MS	F	P-value	F crit
Between Groups	246.743	7	35.24901	2.025722	0.114803	2.657197
Within Groups	278.4115	16	17.40072			
Total	525.1545	23				

The F-value is smaller than F-critical and the p-value is greater than the alpha level selected (0.05). We fail to reject the null hypothesis and conclude that all samples belong to the same population.

From tables 7.9 to 7.20 is it possible to conclude that the mixture properties that present statistical significance are BBR creep stiffness at -12°C and -24°C, BBR m-value at -12°C and -24°C, BBR strength at -24°C, BBR strain at failure at -12°C and SCB fracture energy at -12°C.

7.4 MIXTURES TUKEY ANALYSIS

Since ANOVA only indicates if one or more mixtures have different means, it is necessary to run an additional test to find out the specific differences. Tukey's method, a pairwise comparison technique, was chosen because it constructs simultaneous confidence intervals for differences of all pairs of means and controls the probability of making one or more Type I errors.(Oehlert, 2000)

The confidence intervals and boxplot were generated for all mixtures and corresponding properties. Figures 7.10 (a) to 7.16 (a) show the pairwise confidence intervals and Figures 7.10 (b) to 7.16 (b) show the boxplot for pairwise comparison. The boxplots provide a visual interpretation of the confidence intervals where cells are grouped according to their means. Cells with the same color and letter belong to the same group.

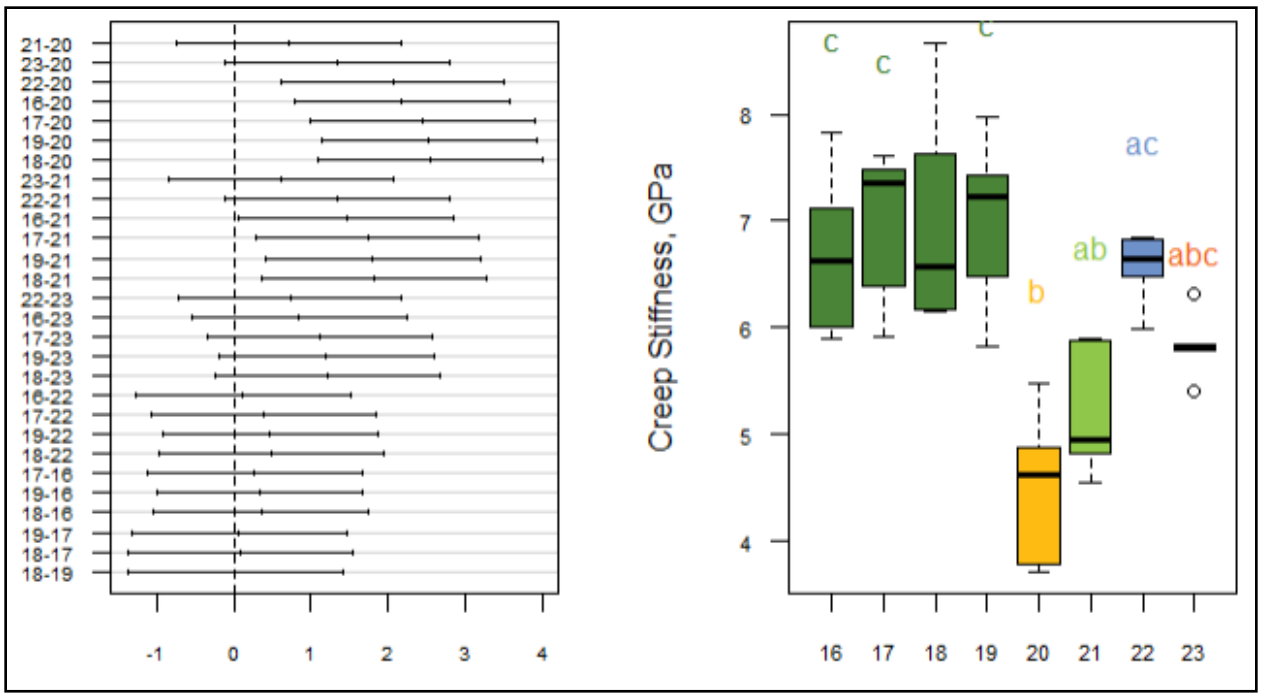

Figure 7.10: (a) Confidence intervals (Tukey) for BBR Creep Stiffness at -12°C. (b) Boxplot for pairwise comparison.

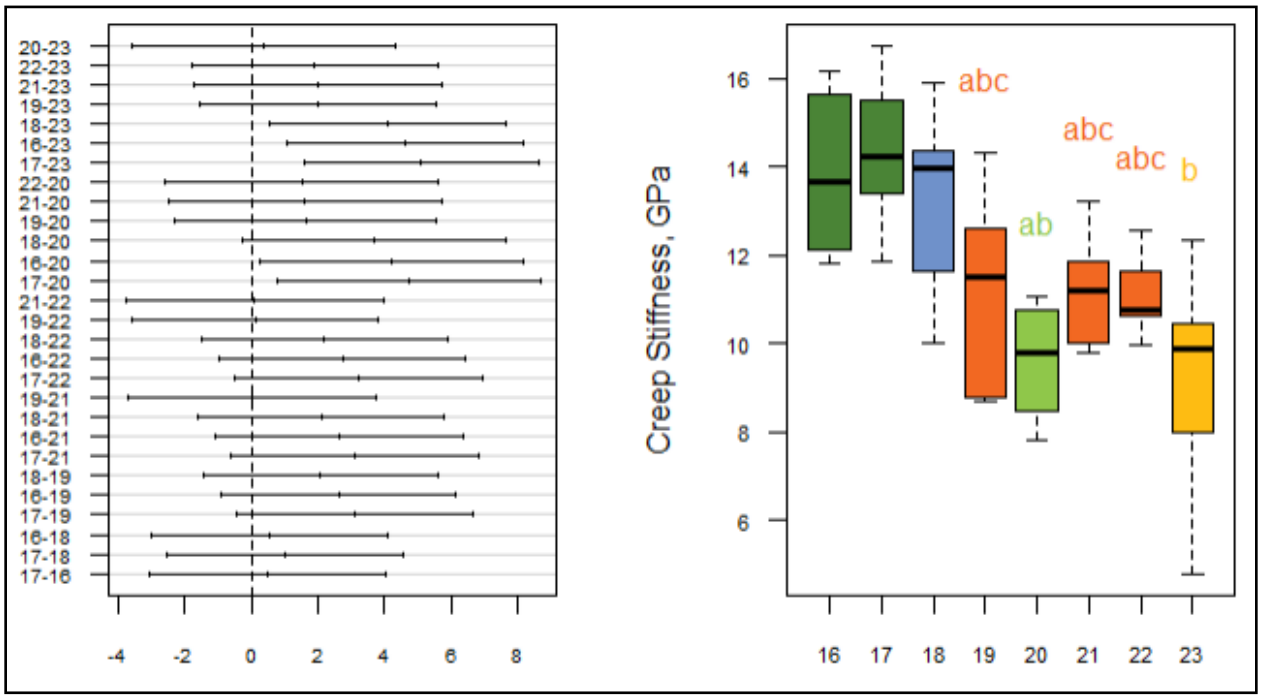

Figure 7.11: (a) Confidence intervals (Tukey) for BBR Creep Stiffness at -24°C. (b) Boxplot for pairwise comparison.

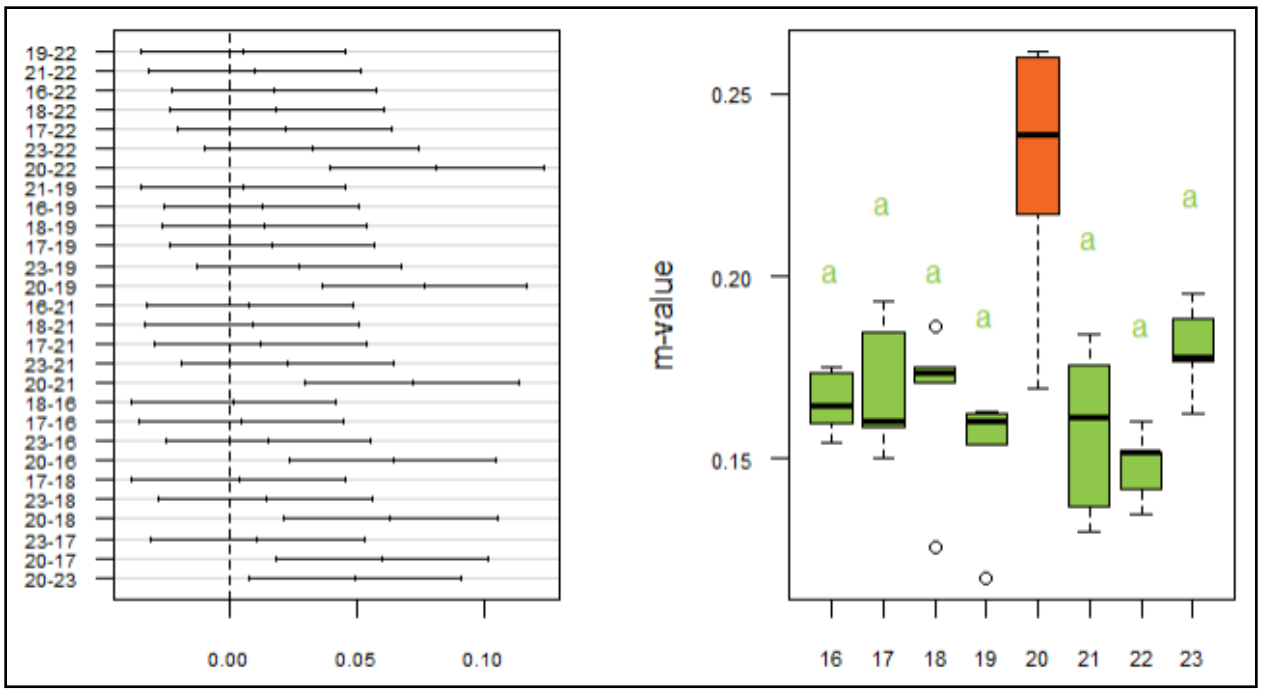

Figure 7.12: (a) Confidence intervals (Tukey) for BBR m-value at -12°C. (b) Boxplot for pairwise comparison.

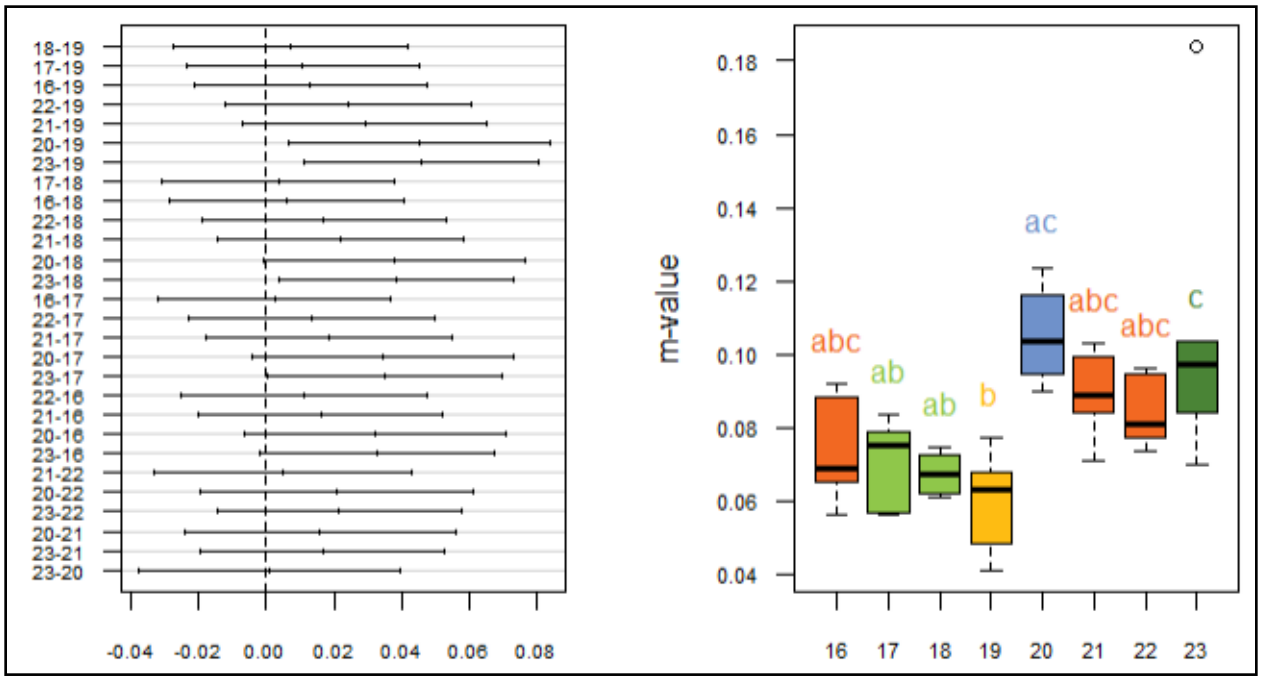

Figure 7.13: (a) Confidence intervals (Tukey) for BBR m-value at -24°C. (b) Boxplot for pairwise comparison.

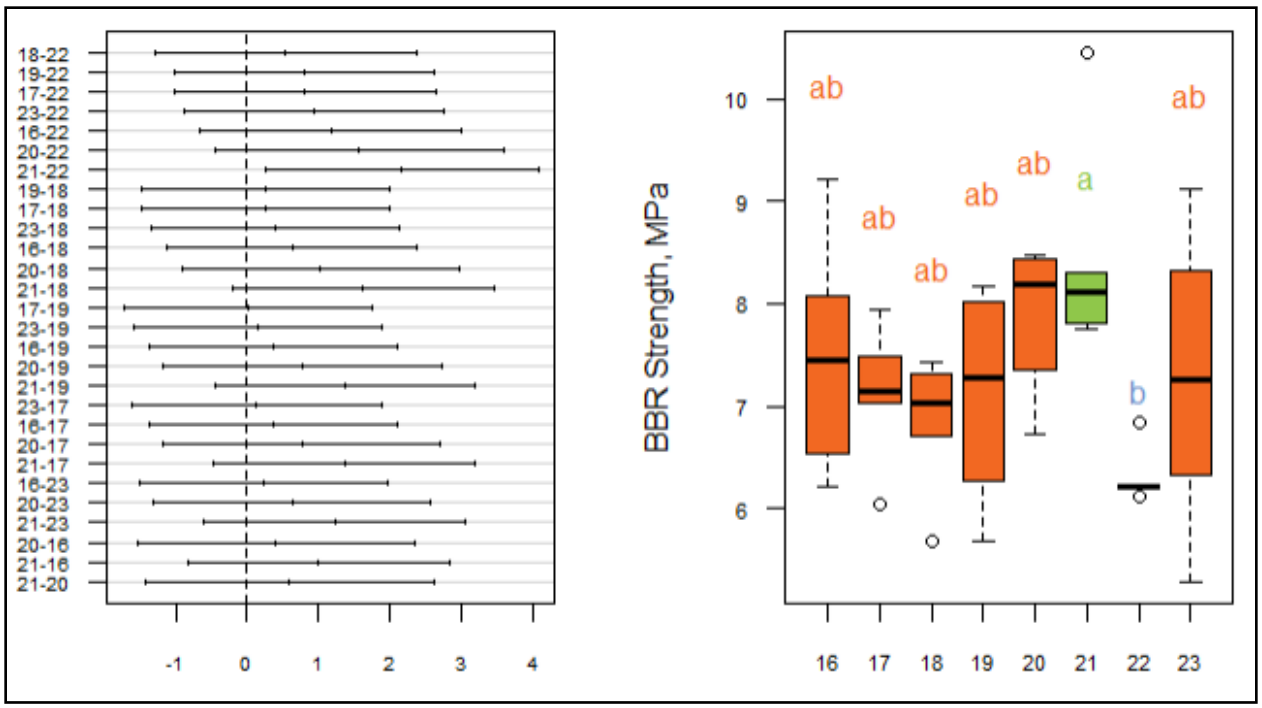

Figure 7.14: (a) Confidence intervals (Tukey) for BBR strength at -24°C. (b) Boxplot for pairwise comparison.

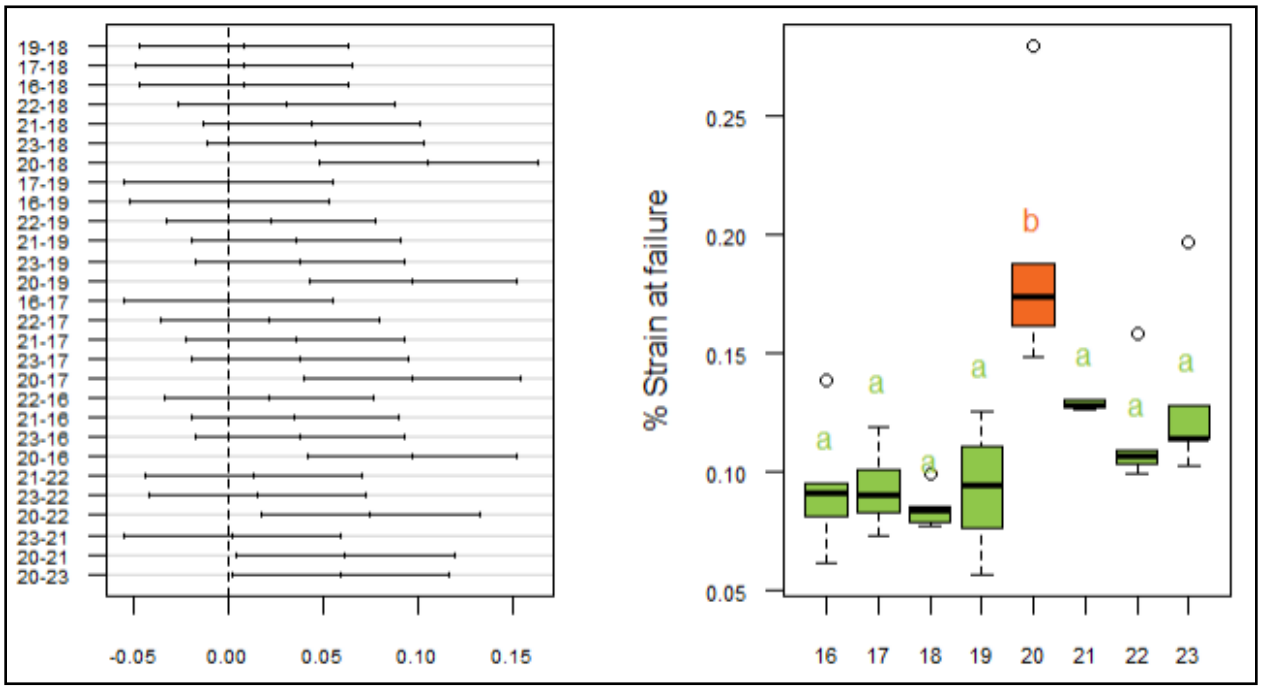

Figure 7.15(a) Confidence intervals (Tukey) for BBR % strain at failure at -12°C. (b) Boxplot for pairwise comparison.

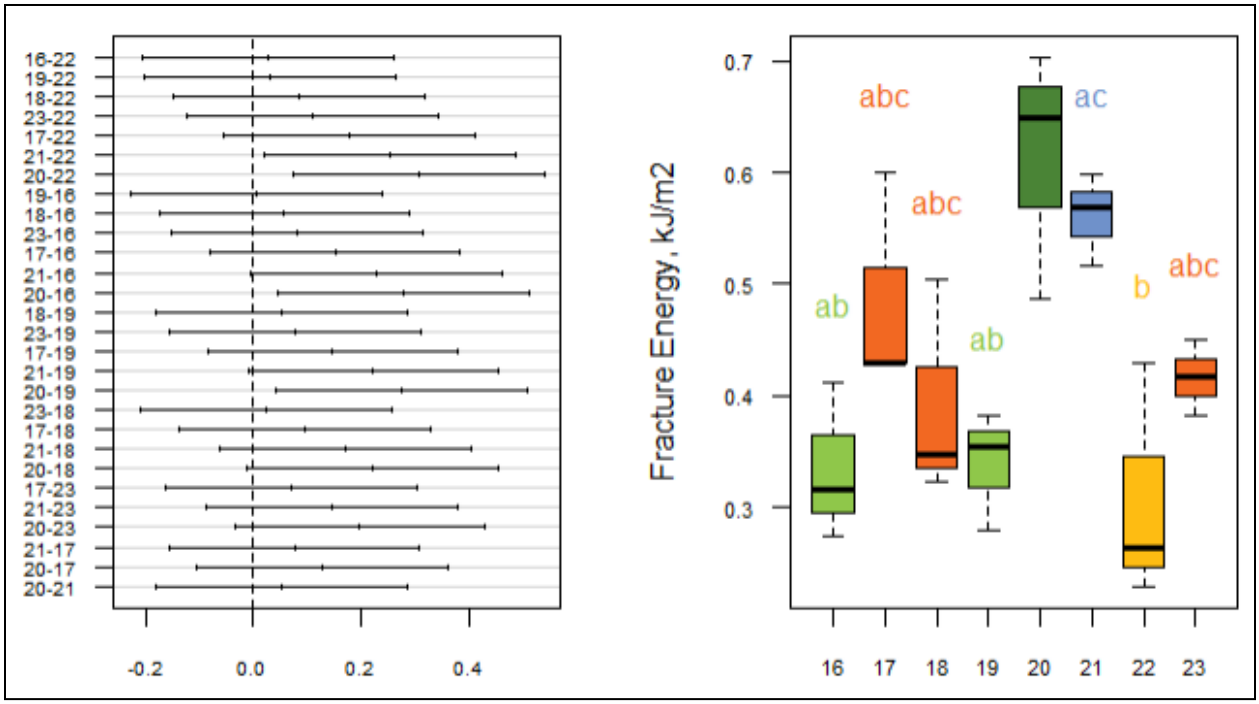

Figure 7.16: (a) Confidence intervals (Tukey) for fracture energy at -12°C. (b) Boxplot for pairwise comparison.

Conclusions

A summary of the boxplots from figures 7.10 to 7.16 is presented in figure 7.17. For each property, cells filled with the same pattern have means that belong to the same group. The summary presented in figure 7.17 does not contain entries for all temperatures because the boxplots and Tukey analyses were performed only on parameters that had a significant result in the ANOVA test. For example, IDT creep and strength placed all mixtures in the same group.

	Temperature	Cells							
		16	17	18	19	20	21	22	23
Mixture BBR Creep Stiffness (60s), GPa	-12C								
	-24C								
Mixture m-value (60s)	-12C								
	-24C								
Mixture BBR Strength, MPa	-24C								
Mixture BBR Strain @ Failure, %	-12C								
Fracture Energy, kJ/m2	-12C								

Figure 7.17: Summary of boxplots for mixture results.

A number of conclusions can be drawn. Cells 16, 17, 18 and 19, built with the same binder type, are in the same group for most of the determined properties. The only significant differences are observed for S(60s) and m(60s) at -24°C and Fracture Energy at -12°C.

For almost all of the mixture properties analyzed, cell 20 mixture is in a different group than other mixtures. This mixture has the highest percentage of RAP, 30%, which may explain this observation. Cell 23 mixture, which has a highly modified binder, is also in a different group for BBR creep stiffness at both temperatures and m-value at -24°C.

Overall, it is observed that for some properties, there is no clear separation between the mixtures prepared with the PG-22 binder and the mixtures prepared with the PG-34 binders. One possible explanation is given by the fact that the mix designs have RAP and RAS contents that could influence in which group the mixture is placed.

7.5 CORRELATIONS

In order to measure the strength and direction of the relationships between mixtures properties and design properties, correlation matrices were calculated based on Pearson's correlation. The correlation coefficients are summarized in tables 7.21 and 7.22. The matrix was generated with data from cells 16 to 23 at -12°C and at -24°C. The coefficients with values larger than 0.75 are highlighted in bold.

The results show that coefficients change with temperature and correlations that are significant at one temperature are not significant at the other temperature, which indicates the need to perform testing at multiple temperatures. The only exception is the correlation between the BBR m-value and BBR failure strain, who have strong positive correlations at both temperature. One other significant observation is the high correlation values between mixture fracture energy and BBR mixture S(60s), m(60s), and strength at -12°C.

No significant correlations are observed between the mechanical properties and the mix design parameters, most likely due to the different combinations of design parameters in each mix design. The only exception is the negative correlation between total AC % and fracture toughness at -24°C. However, a lower asphalt content can have a negative effect on other important properties of the mixture.

Table 7.21: Correlation matrix for properties from cells 16 to 23 at -12°C.

	1	2	3	4	5	6	7	8	9	10	11	12	13	14	15
1. Mixture IDT S(60s) (GPa)	1.00														
2. Mix IDT Strength, MPa	-0.42	1.00													
3. Mix BBR m-value (60s)	-0.69	0.30	1.00												
4. Mix BBR S(60s)	0.80	-0.20	-0.88	1.00											
5. Mix BBR Failure Strain, %	-0.75	0.39	0.81	-0.92	1.00										
6. Mix BBR Strength, MPa	-0.67	0.64	0.69	-0.62	0.64	1.00									
7. Fracture Energy Gf	-0.75	0.23	0.79	-0.80	0.63	0.79	1.00								
8. Fracture Toughness	-0.45	0.31	0.07	-0.30	0.16	0.51	0.59	1.00							
9. VMA	0.09	0.00	0.05	0.22	-0.25	0.43	0.26	0.07	1.00						
10. Design Air void (Va)	-0.34	-0.30	0.28	-0.36	0.16	-0.25	0.33	0.06	-0.46	1.00					
11. RAP %	-0.23	0.53	0.59	-0.57	0.74	0.46	0.30	-0.04	-0.29	-0.04	1.00				
12. RAS %	-0.06	0.03	-0.07	0.37	-0.39	-0.14	-0.11	-0.33	0.35	0.22	-0.48	1.00			
13. Total AC %	0.53	-0.27	-0.51	0.41	-0.18	-0.23	-0.48	-0.31	0.22	-0.57	-0.01	-0.29	1.00		
14. Virgin AC %	0.42	-0.52	-0.57	0.26	-0.28	-0.31	-0.31	0.19	-0.01	-0.37	-0.33	-0.61	0.64	1.00	
15. % Effective AC	0.41	0.18	-0.20	0.41	-0.29	0.31	-0.16	-0.04	0.75	-0.90	-0.04	-0.05	0.50	0.26	1.00

Table 7.22: Correlation matrix for properties from cells 16 to 23 at -24°C.

	1	2	3	4	5	6	7	8	9	10	11	12	13	14	15
1. Mixture IDT S(60s) (GPa)	1.00														
2. Mix IDT Strength, MPa	-0.65	1.00													
3. Mix BBR m-value (60s)	-0.55	0.57	1.00												
4. Mix BBR S(60s)	0.48	-0.78	-0.55	1.00											
5. Mix BBR Failure Strain, %	-0.36	0.64	0.83	-0.55	1.00										
6. Mix BBR Strength, MPa	-0.36	0.21	0.19	-0.45	0.24	1.00									
7. Fracture Energy Gf	-0.02	0.31	0.47	-0.69	0.40	0.25	1.00								
8. Fracture Toughness	-0.14	0.27	0.45	-0.50	0.37	0.34	0.90	1.00							
9. VMA	0.13	-0.48	-0.31	0.41	-0.17	-0.14	-0.07	0.10	1.00						
10. Design Air void (Va)	0.03	-0.15	0.55	0.15	0.24	0.00	0.04	0.03	-0.46	1.00					
11. RAP %	0.09	0.60	0.35	-0.37	0.74	-0.02	0.25	0.17	-0.29	-0.04	1.00				
12. RAS %	-0.05	-0.44	-0.19	0.73	-0.42	-0.22	-0.40	-0.03	0.35	0.22	-0.48	1.00			
13. Total AC %	0.06	-0.09	-0.54	0.18	-0.21	-0.06	-0.66	-0.77	0.22	-0.57	-0.01	-0.29	1.00		
14. Virgin AC %	0.00	-0.10	-0.30	-0.27	-0.27	0.18	-0.10	-0.40	-0.01	-0.37	-0.33	-0.61	0.64	1.00	
15. % Effective AC	0.23	-0.19	-0.61	0.13	-0.29	-0.15	-0.04	0.00	0.75	-0.90	-0.04	-0.05	0.50	0.26	1.00

CHAPTER 8: SUMMARY, CONCLUSIONS, AND RECOMMENDATIONS

In this research effort, an investigation was performed to determine if four testing methods can be viably used in the material selection process, quality control, and forensic investigations of asphalt paving materials. These test methods are the Bending Beam Rheometer (BBR) for creep and strength of asphalt mixtures; low temperature SCB fracture testing for asphalt mixtures; E* testing of asphalt mixtures using the IDT configuration; and BBR strength testing of asphalt binders.

The results show that the testing methods investigated provide repeatable results that follow trends similar to the one observed using traditional methods. The results also show that the properties are highly temperature dependent and the ranking observed at one temperature can change at a different temperature. In addition, it is observed that materials with similar rheological properties, such as complex modulus absolute value |E*|, creep stiffness S, and m-value, do not necessarily have the same fracture resistance. These results confirm one more time the need for a fracture/strength test for correctly evaluating cracking resistance of asphalt materials.

The results also show that, in general, the mixtures used in this experiment have similar properties, which may indicate similar service performance. The only exceptions appear to be the mixture from cell 20 that has the highest RAP content and the mixture from cell 23 that contains a highly modified binder; for most properties evaluated, the two mixtures were each grouped separately from the other mixtures (Table 7.17). The results also indicate that, for some properties, there is no clear separation between the mixtures prepared with the PG-22 binder and the mixtures prepared with the PG-34 binders due to the addition of RAP and RAS in the mix design.

A number of follow-up steps are required to fully evaluate the value of these test methods in the selection process. It is recommended that cores are taken at periodic intervals of time and testing is performed on samples obtained from these cores using the methods described in this report. These methods allow for obtaining representative samples from the surface layer of the pavement, where most cracking occurs. Most importantly, distress surveys should be performed periodically and correlations should be developed to determine the best predictors of performance that can be used to better select asphalt paving materials with good cracking resistance.

REFERENCES

AASHTO (American Association of State Highway and Transportation Officials). (2010). Standard specification for performance-graded asphalt binder. Specification M320-10. AASHTO, Washington D. C.

AASHTO (American Association of State Highway and Transportation Officials). (2012). Standard practice for accelerated aging of asphalt binder using a pressurized aging vessel (PAV). Specification R028-12. AASHTO, Washington D. C.

AASHTO (American Association of State Highway and Transportation Officials). (2013). Standard method of test for effect of heat and air on a moving film of asphalt binder (rolling thin-film oven test). Specification T240-13. AASHTO, Washington D. C.

AASHTO (American Association of State Highway and Transportation Officials). (2012). Standard method of test for determining the flexural creep stiffness of asphalt binder using the bending beam rheometer (BBR). Specification T 313-12. AASHTO, Washington D. C.

AASHTO (American Association of State Highway and Transportation Officials). (2012). Standard method of test for determining the fracture properties of asphalt binder in Direct Tension (DT). Specification T 314-12. AASHTO, Washington D. C.

AASHTO (American Association of State Highway and Transportation Officials). Designation: TP 125-(16) Standard Method of Test for Determining the Flexural Creep Stiffness of Asphalt Mixtures Using the Bending Beam Rheometer (BBR). AASHTO, Washington D. C.

AASHTO (American Association of State Highway and Transportation Officials). (2013). Standard Method of Test for Determining the Fracture Energy of Asphalt Mixtures Using the Semicircular Bend Geometry (SCB). Specification TP105. AASHTO, Washington D. C.

AASHTO (American Association of State Highway and Transportation Officials). (2006). Standard Method of Test for Determining Dynamic Modulus of Hot-Mix Asphalt Concrete Mixtures. Specification TP62-03. AASHTO, Washington D. C.

AASHTO (American Association of State Highway and Transportation Officials). (2007). Standard Method of Test for Determining the Creep Compliance and Strength of Hot-Mix Asphalt (HMA) Using the Indirect Tension Test Device. Specification T322-07. AASHTO, Washington D. C.

Anderson, D. A., & Kennedy, T. (1993). Development of SHRP binder specification. *Journal of the Association of Asphalt Pavement Technologies, 62*, 481-507.

Anderson, D. A., & Marasteanu, M. O. (1999). Physical hardening of asphalt binders relative to their glass transition temperatures. *Transportation Research Record, 1661*, 24-37. doi: 10.3141/1661-05

Anderson, D., Christensen, D., Bahia, H. U., Dongre, R., Sharma, M., Antle, C., & Button J. (1994). *Binder characterization and evaluation vol. 3: physical characterization* (SHRPA-369). Washington, D.C. Strategic Highway Research Program, National Research Council.

Arnold, J. C. (1995). The influence of liquid uptake on environmental cracking of glassy polymer. *Materials Science and Engineering A, 197*, 119-124.

Bahia H. U. (1991). *Low-temperature isothermal physical hardening of asphalt cements* (Ph.D. Thesis). Pennsylvania State University, State College, PA.

Basu, A., Marasteanu, M. O., Hesp, S. (2003). Time-temperature superposition and physical hardening effects in low-temperature asphalt binder grading. *Transportation Research Record,* 1829, 1-8. doi: 10.3141/1829-01

Bažant, Z. P., & Planas, J. (1998). Fracture and size effect in concrete and other quasibrittle materials. Boca Raton, FL: CRC Press.

Burgess R. A., O. Kopvillem, & F.D. Young. (1971) Ste. Anne Test Road - Relationship between Predicted Fracture Temperatures and Low Temperature Field Performance. *Proceedings Association of Asphalt Pavement Technologies*, Vol. 40, pp. 148-193.

Cannone Falchetto, A., M. O. Marasteanu, & H. Di Benedetto (2011) Analogical based approach to forward and inverse problems for asphalt materials characterization at low temperatures, *Journal the Association of Asphalt Paving Technologists (AAPT)*, 80, 549-581.

Cannone Falchetto, A., J-L Le,., K. H. Moon, & M. O. Marasteanu (2013). Histogram testing for strength size effect in asphalt mixtures at low temperature. *Road Materials and Pavement Design,* 13 Supplement (1), 52-64. doi: 10.1080/14680629.2015.1084354

Christensen, R. M. (1971). *Theory of viscoelasticity: An introduction*. New York: Academic Press.

Dongré, R. (1994). Development of direct tension test method to characterize failure properties of asphalt cements. Ph.D. Thesis, Pennsylvania State University, State College, PA.

Dongré, R., & J. D'Angelo (1998). Effect of new direct tension test protocol on the Superpave low-temperature specification for bitumen binder. *Bearing Capacity of Roads and Airfields,* 2, 1035–1047.

Ferry, J. D. (1980). *Viscoelastic properties of polymers*. U.S.: Wiley& Sons.

Fréchet, M. (1927). Sur la loi de probabilité de l'écart maximum. *Annales de la Société Polonaise de Mathématique*, 6, 93–116.

G. W. Oehlert. (2000) A first course in design and analysis of experiments. *W. H. Freeman*, New York.

Hopkins I. L., & R. W. Hamming (1957) On creep and relaxation, *Journal of Applied Physics*, 28, 906-909.

Kim, Y., Seo, Y., King, M., & Momen, M. (2004). Dynamic modulus testing of asphalt concrete in indirect tension mode. *Transportation Research Record,* 1891, 163-173.

Le, J.-L., A. Cannone Falchetto, & M. O. Marasteanu. (2013) Determination of strength distribution of quasibrittle structures from size effect analysis. *Mechanics of Materials,* 66, 79-87.

Li, X. & M. O. Marasteanu. (2004) Evaluation of low temperature fracture resistance of asphalt mixtures using the semi-circular bend test. *Journal of the Association of Asphalt Paving Technologists,* 73, 401-426.

Lim, I. L., I. W. Johnson, & S. K. Choi. (1993) Stress intensity factor for semi-circular specimen under three-point bending. *Engineering Fracture Mechanics*, 44(3), 363-382.

Marasteanu O. M., & D. A. Anderson (1999) Improved Model for Bitumen Rheological Characterization. Presented at European Workshop on Performance-Related Properties for Bituminous Binders, Luxembourg.

Marasteanu, M. O., & D. A. Anderson (2000). Comparison of moduli for asphalt binders obtained from different test devices. *Journal of the Association of Asphalt Paving Technologists,* 69, 574-607.

Marasteanu, M. O., A. Basu, S. A. M. Hesp, & V. Voller (2004). Time-temperature superposition and AASHTO MP1a critical temperature for low-temperature cracking. *International Journal of Pavement Engineering*, 5(1), 31-38. doi: 10.1080/10298430410001720792

Marasteanu, M.O., A. Zofka, M. Turos, X. Li, R. Velasquez, X. Li, W. Buttlar, G. Paulino, A. Braham, E. Dave, J. Ojo, H. Bahia, C. J. Bausano, A. Gallistel, & J. McGraw, Investigation of Low Temperature Cracking in Asphalt Pavements: National Pooled Fund Study 776. (Report no. MnDOT 2007-43) Minnesota Department of Transportation, St. Paul, MN.

Marasteanu, M. O., W. Buttlar, G. Paulino, H. Bahia, C. Williams, K. H. Moon, E. Z. Teshale, A. C. Falchetto, M. Turos, E. Dave, S. Ahmed, S. Leon, A. Braham, B. Behnia, H. Tabatabaee, R. Velasquez, A. Arshadi, S. Puchalski, S. Mangiafico, J. Bausano, A. Buss, A. Kvasnak, Investigation of Low Temperature Cracking in Asphalt Pavements, National Pooled Fund Study Phase II (Report no. MnDOT 2012-23). Minnesota Department of Transportation Saint Paul, MN

Marasteanu, M. O., A. Cannone Falchetto, M. Turos, & J-L. Le (2012b). Development of a simple test to determine the low temperature strength of asphalt mixtures and binders (IDEA Program Final Report, NCHRP-151). Washington D. C.: Transportation Research Board of the National Academies.

Marasteanu, M., D. Ghosh, A. Cannone Falchetto, & M. Turos (2017). Testing protocol to obtain failure properties of asphalt binders at low temperature using creep compliance and stress-controlled strength test. *Road Materials and Pavement Design - EATA,* Taylor and Francis, vol. 18 (supplement 2), pp. 352-367, 2017. DOI: 10.1080/14680629.2017.1304246.

Minnesota Department of Transportation Standard Specifications for Construction, (2360) *Plant Mixed Asphalt Pavement,* 2018 Edition, St. Paul, Minnesota.

Moore, D. S., G. P. McCabe & B. A. Craig (2014). Introduction to the practice of statistics. *W. H. Freeman and Company*, New York.

Moskala, E. J. (1998). A fracture mechanics approach to environmental stress cracking in polyethylene terephtalate. *Polymer, 39(3)*, 675-680.

Readshaw, E. E. (1972). Asphalt specifications in British Columbia for low temperature performance. *Journal of the Association of Asphalt Paving Technologists*, 41, 562-581.

Readshaw, E. E. (1972) Asphalt specifications in British Columbia for low temperature performance. *Proceedings Association of Asphalt Paving Technologists*, 41, 562-581.

Romero, P. (2017) Balanced asphalt concrete mix performance, Phase II: Analysis of BBR and SCB tests. Report No. UT-17.21. Utah Department of Transportation, Salt Lake City, UT.

Romero, P., & K. Van Frank (2016) Using the bending beam rheometer for low temperature testing of asphalt mixtures. Report No. UT-16.09. Utah Department of Transportation, Salt Lake City, UT.

Rowe, G. M., S. H. Khoee, P. Blankenship, & K. C. Mahboub (2009). Evaluation of aspects of E* test by using hot-mix asphalt specimens with varying void contents. *Transportation Research Record*, 2127: 164 – 172.

Rubeck, R. A. (1981). Kinetics of environmental stress cracking in high-density polyethylene. *Polymer*, 22(5), 682-686.

Swartz, S. E., & H. C. Siew (1987). Is load control suitable for fracture-energy measurements for concrete? *Experimental Mechanics*, 27(4), 359-365.

Turos, M., A. Cannone Falchetto & M. O. Marasteanu (2012). The flexural strength of asphalt mixtures using the bending beam rheometer. *7th RILEM International Conference on Cracking in Pavements*, 4, 11-20.

Weibull, W. (1939). The phenomenon of rupture in solids*. Proceedings of Royal Swedish Institute of Engineering Research*, 151, 1-45.